NOISE CONTROL IN 3-D ENCLOSURE USING PIEZOELECTRIC ACTUATORS

BY

MD TARIQUE BIN HAMID

A Thesis Presented to the

DEANSHIP OF GRADUATE STUDIES

KING FAHD UNIVERSITY OF PETROLEUM & MINERALS

DHAHRAN, SAUDI ARABIA

In Partial Fulfillment of the
Requirements for the Degree of

MASTER OF SCIENCE

In

AEROSPACE ENGINEERING

MARCH 2015

KING FAHD UNIVERSITY OF PETROLEUM & MINERALS

DHAHRAN- 31261, SAUDI ARABIA

DEANSHIP OF GRADUATE STUDIES

This thesis, written by **MD TARIQUE BIN HAMID** under the direction his thesis advisor and approved by his thesis committee, has been presented and accepted by the Dean of Graduate Studies, in partial fulfillment of the requirements for the degree of **MASTER OF SCIENCE IN AEROSPACE ENGINEERING.**

Dr. Wael G. Abdel Rahman
(Advisor)

Dr. Ahmed Z. Al-Garni
Department Chairman

Dr. Ahmed Z. Al-Garni
(Co-Advisor)

Dr. Yehia A. Khulief
(Member)

Dr. Salam A. Zummo
Dean of Graduate Studies

DEANSHIP OF GRADUATE STUDIES

5/4/15
Date

Dr. Mehmet Sunar
(Member)

Dr. Prasetyo Edi
(Member)

NOISE CONTROL IN 3-D ENCLOSURE USING PIEZOELECTRIC ACTUATORS

MD TARIQUE BIN HAMID

DEPARTMENT OF AEROSPACE ENGINEERING

MARCH 2015

KING FAHD UNIVERSITY OF PETROLEUM & MINERALS

DHAHRAN- 31261, SAUDI ARABIA

DEANSHIP OF GRADUATE STUDIES

This thesis, written by **MD TARIQUE BIN HAMID** under the direction his thesis advisor and approved by his thesis committee, has been presented and accepted by the Dean of Graduate Studies, in partial fulfillment of the requirements for the degree of **MASTER OF SCIENCE IN AEROSPACE ENGINEERING.**

____

Dr. Wael G. Abdel Rahman
(Advisor)

____

Dr. Ahmed Z. Al-Garni
Department Chairman

____

Dr. Ahmed Z. Al-Garni
(Co-Advisor)

____

Dr. Salam A. Zummo
Dean of Graduate Studies

____

Dr. Yehia A. Khulief
(Member)

____

Date

____

Dr. Mehmet Sunar
(Member)

____

Dr. Prasetyo Edi
(Member)

-

Dedicated to my

Beloved and lovely parents

ACKNOWLEDGMENTS

IN THE NAME OF ALLAH, THE MOST BENEFICIENT, THE MOST MERCIFUL

Read! In the Name of your Lord, Who has created (all that exists), Has created man from a clot (a piece of thick coagulated blood). Read! And your Lord is the Most Generous, Who has taught (the writing) by the pen. Has taught man that which he knew not. Nay! Verily, man does transgress all bounds (in disbelief and evil deed, etc.). Because he considers himself self-sufficient. Surely! Unto your Lord is the return.

(Surah 96: Al 'Alaq, 1-8)

All praise is for Allah. We praise Him and seek His help and forgiveness. We seek refuge in Allah from the evil of ourselves and the wickedness of our own deeds. Peace and blessings of Allah be upon our dearest prophet, Muhammad, his family and his companions, and those who follow him until the last Day.

I am grateful to King Fahd University of Petroleum and Minerals, for facilitating me with an outstanding environment for research and education.

I want to express my appreciation to my advisor Dr. Wael G. Abdelrahman, for his help, guidance and efforts in this work. During this thesis work, I have benefited from his precious aid, scientific counsel, as well as his constant availability. Through his personal and scientific qualities, he has taught me how to be a good researcher and have reinforced my passion for the scientific arena. Thank you, my beloved advisor!

My sincere and heart-felt thanks to Prof. Ahmed. Z. Al-Garni, my Co-Advisor and Chairman of Aerospace Engineering Department, due to his valuable suggestions, encouragement and continuous support.

Special and sincere thanks also go to my thesis committee members, Prof. Yehia A. Khulief, Dr. Mehmet Sunar, and Dr. Edi Prasetyo for their cooperation and valuable advice.

I would like to thank Dr. Ahmed Masud, Dr. Salim Ibrir and my buddy Bagus for their continuous support. Also, I would like to thank all the engineers and members at the Aerospace Engineering Department for their support and advice. Their presence was significant in carrying out this task. Thank you, all!

On my personal account, I would like to thank my mother, brother and my sister who have always encouraged me equally through the difficult and the successful moments in my studies. Best regards to all my friends who know how to enrich my social life at the university. Thank you, Sheriff, Khaled, Yazan, Emon, Himu, Ahmed, Abdullah and everyone else.

Finally, I would like to especially thank my wife, Khadiza-tut-Tamanna, who has known how, during the last course of this research work, to provide her love, tenderness and support in both pleasant as well as during more trying moments. Thank you, Khadiza - I love you!

I always pray to Allah (SWT) to make all true Muslims happy and to guide us to the Straight Path and forgive our sins and grant us Jannah. Ameen

TABLE OF CONTENTS

LIST OF TABLES

LIST OF FIGURES

LIST OF ABBREVIATIONS

PZT	:	Piezoelectric Ceramic
PVDF	:	Polyvinylidene fluoride
ANC	:	Active Noise Control
ASAC	:	Active Structural Acoustic Control
SISO	:	Single Input Single Output
MISO	:	Multi Input Single Output
MIMO	:	Multi Input Multi Output
1D	:	One Dimensional
3D	:	Three Dimensional
LMI	:	Linear Matrix Inequality
LQR	:	Linear Quadratic Regulator
LQG	:	Linear Quadratic Gaussian
KF	:	Kalman Filter
RE	:	Riccati Equation
GA	:	General Aviation
SPL	:	Sound Pressure Level
PD	:	Proportional and Derivative
PI	:	Proportional and Integral

ABSTRACT

Full Name : MD TARIQUE BIN HAMID

Thesis Title : Noise control in 3-D enclosure using piezoelectric actuators

Major Field : Aerospace Engineering

Date of Degree : MARCH, 2015

Acoustic noise is a major problem of our day-today's life, and particularly it is one of the greatest concerns for automotive and aerospace industries. Acoustic noise problem plays pivotal role for extensive research to develop noise reduction techniques such as passive, semi-active, and active methods. Active control strategies are much more useful for low frequency noise problems. This thesis deals with the active control of noise in a 3D enclosure representing a model of helicopter cabin. The source of noise is an external force created by spatially bounded Heaviside function with a temporal function on the upper panel to simulate vibrations from helicopter propeller impinging disturbance on the upper surface of the cabin. An analytical state-space finite dimensional approximate model is derived for the structural-acoustic system consists of a 3D rectangular cavity with five acoustically rigid walls and a simply supported flexible plate on the top of cavity suitable for control design. The analytical model is compared with the published analytical and experimental data which are in complete agreement. Piezoelectric patches bonded symmetrically to the top surface of the panel are used as actuators. Microphone and PVDF sensors are used to measure both the pressure inside the cavity and panel displacement. Implementation of an optimal controller (LQG) shows considerable broadband reduction of noise.

ملخص الرسالة

الاسم الكامل:محمد طارق بن حامد

عنوان الرسالة:التحكم في الضجيج في فجوة ثلاثية الأبعاد باستخدام مشغلات كهروإجهادية

التخصص:هندسة الطيران والفضاء

تاريخ الدرجة العلمية:

.

الضجيج الصوتي يعتبر مشكلة كبرى في حياتنا اليومية،وخاصة أنه يعتبر واحدا من أهم المخاوف بالنسبة لصناعة السيارات والطائرات. مشكلة الضجيج الصوتي تلعب دورا محوريا لأبحاث مكثفة لتطوير تقنيات الحد من الضجيج الصوتي مثل تقنية التحكم السلبي، التحكم شبه النشط والنشط، يتناول هذه البحث التحكم النشط للضجيج في فجوة عازلة ثلاثية الأبعاد تمثل نموذج مقصورة لطائرة هليكوبتر، مصدر الضجيج هو قوة خارجية نشأت من قبل دالة هيفيسيد مع دالة زمنية على اللوح العلوي لمحاكاة اهتزازات مروحة الهليكوبتر والتي تؤثر باضطرابات على السطح العلوي للمقصورة، وقد تم إشتقاق نموذج تحليلي تقريبي محدود الأبعاد لنظام هيكلي صوتي والمتكون من تجويف مستطيل الشكل، ثلاثي الأبعاد مع خمسة جدران صلبة ولوح مرن بسيط الإرتكاز على الجزء العلوي من التجويف حيث أنه مناسب لتصميم التحكم، تتم مقارنة النموذج التحليلي مع البيانات التحليلية والتجريبية المنشورة، في هذ البحث إستخدمن اشرائح كهربية إجهادية بشكل متماثل على السطح العلوي من اللوح حيث أستخدمت كمشغلات، وتم استخداما ميكروفون وأجهزة استشعار لقياس الضغط داخل التجويف الصوتي وكذلك إزاحة اللوح ، وبتنفيذ وحدة تحكم الأمثل يظهر انخفاض كبير واسع النطاق في الضجيج.

CHAPTER 1

Literature Review

1.1 Background information

Noise from vibrations of structures can radiate into the free field or into enclosures. Because of the increasing use of lightweight materials in manufacture, structure-borne noise has become a pronounced concern in industry. The noise radiated by machine tools and by engines in workplaces can seriously damage the health of workers and disturbs the life of residents in adjacent communities. In aerospace and automotive industries, the noise in fuselages or cabins, induced by the vibration of the surrounding walls, can significantly influence the comfort of passengers and hence reduce the competitiveness of products. The problem is especially crucial for turbo-propeller aircraft, due to the high-level blade passage noise in the cabin, which limits, to a great extent, its commercial use even though it has high fuel efficiency. This need for noise reduction in practice strongly motivates the research on noise control.

In general, there are two noise control methods - passive control and active control. Up to present, the passive noise control method is still widely used in practice due to its advantage of easy implementation, low cost, and no need for external energy. It works by utilizing sound absorptive materials to absorb the sound energy, and by building barriers and enclosures to block the propagation paths of noise. However, it is only effective for high frequency noise. The control of low frequency noise and vibration is difficult and expensive and, in many cases, not feasible by passive methods. The long acoustical wavelengths involved require the use of large mufflers, heavy enclosures, and extensive structural damping treatments for noise control.

On the other hand, active control methods are suitable for low frequency noise. The idea of using active sound cancellation as an alternative to passive control was first proposed by Paul Lueg in 1930s [1, 2]. The idea is to use actuators (control sources) to introduce a secondary disturbance into the system to cancel the existing disturbance, thus resulting in an attenuation of the original sound. The 'anti-disturbance' can be generated electronically based on a measurement of the primary disturbance using sensors.

After the exposition of the original idea, it was not until the 1950s that the idea was rekindled by Olson [3, 4] who investigated the possibility of active sound cancellation in rooms, in ducts and in headsets and earmuffs. However, limitations in the available electronic control hardware, as well as limitations in control theory at that time, prevented this technology from being commercially realized.

Since the 1980s, especially in the 1990s, thanks to the rapid advances in control theory and microelectronics, research in active noise control has been greatly expanded. Some commercial systems have even become available for controlling low frequency, plane wave sound propagation in air handling ducts. However, in complex cases, such as noise control in aircraft cabins, extensive research is required before a practical system is realized because of a need to understand the physical principles involved.

For the sake of simplicity, the application of active noise control of plane waves propagating in a one-dimensional air duct is used here to explain the different approaches of active control used in the past, which may be divided into two categories: feedforward control and feedback control.

Feedforward controllers rely on the availability of a reference signal which is a measure of the incoming disturbance. This signal must be received by the controller in sufficient time for the required control signal to be generated and output to the control source when the disturbance arrives [6]. For stationary or slowly varying periodic disturbances this time constraint need not be satisfied, as the assumption can be made that the signal during one period will be very similar to that during the previous period [7]. Thus it is relatively easy to obtain a reference signal for a periodic disturbance. The control signal fed to a control source is produced by digitally filtering the reference signal.

To adapt to changes in the disturbance, current practice involves the use of an adaptive algorithm to adjust the characteristics of the digital filter to minimize the downstream residual disturbance, the measure of which is the instantaneous value of the squared signal detected by an ‘error’ microphone. Feedback control systems differ from feedforward systems in the manner in which the control signal is derived. Whereas feedforward systems rely on some predictive measure of the incoming disturbance to generate an appropriate ‘canceling’ disturbance, feedback systems aim to attenuate the residual effects of the disturbance after it has passed. Feedback systems are thus better at reducing the transient response of systems, while feedforward systems are best at reducing the steady state response.

The feedback controller derives a control signal by filtering an error signal, not by filtering a reference signal as is done by a feedforward controller [6]. One question which may be asked is how one decides whether to use a feedforward or a feedback controller for a particular application. The answer is that a feedforward system should be implemented whenever it is possible to obtain a suitable reference signal, because the performance of a feedforward system is, in general, superior to that of a feedback system.

In cases when the reference signal is difficult to obtain, feedback control systems are especially suitable and, indeed, are the only alternative. In an active control system of the interior noise induced by the vibration of surrounding structures, control sources can be acoustical sources such as loudspeakers, or structural sources such as shakers and piezoelectric transducers, and the error sensors can be microphones, polyvinylidene fluoride (PVDF) sensors or accelerometers.

Depending on the type of control sources, the control method may be divided into Active Noise Control (ANC) using acoustical sources and Active Structural Acoustical Control (ASAC) using vibration sources. Some work has been done on the mechanisms behind the two control methods. By experiments on a rectangular panel in free field, authors [8] compared the two active control methods and summarized their mechanisms.

For vibration sources, global attenuation of radiated sound is observed to occur by two main mechanisms. For “on resonance” excitation, the control force has the effect of increasing the total panel input impedance presented to the noise source, thus reducing all radiated sound. For “off resonance” excitation, the control force tends to not significantly modify the panel total response amplitude but rather to restructure the relative phases of the modes, leading to a more complex vibration pattern and a decrease in radiation efficiency.

For acoustical sources, the mechanism is that the acoustical sources tend to create an inverse pressure distribution at the panel surface and thus unload the panel by reducing the panel radiation impedance. Authors [9, 10] studied the mechanism of controlling sound transmission into a coupled enclosure. The physical mechanisms by which acoustical control sources achieve active sound attenuation are less complicated than those of vibration control sources. The control mechanism employed when using optimally tuned acoustical control sources is mode suppression.

At an acoustical resonance a single acoustical mode will dominate the acoustical pressure distribution in the enclosure and, hence, the levels of acoustical potential energy. A single control source can easily excite this same single mode and, hence, quite easily provide a significant reduction over the entire surface of the structure. At a structural resonance, however, several acoustical modes may be significantly excited. For the control source distribution similarly (in relative phase and amplitude) to excite the acoustical modes, control source placement and number can become critical.

Therefore, in general, acoustical control sources are recommended for controlling acoustical resonance. For vibration control sources, there are two possible control mechanisms: for structure controlled response, where the majority of the total system energy is associated with the response of the structure (such as near a structural resonance), sound pressure reduction is obtained by mode suppression (by suppressing the structural vibration amplitude of the controlling mode); for cavity controlled response, where the majority of the total system energy is associated with the response of the enclosed acoustical space (such as near an acoustical resonance), the control force is used to rearrange the structural modes (change the structural modal amplitudes and phases) so that the radiated power from the structure into the cavity is reduced, which is similar to that in the free field. Compared with an ANC system, with light-weight and surface-mounted piezoelectric transducers (PZT actuators and PVDF sensors), an ASAC system is more compact, less intrusive to the host structure and easy to install, which are appealing characteristics in many practical applications such as noise control of vehicle cabins.

Therefore, it prompts great interest of many researchers. Hereafter, the review mainly focuses on the research on active structural acoustical control.

1.2 Literature Review

A significant amount of work has been carried out by various researchers to reduce the noise level in the passenger cabin as a source of discomfort to passengers. Passive control of noise and vibration is a technique that has been adopted extensively in engineering noise and vibration control. The common practice in this approach is to either modify the stiffness of the structure or augment its damping to achieve passive control by avoiding structural resonances or absorbing vibration and/or acoustic energy. However, for the type of problem in this investigation, such passive control techniques are generally not very effective.

In fact, increasing the damping does not reduce the noise and vibration levels appreciably since the excitations are usually neither broadband nor resonant [11]. Moreover, using damping materials is generally ineffective at the low frequencies (50 Hz to 300 Hz) where propeller noise is significant. Also, narrow-band damping, using tuned vibration absorbers can be effective in reducing noise, but the improvement is limited due to the difficulty in keeping the devices tuned in a varying environment. The successful use of active noise control (ANC), where a large number of microphones and speakers are employed, has been reported in various applications with significant noise reductions [5, 8, 11-17]. This approach, generally referred to as noise cancellation, is realized by generating sound waves using secondary sources that interfere with the noise, thereby using the destructive interference of the component waves to reduce the level of the noise. However, the size of the required devices and the complexity of the configuration make the implementation of this approach inside the cabin of an aircraft unattractive.

Active acoustic control is an alternative to the passive techniques. These active methods are not intended to replace currently used passive techniques, but to complement them. Since passive acoustic blankets are effective in attenuating higher frequency acoustic disturbances, the active technique will target lower frequency acoustic disturbances. There are two main types of active acoustic control. They are Active Noise Control and Active Structural Acoustic Control. Active Noise Control (ANC) [14, 15, 18-25] employs secondary acoustic sources to destructively interfere with the disturbances. Generally, the acoustic disturbances are monitored, and the secondary acoustic sources emit sounds so as to cancel the disturbances at discrete performance points.

ANC is most often used when the disturbance has a strong tonal component such as propeller passage frequency or engine RPM and the disturbance source is easily identifiable and compact such as an automobile muffler. However, in the case of broadband and diffuse source oriented disturbances, a measurement of the disturbance is impossible which makes ANC techniques unfeasible. Besides, ANC techniques are usually only successful in achieving attenuation at specific points at which performance microphones have been placed. In fact ANC techniques may significantly amplify noise at points other than these performance points. This is not satisfactory for the broadband acoustic disturbance alleviation problem in which global attenuation is required. Also the need to place microphones near the disturbance sources can damage the structural integrity.

Active Structural Acoustic Control (ASAC) [14, 26-34] on the other hand uses structural actuators to control the enclosing structure, thus affecting the acoustic field within the enclosure. Since ASAC controls the structural vibrations which lead to the enclosed acoustics, it can control the enclosed acoustic field in a global manner. Although ASAC allows global attenuation of the enclosed acoustics using only structural actuators, it has one problem. This is that it can only control the acoustic modes which are closely coupled with the structural modes. The impedance matching control technique is a specific type of ASAC. It uses a dereverberated model of the system's local behavior to derive a controller which achieves global acoustic attenuation without the need for performance microphones distributed throughout the enclosure.

One main advantage to the impedance matching controller is the lack of need for a complex high order model of the structural-acoustic system. The assumption made for impedance matching control is that the local behavior can be modeled accurately using wave modes and that these are sufficient to obtain an effective controller. Impedance matching control designs generally attempt to eliminate the reflection or transmission of energy through some junction or to maximize the energy dissipated by the controller. Although impedance matching control has its origins in structural control, it has been applied to structural-acoustic control to a limited degree.

A good understanding of the underlying physics of a particular noise and vibration problem is an essential part of designing an optimum control system. Therefore, vibroacoustical modeling and coupling analysis are the first step towards any successful ASAC of structure-acoustical systems. Early in 1963, Lyon [35] studied the noise reduction in an enclosure with one flexible wall. Then, the effect of cavities on the natural frequencies of the flexible plate was investigated by Dowell and Vass [36]. Pretlove [37, 38] pointed out that the effects of shallow cavities on the vibration of a plate are not negligible. In 1970s, Dowell et al. [39] developed the well-known acoustoelasticity theory, which has become the theoretical foundation for vibroacoustical modeling and analysis. In this theory, the sound pressure is expanded in terms of the normal modes of the rigid walled cavity; the motion of the flexible wall are also derived in terms of in vacuo-structural normal modes; finally, the complete coupled fluid-structural equations of motion are obtained by means of Green's Theorem and Neumann boundary conditions. Based on this theory, Narayanan and Shanbhag [40] investigated the sound transmission through a sandwich panel into an enclosure. Recently [41-44] and others have done outstanding work on ASAC in 3D enclosure.

Using vibroacoustical models, one can predict the interior sound pressure level. However, to design an effective active structural acoustical control system, the structural acoustical coupling characteristics have to be further analyzed. For regular structures, the coupling in space could be explicitly characterized by the coupling coefficient between structural and acoustical modes expressed as the surface integral of the acoustical mode shape function and the structural mode shape function divided by the vibrating surface.

The in-vacuo structural mode shape functions of the simply supported top panel are represented with a sinusoidal series along longitudinal and lateral directions respectively multiplied by an arbitrary coefficient and each individual mode shape is divided by its corresponding length of the plate. Besides, the acoustical mode shape functions of the rigid walled regular enclosure are represented with a cosine series along x, y, and z directions respectively multiplied by an arbitrary coefficient and each individual mode shape is divided by its corresponding length of the cavity. The geometric coupling relationship between the uncoupled structural and acoustic mode shapes is obtained by taking a surface integral of acoustical mode shape functions and structural mode shape functions over the plate surface area.

Moreover, Snyder and Hansen [10] have shown the modal coupling relation between acoustical mode and structural mode where they have proved that only odd index panel modes couple with even index acoustical enclosure modes, and vice versa.

In his work, Guicking et al [45] controlled the acoustic reflection coefficient of a single degree of freedom structure in a one-dimensional waveguide. The sensors were a pair of microphones which were weighted to give a measure of the incoming acoustic pressure. The feedback gain from the microphone sensors to the single degree of freedom structure was varied manually so that the acoustic reflection coefficient was minimized. Significant reduction in the reflection coefficient was achieved in the frequency range between 100Hz and 800Hz. This was also extended to three dimensional acoustics in which an array of speakers was set up and each speaker was controlled individually using a one dimensional impedance match for reflection. Although reflection coefficients of less than 0.1 were achieved, work of Guicking et al [45] had one major drawback. Since the control gains were varied manually until a desirable result was obtained, no systematic design methodology was followed to determine the optimal impedance matching compensator.

In his work Glaese [46] used a hybrid global/dereverberated model of the structural-acoustic system, in which the structural part of the model is fully reverberant, but the acoustic part is dereverberant, was used. Using an LQG state space formulation, an optimal compensator was obtained which achieved significant attenuation of the first and second acoustic modes. Thus a systematic approach to obtaining an optimal compensator for global acoustic attenuation was provided which used only structural and acoustic sensing at the surface of the enclosing structure. Much of the past research into active acoustic control is based on feedforward techniques in which a measure of the disturbance is available.

Feedforward control using ASAC methods have been used to control acoustic transmission through thin structures into an enclosure, as was done by Balachandran [27]. PZT actuators located on the flexible structure were used with condenser microphone sensors to control the transmission of acoustics generated by a speaker located outside the enclosure. However, the disturbances generated were simply harmonic in nature allowing for the use of a feed-forward control. Since such a measure of the disturbance is not possible in the case of the broadband and diffusive noise sources, feedback control is required. There has been much work done in the past in the field of structural-acoustic control. However, much of this research has focused on feedforward control techniques which are not a viable option in the case of the 3D cabin noise reduction. Therefore feedback control must be used.

Much of the past research utilizing feedback methods used either reflection control or transmission control to attenuate the enclosed acoustics. Although the work [47, 48] controls both the transmission of sound into the enclosure as well as the acoustic cavity modes, it does not use a systematic control design such as linear optimal control. Therefore the work presented here uses a linear optimal control design to simultaneously control the transmission and reflection of sound to attenuate the acoustic levels within an enclosure.

1.3 Importance of the problem

There are many interesting works have been reported in the literature. Most of them dealt with the problems of free field or regularly shaped enclosures. But, most of the structures in industry are irregular, such as aircraft cabins. Before active noise control technology can be applied in practice, many problems have to be investigated. First, the conventional modal coupling coefficient approach for the structural acoustical coupling analysis only works well for regular shaped enclosures. As structures with irregular sound cavities become involved, it becomes laborious. Hence, a novel structural acoustical coupling analysis method suitable to irregular enclosures is required. Second, a better understanding of the fluid-structure coupling of aircraft cabins is still needed. Thirdly, as mentioned above, because of the merits of PVDF sensors, such as lightweight and easy installation, it has stimulated the interests of many researchers to use PVDF structural error sensors to replace microphones in an ASAC system.

However, because PVDF sensors provide vibration signals of structures instead of sound signals, and because different structural modes have different sound radiation abilities, PVDF sensors have to be specially designed to sense those structural modes efficiently radiating sound. Fourthly, most of the work in the literature concerning ASAC deals with free-field problems involving simple structures like beams and plates, or cavity problems with simple types of control sources such as point forces. Research carried out focused more on the use of various optimal approaches than on the design of the ASAC system itself.

Given the increasing concern with the interior noise of aircraft cabins and vehicular cabins, ASAC for cavity noise of complex structures is of particular interest in both industry and academia, in which PZT actuators are usually used as control actuators. As Li et al. [49] mentioned, the control effect of PZT actuators is different from that of point forces, and the fact that PZT actuators generate distributed effects to the structure over the covered area makes the problem of optimal placement design more critical. Therefore, research including a PZT actuator model, and focusing more on the physical problem itself, should be conducted. On the other hand, when an ASAC system consists of PZT actuators and PVDF error sensors, an effective design system is definitely needed.

1.4 Statement of problem

Aircraft cabin noise consists of the air-borne and structural-borne sound generated by the engine, the propeller and the noise due to the aircraft structure interacting with the boundary layer. The noise levels in the aircraft are generally high during both cruise and climb (90 dB -115 dB). The noise is dominated by the low frequency sounds due to the engine and propeller tones. Cabin noise is fatiguing and makes conversation difficult or unintelligible. The dominant tones, usually due to the propeller, are the most fatiguing content in the spectrum but these tones are the hardest to control by traditional passive methods. Reducing this low frequency cabin noise by passive methods is not practical in the aircraft but constitutes the frequency range in which ANC (active noise control) is the most effective.

Pilots and passengers in rotorcraft and in GA (general aviation) aircraft typically rely on passive headsets incorporating an intercom system to provide hearing protection, reduce fatigue and enable conversation. While these headsets provide good noise attenuation, the tones are still present and fatiguing. More recently, active headsets incorporating ANC systems provide an improvement over the passive headsets by eliminating the dominant tones and reducing the broadband component. The use of headsets is cumbersome, restrictive and uncomfortable after extended periods due to 'head squeeze'. ANC aims to reduce cabin noise to provide lower noise levels to allow normal conversation and eliminate the need for headsets. ANC systems eliminate the dominant tones and can provide extensive broadband reductions in some cases.

Single engine GA aircraft and rotorcraft present a unique set of problems due to the aircraft configuration and the restrictive cabin space and weight allowances. The amount of noise reduction due to ASAC in such closed enclosures is still under investigation. It is possible to investigate practical considerations as well as the amount and the spatial extent of noise reductions through the use of PZT sensors and actuators based on ASAC system with modeling and analysis or in laboratory.

1.5 Objectives

The overall objective of this thesis is to reduce the broadband low frequency noise in a 3-Dimensional enclosure using piezoelectric actuator action on the walls of the enclosure. This will be accomplished by proposing a structural acoustical coupling analysis method, and then employing this method to reduce the pressure at specified points inside the 3-D enclosure.

The detailed objectives are as follows:

- Development of an analytical model of the structural-acoustical coupling characteristics of a 3-D enclosure resembling helicopter cockpits. This includes validation of the system eigen-frequencies using available analytical and experimental results.
- Development of an ASAC system consisting of PZT actuators on one of the 3-D enclosure walls and microphones and PVDF error sensors at selected points simulating points of interest in helicopter cockpits.

1.6 Thesis Organization

The organization of the remainder of this thesis is broken down into five chapters. In chapter 2, active noise control of 1-D rectangular Duct is presented. Chapter 3 contains coupled system modeling and eigen-frequency validation. Chapter 4 explores an active optimal controller design for effective control of pressure fluctuations in the 3D cavity. Chapter 5 discusses the results. Finally chapter 6 summarizes this thesis work, and discusses additional avenues of future studies.

CHAPTER 2

Active noise control of 1-D rectangular Duct

2.1 Introduction:

Duct/cabin noise either be it in buildings, automobiles, aircrafts, or anything you name it, is a significant noise problem. Generally speaking, noise sources are located outside the duct/cabin. The external noise excites the duct/cabin structure, and the structure transmits noise into the cavity. Noise control can be broadly classified into active, passive, and semi-active methods [50]. Passive and semi-active methods are relatively ineffective in low frequencies. For instance, the thickness of the sound absorbing materials must be comparable to the acoustic wavelength (e.g. the wavelength of a 100 Hz sound can be as long as 3.4m). This requirement leads to a large, bulky, expensive and unpractical system. But the active method is efficient, economical, and useful for the control band of 1 kHz [51]. Paul Lueg in 1930s [1, 2] first proposed the idea of using active sound cancellation as an alternative to passive control .

Either adaptive feedforward control or Helmholtz resonator is usually applied to suppress low-frequency reverberant sound fields. If noise reference signal is available, feedforward systems can be used with the help of error microphone and loudspeaker to cancel noise in one direction. Feedforward systems are the most expensive and complex option for acoustic noise reduction due to the requirement for multiple transducers and a powerful digital signal processor [52].

Helmholtz resonators consist of auxiliary coupled acoustic chambers. Helmholtz resonator is a popular passive technique for the dominant acoustic modes control. Lightly damped acoustic modes can be significantly attenuated. But the resonators are difficult to tune and require impractically large cavity volumes at frequencies below 200 Hz [52]. Authors [52, 53] have introduced a new technique for the control of low-frequency reverberant sound fields. In this new technique, electrical impedance is connected to the terminals of an acoustic loudspeaker, the mechanical dynamics to make acoustic response to emulate a sealed acoustic resonator. No microphone or velocity measurement is required. Of the new techniques, the passive shunt electrical circuit is simply the parallel connection of a capacitor and resistor. For semi-active shunt case, the required electrical circuit requires a series negative resistor and negative-inductor circuit along with a parallel inductor-resistor-capacitor circuit [53]. In this work, the numerical results are presented to verify the tuning capability and the control performance of these two shunt loudspeakers.

2.2 Assumptions and Linearization:

The rectangular duct can be considered as one dimensional if $(L_y/L_x, L_z/L_x \ll 1)$, where L_x, L_y, and L_z are the length, width and height of the duct respectively. As for the nonlinear governing equations relevant to the modeling of an acoustic enclosure are the fundamental equations of fluid mechanics: mass conservation, equation of state, and Euler's equation of motion. Linearization can be achieved in case of small pressure perturbation and zero-mean fluid velocity. The nonlinear governing equation is as the following:

$$\frac{\partial^2 p(x,t)}{\partial x^2} - \frac{1}{c^2}\frac{\partial^2 p(x,t)}{\partial t^2} = \rho_o \frac{dv_1}{dt}\delta(x - L_x) \qquad (2.1)$$

Where $p(x,t)$ is the sound pressure variation measured from the duct end, v_1 is the forced velocity, ρ_0 is the ambient density, and c is the speed of sound.

The closed end boundary conditions are $v(0,t) = v(L,t) = 0$. The linearization process has been described in details in [6].

2.3 Difference between Loudspeaker and Shunt Loudspeaker

The electromechanical loudspeaker is the most commonly used actuator in active noise control (ANC) applications [53-55]. Loudspeakers normally behave like band-pass filters, with frequency dependent magnitude weighting and phase shift. By connecting a shunt circuit to a loudspeaker, the natural frequency and damping ratio of the loudspeaker can be modified [53]. The mechanism of the shunt loudspeaker to control noise is to add damping to the target acoustic mode. Such a shunt loudspeaker behaves like a Helmholtz resonator which dissipates acoustic energy from the system [52]. As a primary advantage, the proposed solution for controlling the sound level eliminates expensive sensors and bulky control electronics as required by ANC systems. The shunt loudspeaker discussed herein passively controls the targeted mode, removing acoustic spillover in the control bandwidth, and allows global attenuation with single actuator [53].

2.4 Shunt loudspeaker model

Figure 1 shows a generic schematic of a shunt loudspeaker. There are two inputs for the loudspeaker such as the acting pressure on the speaker face and the current to the coil. The output is the displacement of the loudspeaker. Since the loudspeaker is a coupled electromechanical system, two differential equations are needed to describe their behaviors.

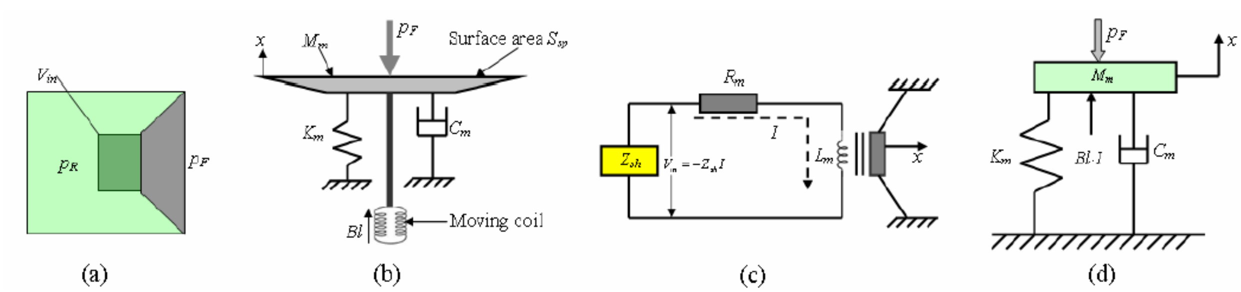

Figure 1 (a)The loudspeaker model; (b) Mechanical schematic of loudspeaker; (c) Electrical schematic of loudspeaker; (d) Mechanical model of loudspeaker [52, 53].

The mechanical dynamics of loudspeaker cone shown in Figure 1 can be written as [55]

$$M_m\ddot{x} + C_m\dot{x} + K_m x = BlI - pS_{sp} \tag{2.2}$$

$$p = p_F - p_R \tag{2.3}$$

$$p_R = -\frac{S_{sp}\rho_o c_o^2}{V_s}x \tag{2.4}$$

Substituting equations (2.3) and (2.4) in equation (2.2) renders the following:

$$M_m\ddot{x} + C_m\dot{x} + (K_m + \frac{S_{sp}\rho_o c_o^2}{V_s})x = BlI - P_F S_{sp} \tag{2.5}$$

Let assume $K_T = K_m + \frac{S_{sp}\rho_o c_o^2}{V_s}$ for simplification, and Eq. (2.5) can be written in the following state space model

$$\begin{bmatrix} \dot{x} \\ \ddot{x} \end{bmatrix} = \begin{bmatrix} 0 & 1 \\ -\dfrac{K_T}{M_m} & -\dfrac{C_m}{M_m} \end{bmatrix} \begin{bmatrix} x \\ \dot{x} \end{bmatrix} + \begin{bmatrix} 0 & 0 \\ \dfrac{Bl}{M_m} & -\dfrac{S_{sp}}{M_m} \end{bmatrix} \begin{bmatrix} I \\ p_F \end{bmatrix} \quad (2.6)$$

From Eq. (2.5)-(2.6) and Figure 1(d), it is found that the loudspeaker can be considered as a spring-mass-damper system subjected to an applied force BlI (loudspeaker force factor (*Bl*) multiplied with supplied current (*I*)) and applied pressure p_F. If $BlI = 0$ (open circuit); the loudspeaker can be considered as a passive acoustic absorber [53].

It is noteworthy that the voice coil Bl couples the electrical and mechanical systems in the loudspeaker. A shunt circuit connected to the terminals of a loudspeaker can be designed to modify the response (natural frequency and damping) of the loudspeaker. The electrical behavior of the loudspeaker can be written as [53, 55]

$$L_m \dot{I} + R_m I = V_{in} - Bl\dot{x} \quad (2.7)$$

V_{in} is the shunt voltage applied to the coil, and other parameters stated in the above equations are given in

Table 1. Combining equations (2.6) and (2.7), the shunt loudspeaker model can be represented by the following state-space form

$$\begin{bmatrix} \dot{I} \\ \dot{x} \\ \ddot{x} \end{bmatrix} = \begin{bmatrix} -\dfrac{R_m}{L_m} & 0 & -\dfrac{Bl}{L_m} \\ 0 & 0 & 0 \\ \dfrac{Bl}{M_m} & -\dfrac{K_T}{M_m} & -\dfrac{C_m}{M_m} \end{bmatrix} \begin{bmatrix} I \\ x \\ \dot{x} \end{bmatrix} + \begin{bmatrix} 1/L_m & 0 \\ 0 & 0 \\ 0 & -\dfrac{S_{sp}}{M_m} \end{bmatrix} \begin{bmatrix} V_{in} \\ p_F \end{bmatrix} \quad (2.8)$$

The shunt circuit of the loudspeaker showed in Figure 1(c) can be regarded as shunt impedance Z_{sh} and the shunt voltage can be defined as

$$V_{in} = -Z_{sh}I \tag{2.9}$$

Combining equations (2.8) and (2.9) turns into the following

$$\begin{bmatrix} \dot{I} \\ \dot{x} \\ \ddot{x} \end{bmatrix} = \begin{bmatrix} -\dfrac{Z_{sh} + R_m}{L_m} & 0 & -\dfrac{Bl}{L_m} \\ 0 & 0 & 0 \\ \dfrac{Bl}{M_m} & -\dfrac{K_T}{M_m} & -\dfrac{C_m}{M_m} \end{bmatrix} \begin{bmatrix} I \\ x \\ \dot{x} \end{bmatrix} + \begin{bmatrix} 0 \\ 0 \\ -\dfrac{S_{sp}}{M_m} \end{bmatrix} [p_F] \tag{2.10}$$

Due to the nature of the shunt impedance, it is not realistic to combine equations (2.8) and (2.9). Hence, equations (2.8) and (2.9) turn to the following transfer function with input velocity $\dot{x}$ and circuit current I assuming $s = j\omega$

$$H_{sp}(s) = \frac{I}{\dot{x}} = -\frac{Bl}{L_m s + R_m + Z_{sh}} \tag{2.11}$$

From equations (2.6) and (2.11), two subsystems viz. a mechanical model and an electrical model are obtained. The actual realization of these two models is performed using **sysic** (system interconnection) in MATLAB for simulation.

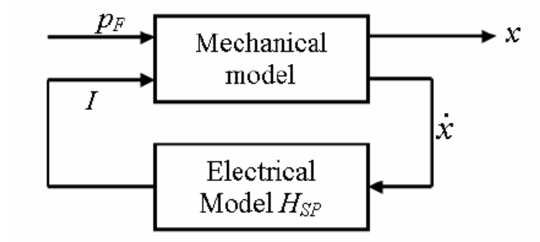

Figure 2 The interconnection of the mechanical and electrical parts of the shunt loudspeaker.

From **Figure 2** and equations (2.6) and (2.11), it can be found that the shunt circuit can be regarded as a feedback controller. Clearly, if the electrical current I is proportional to the displacement x or acceleration $\ddot{x}$, the natural frequency of shunt loudspeaker can be tuned. Alternatively, if I is proportional to $\dot{x}$, the damping of the shunt loudspeaker can be tuned [53].

In this study, two design solutions are presented. The first shunt circuit is purely passive using a capacitor-resistor circuit. The second is a semi-active circuit, which requires a series negative resistor, a negative-inductor circuit and a parallel inductor-resistor-capacitor circuit. These circuits will be discussed in detail in the next sections.

Table 1 The loudspeaker and duct parameters

Duct		Loudspeaker	
Parameter	Value	Parameter	Value
Length, $L_x(m)$	4	Cone area $S_{sp}(m^2)$	207×10^{-4}
Width, $L_y(m)$	0.25	Moving mass $M_m(kg)$	37×10^{-3}
Height, $L_z(m)$	0.25	Natural frequency $\omega_n(Hz)$	28
Air density, ρ_o (kg/m^3)	1.239	Speaker box volume $V_s(m^3)$	207×10^{-5}
Sound speed, $c_o(m/s)$	340	Force Factor Bl (Tm)	9.9
Damping ratio, ζ_p	assumed	Inductance $L_m(H)$	37×10^{-5}
		Resistance $R_m(\Omega)$	6.2

2.5 Passive shunt circuit

Natural frequency of the loudspeaker can be tuned by using a purely passive shunt circuit as show in **Figure 3.** The impedance of the shunt circuit can be written as

$$Z_{sh} = \frac{R_s}{1 + j\omega C_s R_s} \tag{2.12}$$

Where C_s and R_s are shunt capacitance and shunt resistance respectively. The transfer function for electrical part of the loudspeaker H_{SP} can be expressed as

$$H_{sp}(s) = -\frac{Bl}{L_m s + R_m + \frac{R_s}{1 + sC_s R_s}} \tag{2.13}$$

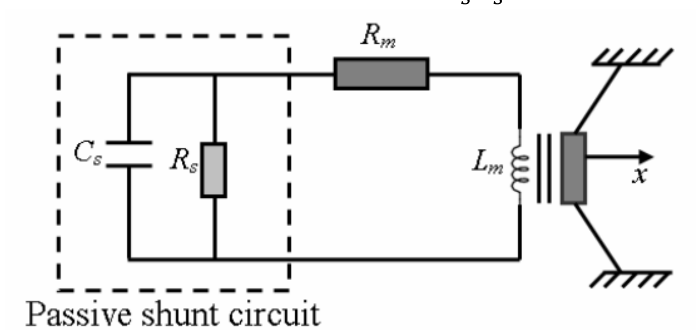

Figure 3 Passive shunt circuit

The natural frequency of loudspeaker can be reduced by increasing value of the shunt capacitance Cs. It is noteworthy that the passive shunt circuit cannot increase the natural frequency of the shunt loudspeaker [53]. Therefore the selection of a suitable loudspeaker is a very important issue in the design of the passive shunt loudspeaker.

2.6 Semi-active shunt circuits

From **Figure 2**, it is clear that the natural frequency and damping ratio of the loudspeaker can be tuned independently of the transfer function of electrical model. H_{SP} is a proportional-Integral-derivative (PID) controller. It can be implemented by using a semi-active shunt circuit including a series negative-resistor, a negative-inductor circuit and a parallel inductor-resistor-capacitor circuit, as shown in **Figure 4**.

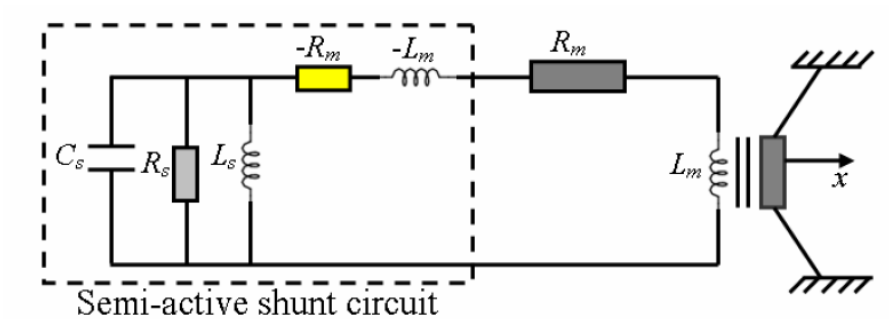

Figure 4 Semi-active shunt circuit.

The impedance for the semi-active shunt circuit, Z_{sh} can be written as following:

$$Z_{sh} = -j\omega L_m - R_m + \left(\frac{1}{\frac{1}{R_s} + \frac{1}{L_s s} + C_s s} \right) \qquad (2.14)$$

Where $R_s, L_s, and\ C_s$ are shunt resistance, shunt inductance, and shunt capacitance respectively. Substituting equations (2.14) into (2.11) turns H_{SP} as a PID controller as following:

$$H_{SP} = -\frac{Bl}{\frac{1}{R_s} + \frac{1}{L_s s} + C_s s} \qquad (2.15)$$

The inferred relationship between loudspeaker and shunt circuit parameters from (2.15) is given in Table 2. It is noteworthy that the natural frequency of the loudspeaker can be tuned by changing the values of Ls and Cs, while the amplitude of frequency responses remain the same. This means that the damping ratio of the shunt loudspeaker does not change. Similarly, the natural frequency of loudspeaker maintains the same value, while the damping ratio is reduced when the values of Rs are changed.

Table 2 The shunt circuit parameters

Shunt circuit parameter	Value
Shunt capacitance $C_s(\mu F)$	$C_s \ \alpha \ M_m$
Shunt inductance $L_m(H)$	$L_s \ \alpha \ 1/\mathrm{K_s}$
Shunt Resistance $R_s(\Omega)$	$R_s \ \alpha \ 1/\zeta_{spk}$

2.7 Noise control performances with shunt loudspeakers

The theoretical study is focused on noise control in a rigid rectangular duct with shunt loudspeakers based on a state-space model. Figure 5 shows a rigid duct consisting of a shunt loudspeaker located at $X_{sh} = 3.88m$, one primary loudspeaker used as disturbance speaker located at $X_p = 0 \ m$, and one microphone located at the right end $X_m = 4m$ to measure the pressure in the duct. The physical parameters of the loudspeakers and duct are listed in

Table 1. The dimensions L_y and L_z of the duct are sufficiently small compared to its length L_x (L_y/L_x , $L_z/L_x \ll 1$) that acoustic waves travel along the length of the duct with planar wave fronts. This assumption enables us to treat the duct as one-dimensional waveguide with spatial coordinate x, where $0 \leq x \leq L_x$ [6].

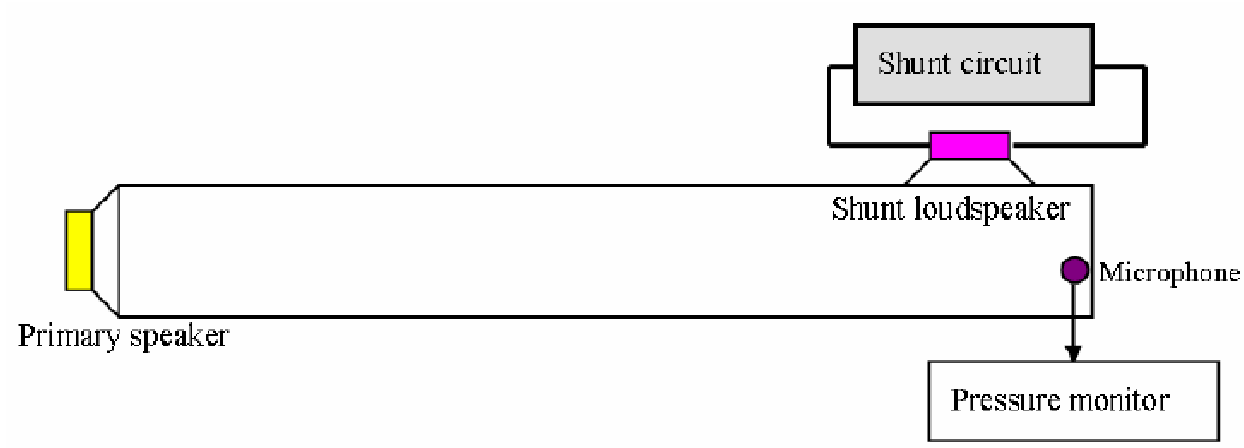

Figure 5 The duct with shunt loudspeaker.

When the frequency is less than the cut-on/off frequency, the acoustic response of the duct illustrated in Figure 5 can be approximated by considering a one-dimension model. The cut-off frequency and cut-on angular velocity can be calculated by $f_{co} = c_0/(2L_y) = 680\ Hz$ and $\omega_{co} = (\pi c_0)/L_y = 4273\ rad/s$ [53, 54]. The authors [53] have considered the control of the duct pressure below 300Hz. In addition, the damping ratio for an arbitrary rectangular enclosure has been assumed as $\zeta_p = 0.001 - 0.003$ from [56].The modal pressure in duct can be written as the followings [52, 53, 55]

$$\ddot{P}_n + 2\zeta_n\omega_n\dot{P}_n + \omega_n^2 P_n = \rho_o c_o^2(F_{p,n} + F_{sh,n}) \tag{2.16}$$

$$F_{p,n} = \ddot{x}_p\Omega_{\mathrm{n}}(X_p)S_{sp} \tag{2.17}$$

$$F_{sh,n} = \ddot{x}_{sh}\Omega_n(X_{sh})S_{sp} \tag{2.18}$$

$$\Omega_n(X) = \sqrt{\frac{2}{L_x}}\cos\left(\frac{n\pi X}{L_x}\right) \tag{2.19}$$

$$\begin{bmatrix}\dot{P}\\ \ddot{P}\end{bmatrix} = \begin{bmatrix}0_{N\times N} & I_{N\times N}\\ -\omega_p^2 & -2\zeta_p\omega_p\end{bmatrix}\begin{bmatrix}P\\ \dot{P}\end{bmatrix} + \begin{bmatrix}0_{N\times 1} & 0_{N\times 1}\\ S_{sp}\Omega_p & S_{HR}\Omega_{sh}\end{bmatrix}\begin{bmatrix}\ddot{x}_p\\ \ddot{x}_{sh}\end{bmatrix} \tag{2.20}$$

Where$\omega_p = diag(\omega_1, \omega_2, \ldots, \omega_N)$, $\zeta_p = diag(\zeta_1, \zeta_2, \ldots, \zeta_N), P = [P_1, P_2, \ldots, P_N]^T, \Omega_p = \left[\Omega_1(X_p), \Omega_2(X_p), \ldots, \Omega_N(X_p)\right]^T, \Omega_{sh} = [\Omega_1(X_{sh}), \Omega_2(X_{sh}), \ldots, \Omega_N(X_{sh})$, and $P_n, \omega_n, and\ \zeta_n$ are the modal pressure, natural frequency and damping ratio of n^{th} acoustic mode of the duct. Whereas, $F_{p,n}, F_{sh,n}\ and\ \Omega_n$ are the n^{th} modal force due to primary loudspeaker, shunt loudspeaker, and n^{th} acoustic mode shape of the rigid duct. Besides, $x_p\ and\ x_{sh}$ are the displacements of the primary and shunt loudspeakers. The natural frequency of n^{th} mode for a rectangular enclosure can be calculated by the following equation from [54].

For 3-D case
$$\omega_n = \frac{c}{2}\sqrt{\left[\frac{n_x}{L_x}\right]^2 + \left[\frac{n_y}{L_y}\right]^2 + \left[\frac{n_z}{L_z}\right]^2} \tag{2.21}$$

For 1-D case
$$\omega_n = \frac{c}{2} \times \frac{n_x}{L_x}\ ; n_x = n^{th}\ mode\ along\ length \tag{2.22}$$

Where c is the speed of sound, $n_x, n_y, and\ n_z$ are number of modes along $x, y, and\ z$ directions respectively.

Moreover, there are three output parameters, i.e. p_p, the pressure at primary speaker location X_p, p_{sh}, the pressure at the shunt loudspeaker location X_{sh}, and p_m, the pressure at the monitor microphone location X_m. Besides, $\Omega'_p, \Omega'_{sh}, and\ \Omega'_m$ are mode shape functions at the primary speaker location, at the shunt loudspeaker location, and at the monitor microphone location respectively. Outputs are written as

$$\begin{bmatrix} p_p \\ p_{sh} \\ p_m \end{bmatrix} = \begin{bmatrix} \Omega'_p & 0 \\ \Omega'_{sh} & 0 \\ \Omega'_m & 0 \end{bmatrix} \begin{bmatrix} P \\ \dot{P} \end{bmatrix} \tag{2.23}$$

2.8 Results and Discussion

The loudspeakers and duct subsystems have been coupled using $sysic$ and Simulink in Matlab. Figure **6** shows the diagram of the loudspeaker-duct system interconnection taken from [53].

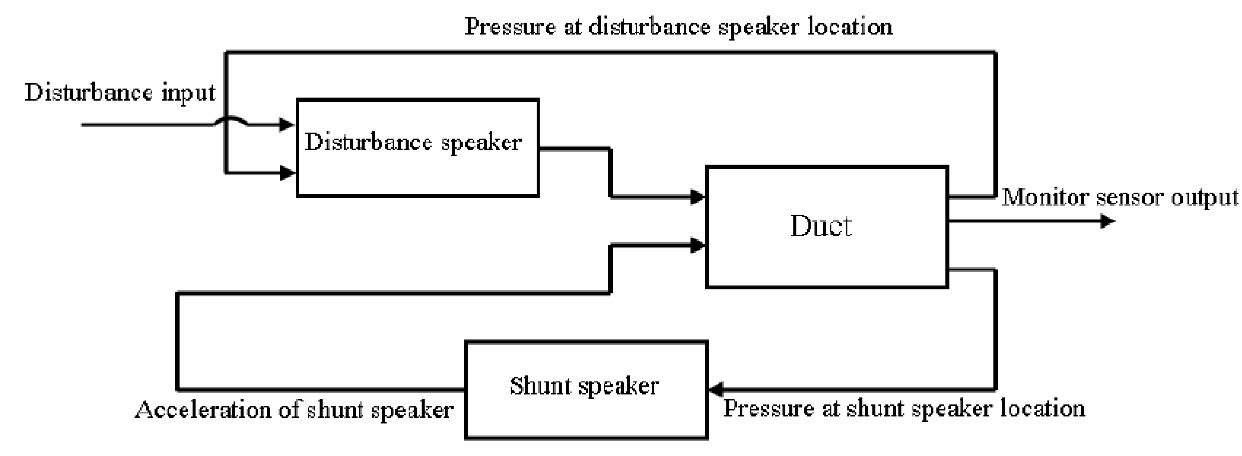

Figure 6 The duct–shunt loudspeaker system.

In Figure 7, the blue line depicts the uncontrolled response measured at the end of the duct, and green line portrays how the passive shunt loudspeaker reduces the noise from the duct system. As the formulation of the passive shunt circuit shows when C_s value is increased the natural frequency decreases provided $R_s \to \infty$, but decreasing the C_s value cannot increase the natural frequency. Hence selection of a proper loudspeaker is of tremendous importance.

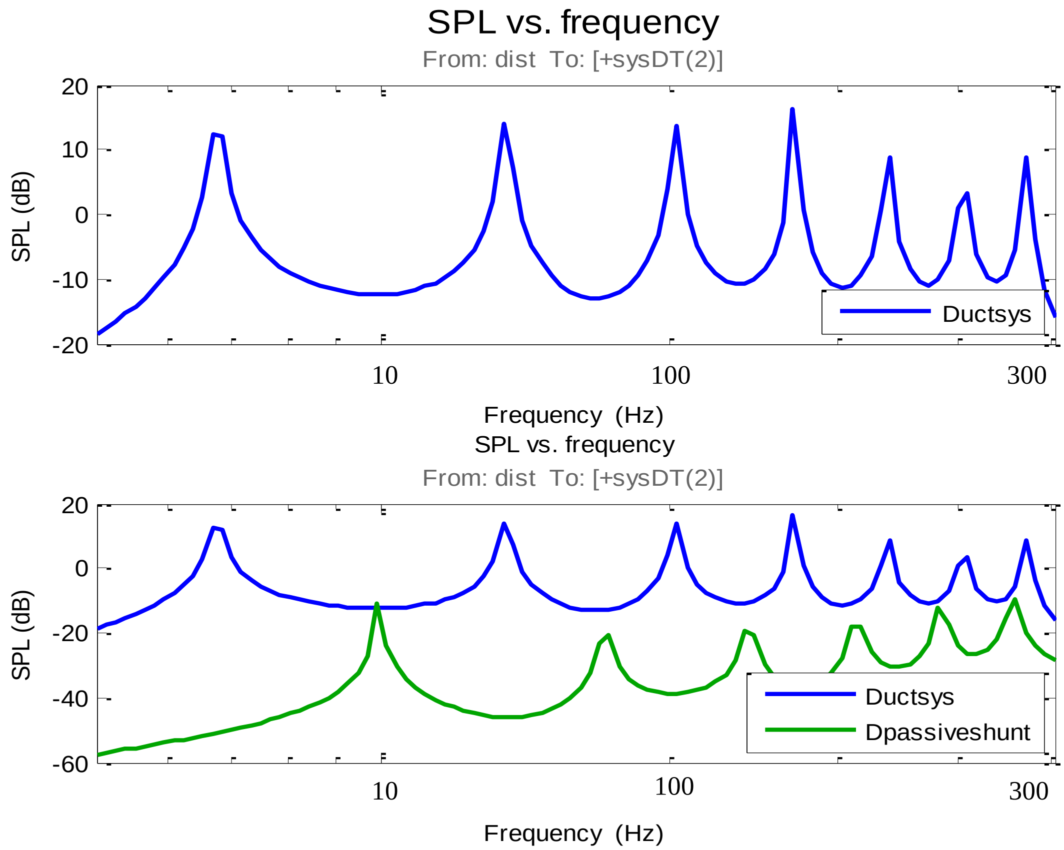

Figure 7 The passive shunt loudspeakers with $\boldsymbol{C_s = 37\mu F \ and \ R_s = 100M\Omega}$

All figures are plotted in the frequency domain in the range of $\omega = 31.8\,Hz - 317.6\,Hz$. Figure 8 shows how well the semi-active shunt loudspeaker works to reduce noise. But as the L_s ,which acts as an integrator, value is increased above 5.685 mH, there is a different modulation of noise signal shown in Figure 9 which can create more noise if the proper value is not selected. Similarly, increasing the C_s, which works as a derivative parameter, value beyond $3700\mu F$, the frequency response start showing an inverted trend as shown in Figure 10 which can in effect intensify noise. So, proper selection of $C_s \ and \ L_s$ values are of tremendous importance. Besides, any R_s value can be taken except $R_s \ll 1$.

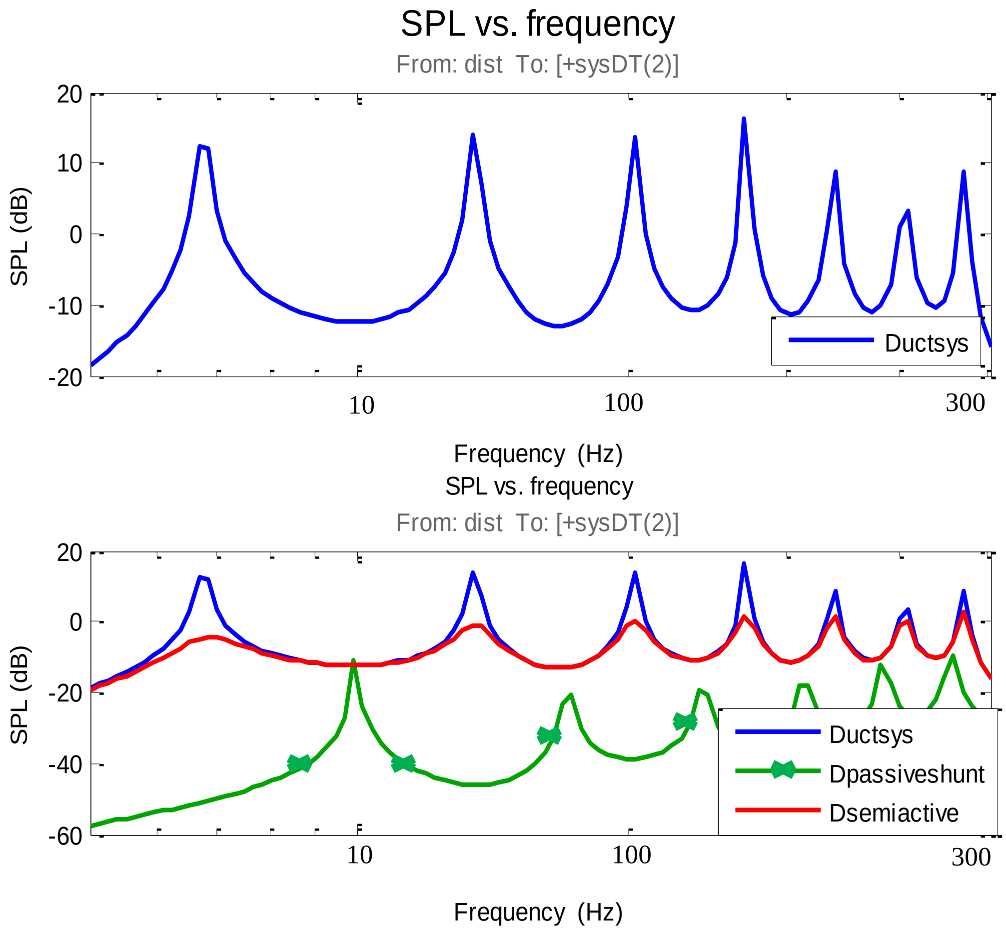

Figure 8 The passive and semi-active shunt loudspeakers with $\mathbf{C_s = 37\mu F, R_s = 10\Omega, \text{and } L_s = 5.685\ mH}$

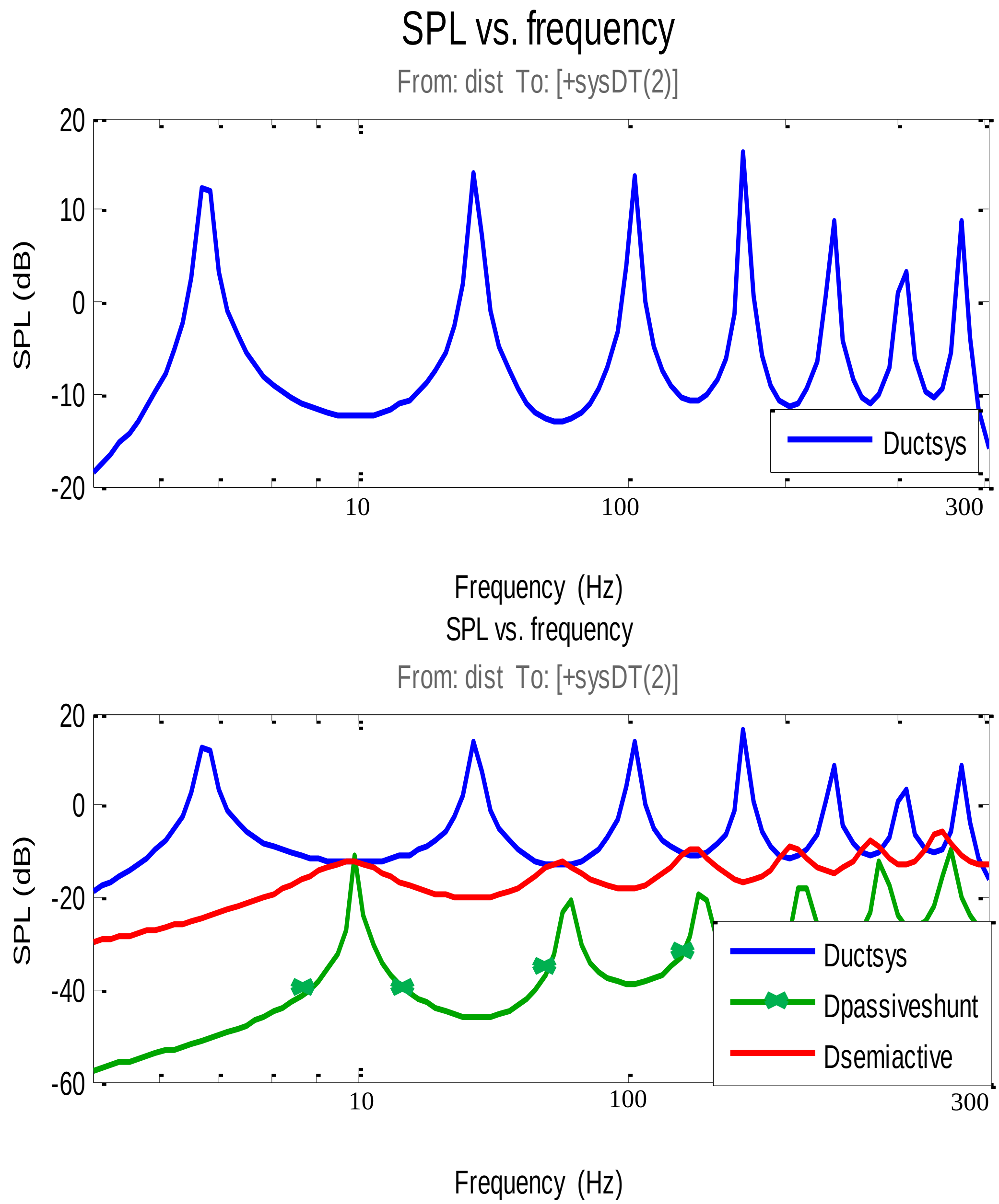

Figure 9 The passive and semi-active shunt loudspeakers with $\boldsymbol{C_s = 37\mu F, R_s = 10\Omega, and\ L_s = 56.85\ mH}$

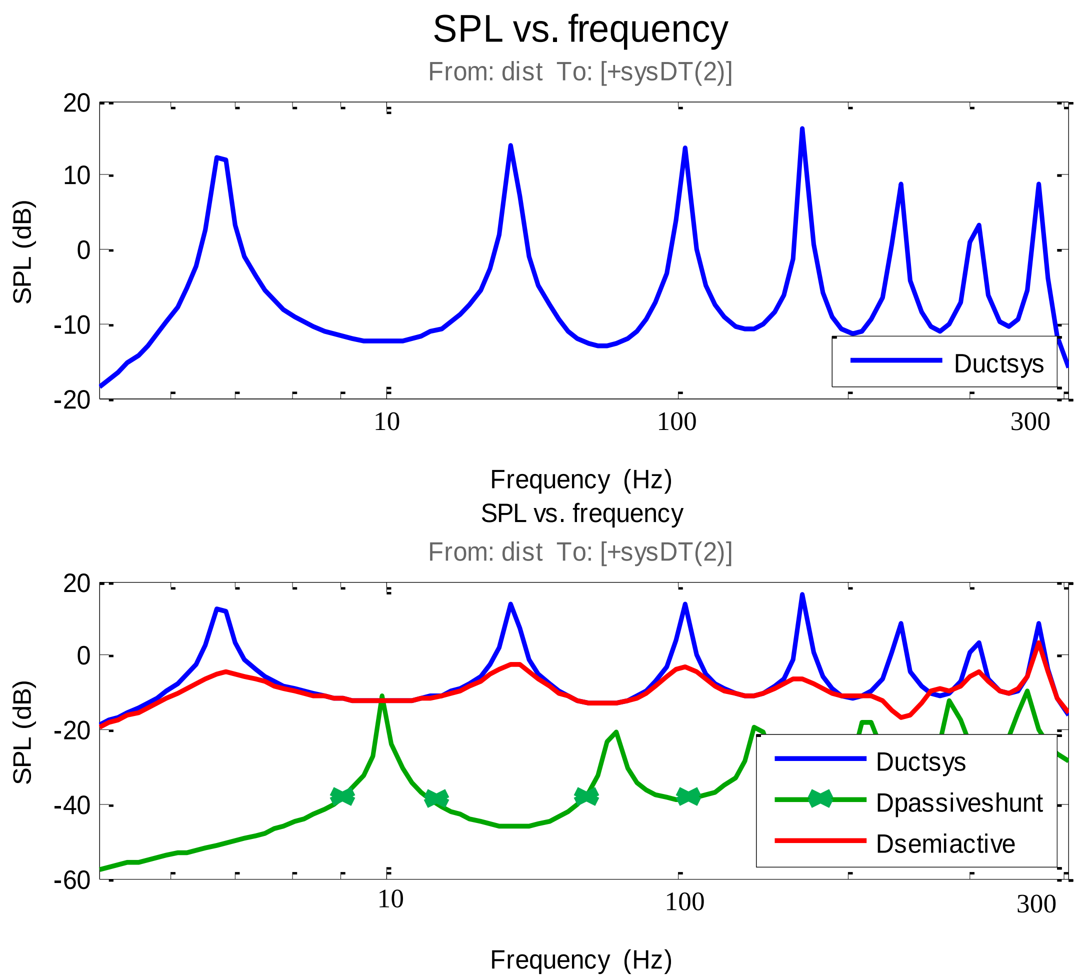

Figure 10 The passive and semi-active shunt loudspeakers with $\boldsymbol{C_s = 3700\mu F, R_s = 10\Omega, and\ L_s = 56.85\ mH}$

CHAPTER 3

System Modeling and Eigen-frequency Validation

3.1 Modeling of three dimensional (3D) System

The structural-acoustic system consists of a three dimensional rectangular cavity. The enclosure has five acoustically rigid walls. It has a simply supported flexible steel /aluminum plate on the top of cavity. A harmonic plane wave incident on the flexible plate or any external force creating disturbance on the plate can be considered as the prime source of external excitation. Piezoelectric actuators on the flexible plate function to control sound pressure level (SPL) in the cavity. The key purpose of the controller is to reduce noise in the cavity globally.

There are three distinct coordinate systems in this system modeling. Sound field in the cavity is specified with $\boldsymbol{x}(x_1, x_2, x_3)$; thin flexible plate vibration is demarcated with $\boldsymbol{y}(y_1, y_2)$; and the external incident wave is drawn with r. The three dimensional (3D) enclosure with attached piezoelectric patches and labeled coordinate system is shown in **Figure 11**. Dimension of the cavity and material properties of flexible plate (aluminum and steel) and properties of air in the cavity are listed in Table 3 which is taken from [58].

Table 3 Materials properties and dimensions of the cavity

Parameters	Value	Unit	Definition
L_1	2	m	Cavity length
L_2	0.6	m	Cavity width
L_3	0.9	m	Cavity height
h_p	7	mm	Plate thickness
$E_{p,steel}$	207	GN/m^2	Young's Modulus
ρ_p	7870	Kg/m^3	Density of steel Plate
ν_p	0.29	-	Poisson's ratio steel
$E_{p,Al}$	71	GN/m^2	Young's Modulus
$\rho_{p,Al}$	2770	Kg/m^3	Density of Al Plate
$\nu_{p,Al}$	0.33	-	Poisson's ration Al plate
ρ_0	1.21	Kg/m^3	Density of air
c_0	340	m/s	Phase/air speed
ξ_p	0.01	-	Structural damping ratio
ξ_a	0.01	-	Acoustic damping ratio

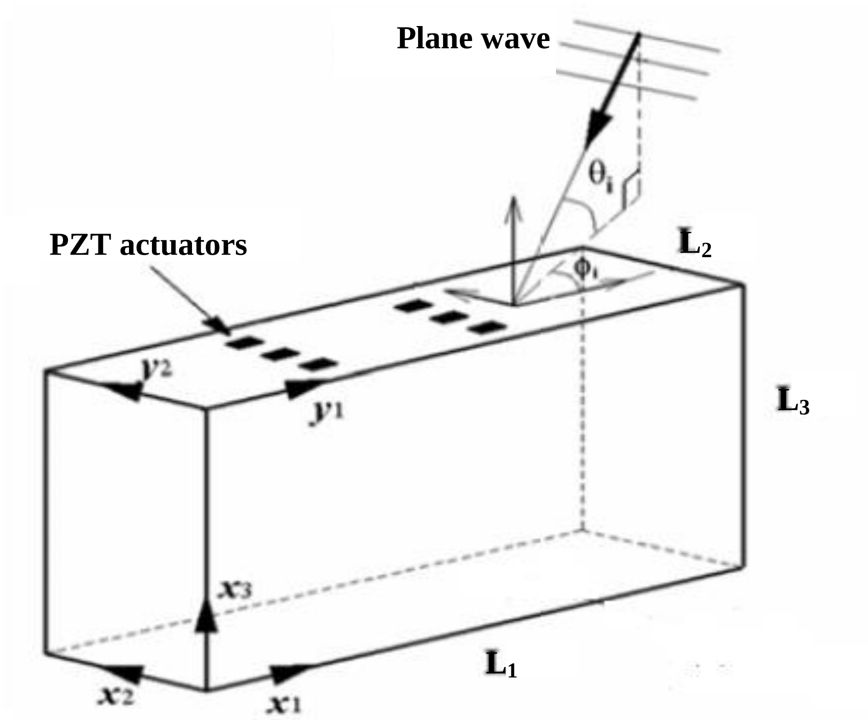

Figure 11 A 3D rectangular enclosure with attached piezoelectric actuators and external disturbance

3.2 System modeling and Uncertainties

Proper modeling of any system is of tremendous importance. Certain preconditions are, nevertheless, usually set to avoid difficulties in system modeling. But due to the soaring and leaping advent of computing technology those assumptions can be minimized if proper research methodologies are put on place on time. System uncertainties can mainly be divided into four categories such as

a) Parameter uncertainties

Uncertainties evolve from any unknown parameter or parameters are defined as parameter uncertainties. As for the 3D enclosure considered here, parameter uncertainties can arise from PZT actuator attached with glue to the flexible plate.

b) Unmodeled dynamics

To reduce the complexity of the analytical model, researchers simplify the model with certain assumptions where they ignore some dynamics which can be termed as Unmodeled or missing dynamics that do not change the system dynamics above all. Since the dimensions of actuator and sensor patches are much smaller compared to that of the thin plate, the actuator and sensor dynamics were usually overlooked in this work. Besides, other hardware dynamics was not considered, and cavity wall was assumed as rigid acoustically. As for theoretical derivation, the plate is assumed to be simply supported on its four sides. Besides, the initial displacements and velocities at all points on the plate are taken as zero.

c) External additive inputs

Any input apart from the considered inputs is defined as external additive inputs or external disturbances. In this case, the external additive inputs can be variation in temperature and in air flow.

d) Measurement errors

Error resulted in from sensors data is called measurement error. Measurement error can lead to fatal result if not properly calibrated with accuracy, repeatability, precision and reproducibility. In this case, measurement error can arise from PVDF sensors and microphones.

A system considering the above uncertainties can be written as following:

$$\dot{x} = \big(A(\theta) + \Delta A(\theta)\big)x + (B + \Delta B)u + D_1\xi$$

$$y = (C + \Delta C)x + (D + \Delta D)u + D_2\zeta$$

Where θ is a vector of uncertain parameters, $\Delta A\ and\ \Delta B$ are unmodeled dynamics, and $\xi\ and\ \zeta$ are seen as external disturbances. This system can be modeled with certain norm-bounded uncertainties and stability can be ensured using LMI via Schur complement. Readers are highly encouraged to see any robust control book for further understanding with [60-62].

3.3 Vibration of the thin flexible plate

Plates are primarily flat elements with thicknesses smaller compared with the remaining dimensions. Plates of technical significance are often termed as thin when the ratio of the thickness to the smaller span length is less than 1/20. Homogeneous thin elastic plate vibration equation can be written as Meirovich [63] using Hamilton's principle:

$$D_p\nabla^4 W(t,y) + C_p\frac{\partial W(t,y)}{\partial t} + h_p\rho_p\frac{\partial^2 W(t,y)}{\partial t^2} = F_p(t,y) \quad (3.1)$$

$$F_p(t,y) = f_{PZT}(t,y_{PZT}) + p_{in}(t,y) - p_{out}(t,y) \quad (3.2)$$

Where, $W(t,y)$ is the vibration amplitude in location $\boldsymbol{y}(y_1,y_2)$on the thin plate at time t; F_p is the pressure summation on the plate; C_p represents posteriori damping factor of the plate; D_p is the flexural rigidity of the plate $\left(D_p = \frac{E_p h_p^3}{12(1-\nu_p^2)}\right)$; f_{PZT} is the force density summation from PZT actuators; p_{out} and p_{in} are external and internal pressure loading on the plate respectively. Here thin flexible plate is assumed to have simply supported boundary conditions. Then ω_p, natural frequency and φ_p, mode shape function of vibrating plate are achieved using variable separation method turning the above non-homogeneous equation into homogeneous equation as [5, 48, 54]:

$$\omega_{p,uv} = \sqrt{\frac{D_p}{h_p \rho_p}} [\gamma_u^2 + \gamma_v^2] \qquad u, v = 1, \dots, \infty \tag{3.3}$$

$$\varphi_{p,uv} = 2 \sin(\gamma_u) \sin(\gamma_v) \qquad u, v = 1, \dots, \infty \tag{3.4}$$

Where $\gamma_u = \frac{u\pi}{L_1}, \gamma_v = \frac{v\pi}{L_2}$

Thin flexible plate vibration amplitude can be appraised with the summation of modal coordinates multiplied by mode shape functions according to finite approximation (expansion) theorem as [48, 58]

$$W(t, y) \approx \sum_{m=1}^{N_p} \eta_m(t) \varphi_m(y) \tag{3.5}$$

Where $\eta_m(t)$ is a time-dependent coefficient; $\varphi_m(y)$ is a mode shape function sorted by increase of frequency and N_p is the total mode number on the plate. Equation (3.5) is substituted into equation (3.1). Then surface integral on the plate surface is taken. After that the differential equation of plate vibration is written as [27, 48, 58, 59] using orthogonal properties of modal functions:

$$\ddot{\eta}_m(t) + 2\xi_{p,m}\omega_{p,m}\dot{\eta}_m(t) + \omega_{p,m}^2 \eta_m(t) = 1/m_p [g_{PZT,m}(t) + g_{PIN,m}(t) + g_{POUT,m}] \tag{3.6}$$

$$g_{PZT,m} = \iint_{S_p} \varphi_m f_{PZT}(t, y_{PZT}) ds, g_{Pin,m} = \iint_{S_p} \varphi_m p_{in} ds,$$

$$g_{Pout,m} = \iint_{S_p} \varphi_m p_{out} ds\,, \qquad m = 0,1, \ldots N_p \tag{3.7}$$

Where m_p and S_p are mass and area of the thin plate; $g_{PZT,m}$, is generalized force owing to PZT actuators. Besides, $g_{Pin,m}$and $g_{Pout,m}$ are generalized internal and external pressure on the plate respectively. The sum of the incident wave with pressure p_i and the reflected wave with pressure p_r results in as external loading p_{out} [47]. The dynamic interaction is much stronger from structure to acoustics than from acoustics to structure. As a result, p_r, radiation-damping term, can be overlooked which turns into $p_{out} = 2p_i$. The plane wave is assumed to be produced by a distant large speaker. p_i, incident pressure, can be written in coordinate $\boldsymbol{r}$ as

$$p_i(t, \boldsymbol{r}) = p_{i0} \mathrm{e}^{\mathrm{j}\omega_\mathrm{i}\mathrm{t}-\mathrm{j}\overrightarrow{K_i}.\mathbf{r}} \tag{3.8}$$

Where $\overrightarrow{K_i}$ is the vector of wave number; $\omega_i$is the natural frequency of plane wave and p_{i0} is power of speaker (assuming unit here). Equation (3.8) is substituted into equation (3.7) to obtain the generalized outer pressure as [64]:

$$g_{Pout,m} = 4S_p I_{u(m)} I_{v(m)} \tag{3.9}$$

Where

$$I_u = \frac{u\pi\left[1-(-1)^u \mathrm{e}^{-\mathrm{jK_iL_2\sin\theta_i\cos\varphi_i}}\right]}{(u\pi)^2 - (K_i L_1 sin\theta_i cos\varphi_i)^2} \tag{3.10}$$

$$I_v = \frac{v\pi\left[1-(-1)^v \mathrm{e}^{-\mathrm{jK_iL_2\sin\theta_i}sin\varphi_\mathrm{i}}\right]}{(v\pi)^2 - (K_i L_1 sin\theta_i sin\varphi_i)^2} \tag{3.11}$$

$$K_i = \frac{\omega_i}{c} \tag{3.12}$$

c is phase speed with frequency. Constant phase speed of any wave with its frequency is termed as non-dispersive wave. But varying phase speed of any wave with its frequency is called dispersive wave. Besides, an external force can be used to cause vibration in the plate. This external force can be expressed as $f(t, x_1, y_1) = f(t)g(x_1, y_1)$. Then $f_{uv}(t)$ can be expressed as the following

$$f_{uv}(t) = \left[\frac{1}{S_1}\int\int_{S_1} g(x_1, y_1)\varphi(x_1, y_1)dS_1\right] f(t) = \gamma_{uv} f(t)$$

Where $g(x_1, y_1)$ is a spatially bounded Heaviside or delta function, whereas $f(t)$ is any temporal function.

3.4 Piezoelectric actuators

The piezoelectric actuators induce internal moments, $M^k_{y_1,y_1}$ and $M^k_{y_2,y_2}$. The PZT patch extends in the y_1 and y_2 directions on the flexible plate due to their bending nature. These internal moments can be obtained as [65]:

$$\begin{aligned} M^k_{y_1,y_1} = M^k_{y_2,y_2} \\ &= C_0\varepsilon^k_{PZT}\left[H\left(y_1 - x^k_{PZT,1}\right) - H\left(y_1 - x^k_{PZT,2}\right)\right] \\ &\times \left[H\left(y_2 - y^k_{PZT,1}\right) - H\left(y_2 - y^k_{PZT,2}\right)\right] \end{aligned} \tag{3.13}$$

Where
$$\varepsilon^k_{PZT} = \frac{d_{31}V^k_{PZT}}{h_{PZT}} \tag{3.14}$$

And $x^k_{PZT,1}$ and $x^k_{PZT,2}$ are the initial and ending position of the k^{th} piezoelectric actuator in the y_1 direction, whereas $y^k_{PZT,1}$ and $y^k_{PZT,2}$ are the initial and ending position of the k^{th} piezoelectric actuator in the y_2 direction. Besides, V^k_{PZT} and ε^k_{PZT} are the applied voltage and resultant strain in the direction of polarization of the k^{th} PZT patch. $H(.)$ denotes a step Heaviside function and C_0 is the piezoelectric coefficient can be obtained as a function of piezoelectric material:

$$C_0 = -\frac{2}{3}\left(\frac{1+\nu_{PZT}}{1-\nu_p}\right) \times \left(\frac{E_p h_{p2}^2 P_{PZT}}{1+\nu_p-(1+\nu_{PZT})P_{PZT}}\right) \tag{3.15}$$

Where

$$P_{PZT} = -\frac{E_{PZT}}{E_p}\frac{(1-\nu_p^2)}{1-\nu_{PZT}^2}K_{PZT}; \quad K_{PZT} = \frac{\frac{3}{2}h_{PZT}h_{p2}(h_{PZT}+2h_{p2})}{(h_{p2}^2+h_{PZT}^2)+3h_{p2}h_{PZT}^2} \tag{3.16}$$

and h_{p2} represents half of the plate thickness. Dimensions and material properties of PZT actuators are enlisted in Table 4. In this work, the plate dimensions are much bigger than to that of PZT patch. Hence, it is assumed that the plate dynamics is not affected with bonded PZT patches. f_{PZT}, piezoelectric induced force density can be obtained as [58]:

$$f_{PZT} = \sum_{k=1}^{N_{PZT}} \left[\frac{\partial^2 M_{y_1,y_1}^k}{\partial y_1^2} + \frac{\partial^2 M_{y_2,y_2}^k}{\partial y_2^2}\right] \tag{3.17}$$

Then moment's equation (3.13) is substituted into equation (3.17) to replace the resultant into equation (3.7). Thus, a generalized modal force can be obtained as a function of applied voltage [58]:

$$g_{PZT,m}(t) = \sum_{k=1}^{N_{PZT}} B_{PZT,m,k} V_{PZT}^k(t) \qquad m = 1, \dots, N_p \tag{3.18}$$

Where

$$B_{PZT,m,k} = \frac{C_0 d_{31}}{h_{PZT}} \left[\cos\left(\gamma_u x_{PZT,1}^k\right) - \cos\left(\gamma_u x_{PZT,2}^k\right)\right] \times \left[\cos\left(\gamma_v y_{PZT,1}^k\right) - \cos\left(\gamma_v y_{PZT,2}^k\right)\right]\left(-\frac{2(\gamma_u^2 + \gamma_v^2)}{\gamma_u \gamma_v}\right) \tag{3.19}$$

$where\ k = 1, \dots, N_{PZT}$

Table 4 Material properties and dimensions of PZTs

Parameters	Value	Unit	Definition
L_{xPZT}	80	mm	Patch length
L_{yPZT}	60	mm	Patch width
h_{PZT}	1	mm	Patch thickness
E_{PZT}	63	GN/m^2	Young’s Modulus
ρ_{PZT}	7650	Kg/m^3	Density of patch
ν_{PZT}	0.3	-	Poisson’s ratio
d_{31}	166	pico m/V	Strain Constant

3.5 3D cavity acoustic pressure

The thin flexible plate on top of the cavity is set to vibration, and this plate vibration functions as external disturbance of the 3D cavity. Thus, entire boundary condition of the cavity is assumed as rigid boundary. Moreover, vibration of the plate is assumed as the fluctuating volume flow per unit volume of the cavity, that is equivalent to : $\rho_0 \delta(x_3 - L_3) \partial W(t, x_1, x_2)/\partial t$ [66]. The correlation between pressure and density can be obtained according to mass and moment conservation equations as $P(t,x) = c_0^2 \rho(t,x)$ from [41, 48, 58]; where c_0 is the speed of sound.

$$\nabla^2 P(t,x) - C_a \frac{\partial P(t,x)}{\partial t} - \frac{1}{c_0^2} \frac{\partial^2 P(t,x)}{\partial t^2} = F_a \tag{3.20}$$

Where $$F_a = -\rho_0 \frac{\partial^2 W(t, x_1, x_2)}{\partial t^2} \delta(x_3 - L_3) \tag{3.21}$$

and $P(t, x)$ represents the pressure in location $x(x_1, x_2, x_3)$ in the cavity; ρ_0 is the air density at equilibrium state in the cavity; F_a is the excitation force in cavity originated from vibration of the plate; and C_a is the acoustic damping operator. The cavity boundary conditions are:

$$\nabla P(t, x).n = 0 \qquad on\ \Omega_B \tag{3.22}$$

Where, n is the normal direction pointed outward at all points on surface of cavity, Ω_B. Boundary condition from equation (3.22) is inserted into wave equation (3.20). Then, ω_a, cavity natural frequencies and ψ_a, acoustic mode shape functions are obtained using separation of variables method as [41, 48, 58]:

$$\omega_{a,k_1k_2k_3} = c_0\pi\sqrt{\left[\left(\frac{k_1}{L_1}\right)^2 + \left(\frac{k_2}{L_2}\right)^2 + \left(\frac{k_3}{L_3}\right)^2\right]}; \tag{3.23}$$

$$k_1, k_2, k_3 = 0,1, \dots, \infty$$

$$\psi_{a,k_1k_2k_3} = A_{k_1k_2k_3}\cos(\frac{k_1\pi}{L_1}x_1)\cos(\frac{k_2\pi}{L_2}x_2)\cos(\frac{k_3\pi}{L_3}x_3) \tag{3.24}$$

Acoustic pressure in the cavity can be appraised with the summation of modal coordinates multiplied by acoustic mode shape functions according to finite approximation (expansion) theorem as [48, 58]:

$$P(t, x) \approx \sum_{n=0}^{N_a} \psi_n(\boldsymbol{x})\, q_n(t) = \boldsymbol{\Psi}^T \boldsymbol{q} \tag{3.25}$$

Where $q_n(t)$ are the time-dependent coefficients; $\psi_n(x)$ is an acoustic mode shape function organized by increasing frequency and N_a is the total mode number in the cavity. Since the acoustic mode number is counted from ‘0’ (zero), the length of vectors $\boldsymbol{\Psi}$ and $\boldsymbol{q}$ consist of $\psi_n(x)$ and $q_n(t)$ elements, respectively is $N_a + 1$. Then, pressure amplitude from equation (3.25) is substituted into the wave equation (3.20). After that, a volume integral is taken in the 3D cavity provided acoustic mode shape functions are orthogonal. The acoustic pressure differential equation is derived as:

$$\ddot{q}_n(t) + 2\xi_{a,n}\omega_{a,n}\dot{q}_a(t) + \omega_{a,n}^2 q_n(t) = N_{a,n} \qquad n = 0,1,\ldots,N_a \tag{3.26}$$

Where

$$N_{a,n} = \iiint\limits_{V_a} \Psi_n F_a dV \tag{3.27}$$

where V_a denotes 3D cavity volume and $N_{a,n}$ is the generalized acoustic pressure from acoustic piston sources and flexible plate vibration.

3.6 Structural-acoustic equations of the 3D Coupled system

The vibro-acoustic coupling between acoustic cavity and flexible plate is presented in this section. It is essential to have a coupling relationship for the system in order to control and reduce sound field in the cavity. For this, the cavity pressure from equation (3.25) is substituted in equations (3.6) and (3.7) which turns into a coupling relation between acoustic pressure in the cavity and vibration of the plate.

Then, plate vibration amplitude from equation (3.5) is inserted into equation (3.21) and F_a is injected into equations (3.26) and (3.27). Consequently, two simplified coupled equations are obtained as [48, 58, 59]:

$$\ddot{\eta}_m(t) + 2\xi_{p,m}\omega_{p,m}\dot{\eta}_m(t) + \omega_{p,m}^2\eta_m(t) = \frac{1}{m_p}\left[g_{PZT,m} + \sum_{n=0}^{N_a} c_{n,m}\, q_n(t)\right] \qquad m = 1, \dots, N_p \tag{3.28}$$

$$\ddot{q}_n(t) + 2\xi_{a,n}\omega_{a,n}\dot{q}_a(t) + \omega_{a,n}^2 q_n(t) = \frac{\rho_0 c_0^2}{V_a}\sum_{m=1}^{N_p} c_{nm}\ddot{\eta}_m(t); \quad n = 0,1, \dots, N_a \tag{3.29}$$

Where
$$c_{n,m}(t) = \iint_{S_p} \varphi_m(y_1, y_2)\Psi_n(y_1, y_2, L_3)dS \tag{3.30}$$

and $c_{n,m}$ is the geometric coupling coefficient between the uncoupled acoustic mode shapes and structural mode shape functions and $\xi_{p,m}$ and $\xi_{a,n}$are the plate and the cavity modal damping, respectively. Now, state space domain is crucial in order to calculate coupled modal functions and coupled resonant frequencies. Hence, coupled system is transformed into state-space domain. Hence, the state variables can be taken as [48, 58, 59]:

$$\begin{cases} \boldsymbol{x}_{state}^a(2n) = x_n^a \\ \boldsymbol{x}_{state}^a(2n+1) = y_n^a \end{cases} \begin{cases} \boldsymbol{x}_{state}^p(2m-1) = x_m^p \\ \boldsymbol{x}_{state}^p(2m) = y_m^p \end{cases}; \quad \boldsymbol{x}_{state} = \begin{Bmatrix} \boldsymbol{x}_{state}^p \\ \boldsymbol{x}_{state}^a \end{Bmatrix} \tag{3.31}$$

Where

$$\begin{Bmatrix} x_m^p \\ y_m^p \end{Bmatrix} = \begin{Bmatrix} \eta_m(t) \\ \dot{\eta}_m(t) \end{Bmatrix}\ and\ \begin{Bmatrix} x_n^a \\ y_n^a \end{Bmatrix} = \begin{Bmatrix} q_n(t) \\ \dot{q}_n(t) \end{Bmatrix}; \quad m = 1, \dots, N_p \,\&\, n = 0,1, \dots, N_a \tag{3.32}$$

Derivative of state variables is written from equations (3.28) and (3.29), and the simplified state equation is obtained as:

$$\begin{bmatrix} \boldsymbol{E}_{11} & \boldsymbol{0} \\ \boldsymbol{E}_{21} & \boldsymbol{E}_{22} \end{bmatrix} \begin{Bmatrix} \dot{\boldsymbol{x}}_{state}^{p} \\ \dot{\boldsymbol{x}}_{state}^{a} \end{Bmatrix} = \begin{bmatrix} \boldsymbol{A}_{11} & \boldsymbol{A}_{12} \\ \boldsymbol{0} & \boldsymbol{A}_{22} \end{bmatrix} \begin{Bmatrix} \boldsymbol{x}_{state}^{p} \\ \boldsymbol{x}_{state}^{a} \end{Bmatrix} + \begin{bmatrix} \boldsymbol{D}_{PZT} \\ \boldsymbol{0} \end{bmatrix} \boldsymbol{v}_{PZT} + \frac{1}{h\rho_0} \begin{bmatrix} \boldsymbol{B}_{11} \\ \boldsymbol{0} \end{bmatrix} f(t) + \boldsymbol{d}_{PW} \tag{3.33}$$

$$\begin{bmatrix} w(x,y,z,t) \\ p(x,y,z,t) \end{bmatrix} = \begin{bmatrix} \boldsymbol{C}^{(\boldsymbol{w})} & \boldsymbol{0} \\ \boldsymbol{0} & \boldsymbol{C}^{(\boldsymbol{p})} \end{bmatrix} \begin{bmatrix} \boldsymbol{x}_{state}^{p} \\ \boldsymbol{x}_{state}^{a} \end{bmatrix}$$

where $\boldsymbol{C}^{(w)} = [\alpha_i(x)\beta_i(y)] = \sin(\frac{i\pi x}{L_x})\sin(\frac{j\pi y}{L_y})$ from [41, 67], $\boldsymbol{C}^{(p)} = \left[\psi_{a,k_1k_2k_3}\right]$ from equation (3.24). **Appendix A** contains elaboration of other coefficients. The inverse of $\boldsymbol{E_{state}}$ matrix is used to transform above equation into standard state space equation. Lastly, the state-space equation in standard from is derived as:

$$\dot{\boldsymbol{x}}_{state} = \boldsymbol{A}_{state}\boldsymbol{x}_{state} + \boldsymbol{D}'_{PZT}\boldsymbol{v}_{PZT} + \boldsymbol{B}' f(t) + \boldsymbol{d}'_{PW}$$
$$\boldsymbol{y} = \boldsymbol{C}\boldsymbol{x}_{state} \tag{3.34}$$

Where

$$\boldsymbol{E}_{state} = \begin{bmatrix} \boldsymbol{E}_{11} & \boldsymbol{0} \\ \boldsymbol{E}_{21} & \boldsymbol{E}_{22} \end{bmatrix} \qquad \boldsymbol{A}_{state} = \boldsymbol{E}_{state}^{-1} \begin{bmatrix} \boldsymbol{A}_{11} & \boldsymbol{A}_{12} \\ \boldsymbol{0} & \boldsymbol{A}_{22} \end{bmatrix}$$
$$\boldsymbol{D}'_{PZT} = \boldsymbol{E}_{state}^{-1} \begin{bmatrix} \boldsymbol{D}_{PZT} \\ \boldsymbol{0} \end{bmatrix}, \qquad \boldsymbol{B}' = \boldsymbol{E}_{state}^{-1} \times \frac{1}{h\rho_0} \begin{bmatrix} \boldsymbol{B}_{11} \\ \boldsymbol{0} \end{bmatrix} \tag{3.35}$$
$$\boldsymbol{d}'_{PW} = \boldsymbol{E}_{state}^{-1}\boldsymbol{d}_{PW}$$

3.7 Resonant frequencies

Uncoupled and coupled resonant frequencies of the 3D system are calculated with earlier sections' derived equations in this section. Equation (3.3) is used to calculate the uncoupled resonant frequencies of the simply supported plate. Equation (3.23) determines the uncoupled resonant frequencies of the 3D cavity with rigid walls. Then, the resonant frequencies of coupled system are derived from the eigenvalues of matrix $\boldsymbol{A}_{state}$ provided in equation (3.35). The calculated uncoupled and coupled resonant frequencies are enlisted in Table 5 where the results have been compared with Hanif and Ohadi [58] which turn in with complete agreement.

Furthermore, geometric coupling coefficients between the uncoupled acoustic and structural mode shape functions are enlisted in Table 6. The results of Table 6 were compared with the corresponding results of Table 2 in reference [64] for validation of the system modeling. It shows the complete agreement for geometric coupling coefficients. Besides, another analytical model has been encoded to validate the Eigen-frequencies from [48, 59] where the authors have compared the eigen-frequencies of the analytical model with experimental results that turned into a very close agreement. The model is a rectangular wooden box with one of its surface being the aluminum plate.

Table 5 Coupled and uncoupled resonant frequencies reproduced from [58]

Mode No.	Hanif(2009)	**Present work**			
		Coupled	Plate	Cavity	% difference
0	0	0	*	0	0.00%
1	51.44	51.4995	51.5021	*	0.12%
2	63.66	64.2563	64.2595	*	0.93%
3	85.34	84.9957	*	85	0.41%
4	85.42	85.5176	85.5219	*	0.11%
5	115.26	115.2834	115.2891	*	0.02%
6	153.43	153.5537	153.5614	*	0.08%
7	170.18	169.9915	*	170	0.11%
8	189.04	188.8794	*	188.8889	0.09%
9	193.25	193.2414	193.2511	*	0.00%
10	200.13	200.3285	200.3385	*	0.10%

Table 6 The natural frequencies and geometric mode shape coupling coefficients of each uncoupled system reproduced from [64]

Order		Plate	1	2	3	4	5	7	10
	Type		(1,1)	(2,1)	(3,1)	(4,1)	(5,1)	(6,1)	(7,1)
Cavity		Freq (Hz)	52	64	86	115	154	200	256
1	(0,0,0)	0	0.71	0	0.24	0	0.14	0	0.10
2	(1,0,0)	85	0	0.67	0	0.27	0	0.17	0
3	(2,0,0)	170	-0.33	0	0.60	0	0.24	0	0.16
4	(0,0,1)	189	-1.00	0	-0.33	0	-0.20	0	-0.14
5	(1,0,1)	207	0	-0.94	0	-0.38	0	-0.24	0
6	(2,0,1)	254	0.47	0	-0.85	0	-0.34	0	-0.22
7	(3,0,0)	255	0	-0.40	0	0.57	0	0.22	0

This ductile surface is set to vibrations to generate acoustic disturbances inside the 3D cavity using PZT actuator at the center of the aluminum plate. The parameters of the 3D laboratory acoustic enclosure are shown in **Table 7**. Based on the enlisted parameters in **Table 7**, Fang et al. [48, 59] have obtained a transfer function model given in (3.36) with assumed modes approximation method. A MATLAB script file has been coded to generate eigen-frequencies based on the state-space model and transfer function. The results shown in Table 8 exactly match with the analytical results of [48, 59]. Table 8 shows the comparison. Missing frequencies from the analytical model is designated with the symbol (*) in the second column of the Table 8. Whereas, missing frequencies from the identified model is represented with the symbol (#) in the third column.

The missing frequencies are attributed to the missing dynamics in the analytical modeling. In this analytical modeling, sensor, actuator, and hardware dynamics were neglected due to their apparent insignificance compared to plate dynamics.

In particular, the modes 1, 3, 8, 12, 15, and 20 are missing in the analytical model. The modes 4, 10, 11, 19, 22, 23, and 25 are missing in the identified model. The modes 10 and 11 are very close to 9 and with appropriate damping may collapse onto one. This may be the case for the missing modes 10 and 11 in the identified model. For the same reason, modes 19 and 25 are missing in the identified model. The modes 4, 22, and 23 seem to be highly damped in the experimental data which is why the identification algorithm cannot detect [59]. The frequencies listed in the Table 8 do not account for boundary impedance, i.e., it assumes the perfectly hard boundary with zero transmissibility [48]. Hence the model is verified to go for an optimal controller design.

Table 7 Parameters for 3D apparatus from [48]

Parameter	Value	Parameter	Value
l_x	0.30480 m	l_y	0.38100 m
l_z	0.78740 m	a	0.00630 m
b	0.29850 m	c	0.00630 m
d	0.37470 m	h	0.0008130 m
E	$71.0 \times 10^9\ N/m^2$	μ	0.330
ρ	$2810\ kg/m^3$	c_0	343.0 m/s
ρ_0	$1.1300\ kg/m^3$	x_0	0.12700 m
y_0	0.15240 m	z_0	0.31120 m
x_1	0.15240	y_1	0.19050 m

$$Q_{k_1k_2k_3}(s) = Js^2 \sum_{k_1=0}^{l_1} \sum_{k_2=0}^{l_2} \sum_{k_3=0}^{l_3} \frac{\psi_{k_1k_2k_3}(x_0, y_0, z_0)}{s^2 + 2\zeta_{k_1k_2k_3}\omega_{k_1k_2k_3} + \omega_{k_1k_2k_3}^2} \times \left[\sum_{n=1}^{p_1} \sum_{m=1}^{p_2} \frac{\alpha_{k_1k_2k_3nm}\phi_{nm}(x_{11}, y_{11})}{s^2 + 2\zeta_{nm}\omega_{nm}s + \omega_{nm}^2} \right] \tag{3.36}$$

Table 8 Comparison of analytical and experimental frequencies from [59]

Mode No.	Analytical Fang et. al (2014)	Experimental Fang et. al (2014)	Present work		
			From TF	Coupled System	From A_{state}
			Natural frequencies (Hz)	Damping factors	Natural frequencies (Hz)
1	*		0	-1	0
2	37.5	39.2	37.456	0.001	37.5
3	*	64.0	*	*	*
4	80.8	#	80.848	0.0062	80.8
5	106.4	98.4	106.431	0.0114	106.4
6	149.8	125.5	149.824	0.0166	149.8
7	153.2	157.7	153.169	0.0218	153
8	*	182.4	*	*	*
9	217.8	222.4	217.805	0.0018	217.8
10	221.4	#	221.389	0.0271	221.4
11	222.1	#	222.145	0.0323	221.9
12	*	239.0	*	*	*
13	254.4	251.3	254.418	0.0375	253.9
14	264.8	262.1	264.783	0.0427	264.6
15	*	280.5	*	*	*
16	323.4	327.1	323.394	0.0479	322.6
17	337.1	351.0	337.103	0.0531	336.6
18	382.3	381.0	382.331	0.0583	382.3
19	384.6	#	384.597	0.0635	383.2
20	*	416.7	*	*	*
21	425.7	423.5	425.728	0.0687	425.4
22	435.6	#	435.613	0.0026	435.2
23	438.4	#	438.346	0.074	437.2
24	450.1	454.5	450.131	0.0034	450.1
25	453.6	#	453.573	0.0792	451.7
26	498.0	479.0	498.046	0.0844	497.2
27			500.062	0.0042	499.9

CHAPTER 4

Optimal Controller Design

4.1 Stability Criterion

When designing a feedback control system, a critical issue is to achieve stability. If the feedback gain is too large, then the controller may "overreact" and the closed loop system becomes unstable. A generalized plant using a feedback controller is shown in Figure 12. As illustrated, the signal from the error sensor is $y(t)$. The control signal $u(t)$ is generated through some form of static or dynamic controller H. The basic idea is to produce a secondary disturbance such that it cancels the effect of the primary disturbance at the location of the error sensor.

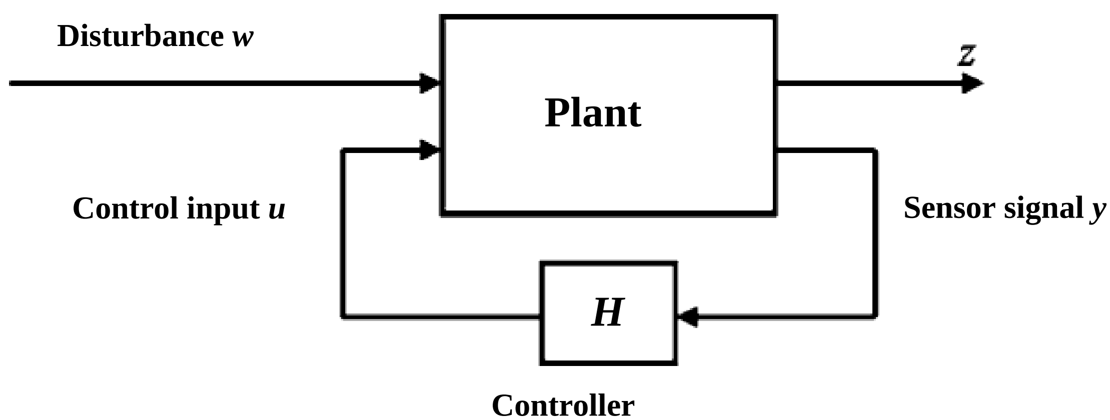

Figure 12 Schematic diagram of the generalized plant with a feedback compensator

The controller is often defined by minimizing the sum of the quadratic square of the signals from error sensors such as accelerometers/PVDF for structural dynamics or microphones for acoustic dynamics. To show the principle of feedback control, a single-channel feedback control system is shown in Figure 13. Standard linear systems theory can be used to derive the response of the system. The closed-loop frequency response can be written as

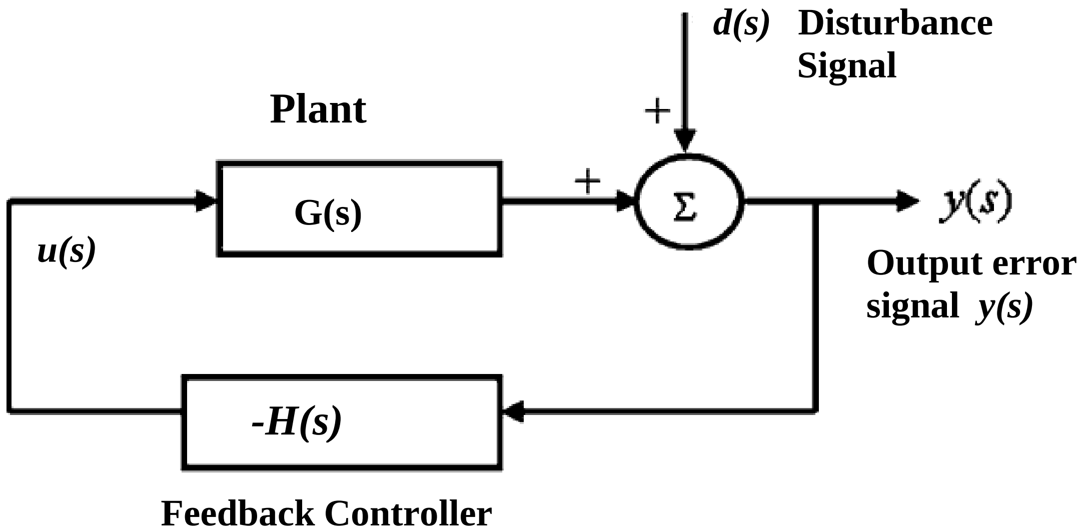

Figure 13 A single-channel feedback control case

$$\frac{y(s)}{d(s)} = \frac{1}{1 + G(s)H(s)} \tag{4.1}$$

where $G(s)H(s)$ is the open-loop frequency response.

Assume that in the working frequency range $[\omega_a, \omega_b]$, the controller is designed to satisfy the following conditions:

1. $|1 + G(s)H(s)| \gg 0 \quad (Large\ open\ loop\ gain)$;

2. $G(s)H(s)\ has\ little\ phase\ shift$

So in equation (4.1) $y(s)/d(s) \ll 1$, and the response is significantly reduced due to the control source.

However, outside the working frequency range, the above conditions may not be satisfied. If the open-loop gain is unity at some frequency where there is also 180^0 phase shift

$$G(s)H(s) = -1(180^0\, phase\ shift\ with\ unit\ gain)$$

Clearly $y(s) \rightarrow \infty$and the system becomes unstable. In designing feedback control systems, there is the trade-off between high open-loop gain in working frequency range and low open-loop gain outside working frequency range [68].

The main drawback using feedback control is the robustness and stability problem associated with feedback designs. Two methods are commonly used to determine closed-loop stability, i.e., root locus criterion and Nyquist criterion [5, 68, 69]. Root locus criterion will be discussed in the following section. For details, MATLAB documentation is decently informative.

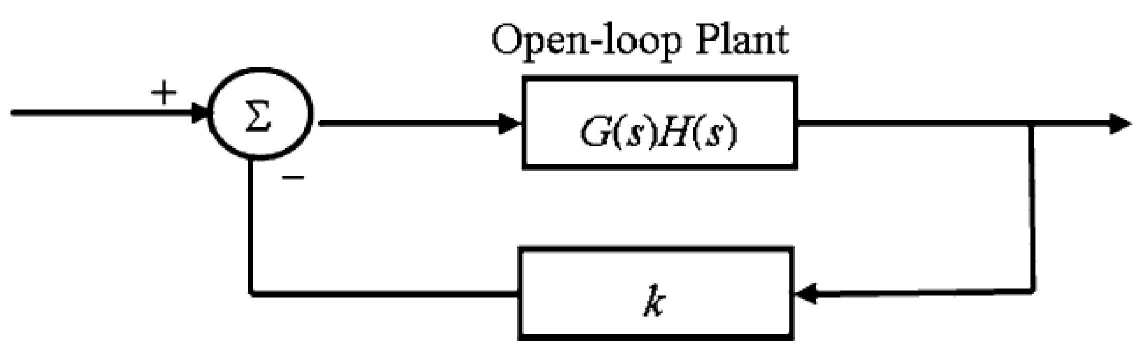

Figure 14 The principle for root locus method

In the discussion of active control systems below, we assume that the open-loop plant and controller are stable for simplification of the analysis. In the feedback control design, the first consideration will be related to closed-loop stability. One way to test for stability is to determine the pole/zeros of the closed-loop system by solving the characteristic equation:

$$1 + G(s)H(s) = 0 \tag{4.2}$$

If and only if all the closed loop poles lie in the left half plane, the system is stable. But the system is considered unstable if any pole lies on the imaginary axis. Basically, the poles are eigenvalues of the state space $\boldsymbol{A_{state}}$ matrix. Numerically poles are calculated from the plant matrices and the resonant frequencies are calculated from the imaginary parts of the poles.

However, in many cases, it is difficult to obtain an explicit pole/zero model for the controlled dynamic response due to delays, considerable variability, or very high-order modes. The root locus method is a graphical means of identifying the closed-loop pole/zeros of a SISO system for all values of the compensator gains according to the open-loop characteristic equation. The root locus method gives the closed-loop pole trajectories as a function of the feedback gain k (assumingnegative feedback, as shown in Figure 14). The advantage of this method is that all of the closed-loop information can be obtained by dealing with the open-loop transfer function. Assume that the open-loop plant G(s)H(s) can be written in the transfer function form:

$$G(s)H(s) = \frac{n(s)}{d(s)} \tag{4.3}$$

The closed-loop poles in Figure 14 are the roots of

$$d(s) + k \cdot n(s) = 0 \tag{4.4}$$

where k is a variable gain that has been factored out of the open-loop transfer function.

From equation (4.4), it can be found that for $k = 0$, the roots of equation (4.4) correspond to $d(s) = 0$ or the open-loop poles, and as k tends to infinity, the roots are$n(s) = 0$ or the zeros of the open-loop system.

Assume that the open-loop plant has n poles and m zeros. It should be noted that the closed-loop system must always have n poles, no matter what we pick k to be. The root locus must have n branches, each branch of which starts at a pole and goes to a zero of the open-loop plant. If the open-loop plant has more poles than zeros (m<n), it means that the open-loop plant has zeros at infinity. The number of root locus branches that go to infinity (asymptotes) is equal to the number of zeros at infinity $(n - m)$. The root locus is essentially the locations of all possible closed-loop poles. We can select a gain from the root locus such that our closed-loop system will perform the way we want. The closed-loop system becomes unstable if any of the selected pole goes on the right half plane,. The poles that are closest to the imaginary axis have the greatest influence on the closed-loop response.

In MATLAB, the function $rlocus$ adaptively selects a set of positive gains k toproduce a smooth plot. Figure 16 and Figure 16 shows the root locus plot from the minimal realization of the coupled system and the transfer function (TF) of the coupled system respectively. Figure 15 shows a pair of pole-zero on the right hand side of the imaginary axis which portrays the system as unstable and Figure 16 depicts that few pairs of pole-zero are on the imaginary axis which shows the system is inherently marginally stable which becomes unstable with slightest disturbance.

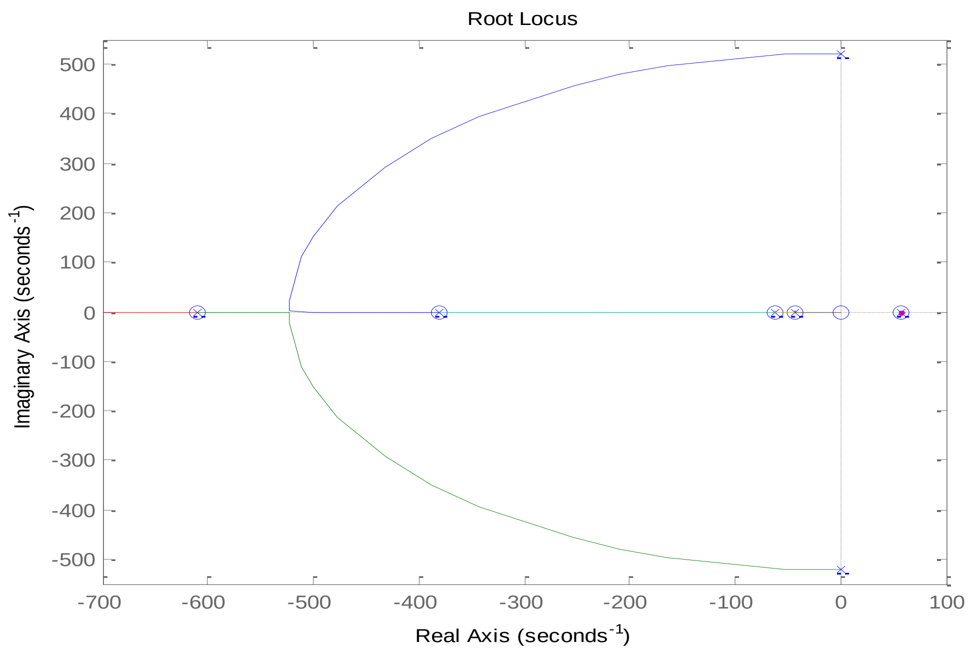

Figure 15 Root Locus plot from the minimal realization of the coupled system

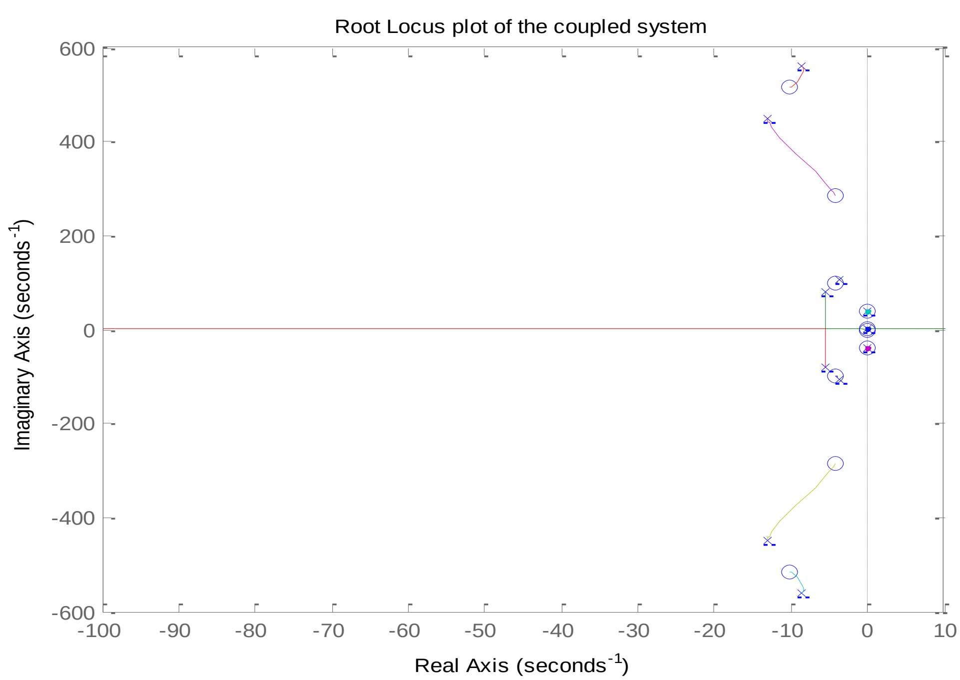

Figure 16 Root Locus plot from the TF of the coupled system

4.2 Stabilizability and Detectability

Stability and controllability are related stabilizability. Poles or eigenvalues of any system can be moved to the left half of the s-plane by a state feedback if the system is controllable. Hence, state feedback is used to stabilize any controllable system. State feedback causes the eigenvalues to move to the open left half of the s-plane. Conversely, a system cannot be stabilized if the system is not controllable.

Lin [70] and others mentioned that an eigenvalue λ_i is not controllable if it cannot be moved by state feedback. Formally, $\lambda_i \in \lambda(A)$ is unstable if $Re(\lambda_i) \geq 0$. $\lambda_i \in \lambda(A)$ is not controllable if $(\forall K)\lambda_i \in \lambda(A + BK)$.

Any linear time invariant system (LTI) can be stabilized if all poles from right half of the s-plane can be placed to the left half of the s-plane. That's to say, all unstable poles must be controllable. Stabilizability postulates two sufficient conditions as

i) If a system is stable, then it is stabilizable
ii) If a system is controllable, then it is stabilizable

It is more complex to check stabilizability with complete set of necessary and sufficient conditions. Hence, eigenvalues are derived from the analytical plant matrix to identify the system if the system is controllable. Controllability is easier to be determined than that of stabilizability. Thus, it is better practice to determine controllability of the system. If the system is controllable, it is stabilizable. Otherwise, it is necessary to check stabilizability.

Moreover, a linear time-invariant system is detectable if all unstable eigenvalues are observable. An eigenvalue $\lambda_i \in \lambda(A) = \lambda(A^T)$ of a LTI system (A, C) is observable if and only if its corresponding eigenvector v_i of A^T satisfies the condition $Cv_i \neq 0$. Detectability of a system can be checked if all unstable poles of the system are observable. In our case, the system is detectable, so it is observable.

4.3 Linear Quadratic Regulator (LQR) Problem

The state-feedback approach can provide a complete model of the global response of the system under control. They are particularly applicable to the control of the first few modes of a structure [71]. The state-feedback approach provides the best performance that can be achieved under an ideal feedback control system (full information and no uncertainty) [69, 72, 73].

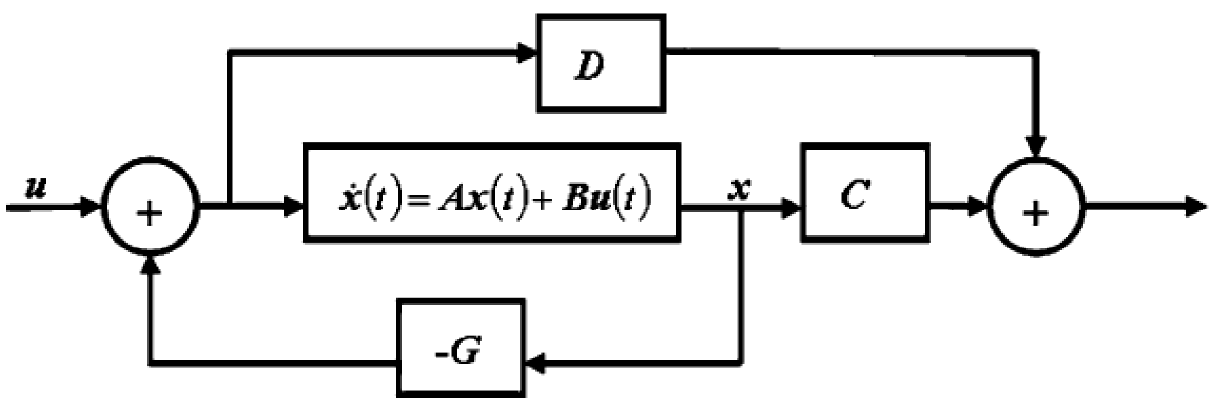

Figure 17 The principle of state feedback

Consider the state-space equation

$$\dot{\boldsymbol{x}}(t) = \boldsymbol{A}\boldsymbol{x}(t) + \boldsymbol{B}\boldsymbol{u}(t) \tag{4.5}$$

Assume that the input vector $u(t)$ can be made proportional to the state vector $x(t)$:

$$\boldsymbol{u}(t) = -\boldsymbol{G}\boldsymbol{x}(t) \tag{4.6}$$

Where G is the state-feedback gain matrix. Substituting equation (4.6) into (4.5) equation,

$$\dot{\boldsymbol{x}}(t) = (\boldsymbol{A} - \boldsymbol{B}\boldsymbol{G})\boldsymbol{x}(t) \tag{4.7}$$

where $(\boldsymbol{A} - \boldsymbol{B}\boldsymbol{G})$ is often referred to as the closed-loop system matrix. Its eigenvalues are the closed-loop poles. The objective is to determine the appropriate state-feedback matrix $\boldsymbol{G}$ such that the eigenvalues of the closed-loop system matrix can be specified as desired. The principle of the state feedback is shown in **Figure 17**. The state-feedback control is often used to predict the best performance that can be achieved. One effective way of designing a full state-feedback control system is to use the optimal linear quadratic regulator (LQR) [69]. LQR provides a means of evaluating the optimal control that can be achieved. LQR problem involves finding the appropriate state-feedback controller that minimizes the following cost function:

$$J = \int_0^\infty (\boldsymbol{x}^T(t)\boldsymbol{Q}\boldsymbol{x}(t) + \boldsymbol{u}^T(t)\boldsymbol{R}\boldsymbol{u}(t))dt \tag{4.8}$$

subject to the state dynamics: $\dot{\boldsymbol{x}}(t) = \boldsymbol{A}\boldsymbol{x}(t) + \boldsymbol{B}\boldsymbol{u}(t)$, where $\boldsymbol{Q}$ is a symmetric positive semi-definite matrix. $\boldsymbol{R}$ is a symmetric positive definite matrix, termed as scalar weighting matrix. In the cost function of equation (4.8), the first term in the integral $\boldsymbol{x}^{\boldsymbol{T}}(t)\boldsymbol{Q}\boldsymbol{x}(t)$is used to minimize the error (cost function), while the second term in the integral $\boldsymbol{u}^T(t)\boldsymbol{R}\boldsymbol{u}(t)$ is to keep the control input as small as possible. Normally $\boldsymbol{R}$ is selected as an identity matrix multiplied by a scalar coefficient r. The large values of r means more emphasis being placed on control cost than on the minimization of cost function. Letting $\boldsymbol{Q} = \boldsymbol{C^T C}$, equation (4.8) can be rewritten as

$$\boldsymbol{J} = \int_0^\infty (\boldsymbol{y}^T(t)\boldsymbol{y}(t) + \boldsymbol{u}^T(t)\boldsymbol{R}\boldsymbol{u}(t))dt \tag{4.9}$$

The optimal control is obtained through full state feedback with control law defined as follows

$$\boldsymbol{u}(t) = -\boldsymbol{G}\boldsymbol{x}(t), \quad \boldsymbol{G} = \boldsymbol{R^{-1} B^T K} \tag{4.10}$$

where $\boldsymbol{K}$ is a symmetric, positive definite, constant coefficient matrix. $\boldsymbol{K}$ is the solution of the algebraic Riccati equation (ARE) [69, 72, 73]:

$$\boldsymbol{A^T K} + \boldsymbol{KA} - \boldsymbol{KBR^{-1}B^T K} + \boldsymbol{Q} = 0 \tag{4.11}$$

In MATLAB, the command lqr is used to calculate the optimal gain matrix $\boldsymbol{G}$.

$$Syntax: \quad [G, \quad K, \quad e] = lqr(A, \quad B, \quad Q, \quad R)$$

where $\boldsymbol{G}$ is the optimal gain matrix; $\boldsymbol{K}$ is the solution of the Riccati equation; $\boldsymbol{e}$ is the closed-loop eigenvalues, i.e., $e = eig(\boldsymbol{A} - \boldsymbol{BG})$; $\boldsymbol{A}$ is the state matrix (before control); $\boldsymbol{B}$ is input matrix due to the control source; and $\boldsymbol{Q}$ is a symmetric positive semi-definite matrix. $\boldsymbol{R}$ is scalar weighting matrix.

4.4 Lyapunov equation to build a stable LQR controller

The precondition to design a LQR for a closed loop system is to ensure the controllability of the given system in (4.5) and the purpose is to minimize the value of cost function given in (4.8).

Controllability can be checked by different ways such as checking the full rank of system made of (A, B). In MATLAB, one can just provide the system matrices with the following command

$$Acon = ctrb(A, B); [r, c] = size(Acon);$$

$$rank(Acon)$$

Where full rank of A_{con} indicates that the system is controllable. Provided all rows and columns are linearly independent, the full rank is achieved when the rank of A_{con} becomes equal to either minimum number of rows or minimum number of columns. Another way is to check the controllability (time dependent system) is to check controllability Grammian of the system where the controllability Grammian is as following

$$Pc = \int_0^{+\infty} e^{At} BB' e^{A' t} dt \tag{4.12}$$

Where Pc is the controllability Grammian which can be solved from the following Lyapunov equation

$$A \times Pc + Pc \times A' + B \times B' = 0 \tag{4.13}$$

Let $Qc = B \times B'$, and the controllability Grammian can be checked from the following MATLAB command

$$Pc = lyap(A, Qc);\ \%\ solves\ the\ lyapunov\ matrix\ equation$$

Where user has to ensure Pc is a full rank matrix to confirm the system is controllable. From the result of optimal control theory [62, 74-81], one can design the control input as follows

$$u = -R^{-1}B'Px \tag{4.14}$$

Where P is the solution of the Riccati equation

$$A'P + PA - PBR^{-1}B'P + Q = 0 \tag{4.15}$$

A given system is stable if the Lyapunov conditions hold. Let $V(x)$ be a quadratic equation, where $V(x)$ is as following

$$\begin{gathered} V(x) = x^T P x \\ \dot{V}(x) = \dot{x}^T P x + x^T P \dot{x} \end{gathered} \tag{4.16}$$

The system is stable if $V(x) > 0 \; and \; \dot{V}(x) < 0$. This implies that

$$\frac{d}{dt}(x'Px) = x'(A'P + PA - 2PBR^{-1}B'P)x = -x'Qx - u'Ru$$

Consequently

$$\int_0^{+\infty} (x'(s)Qx(s) + u'(s)Ru(s))ds \leq x'(0)Px(0)$$

If we start from the above equation the following holds

$$\int_0^{+\infty} (x'(s)Qx(s) + u'(s)Ru(s))ds \leq -\int_0^{+\infty} \frac{d}{dt}(x'Px)$$

The last inequality is expanded as follows

$$\int_0^{+\infty} (x'(s)Qx(s) + u'(s)Ru(s))ds \leq -\int_0^{+\infty} x'(s)(A'P + PA - 2PBR^{-1}B'P)x(s)ds$$

The last inequality is satisfied if the following holds

$$A'P + PA - PBR^{-1}B'P + Q < 0$$

The $\dot{V}(x)$ can be expanded with the help of equation (4.7), (4.14), and (4.15) just as following taking $(A - BG)$ as $(A + BG)$

$$\dot{V}(x) = x^T(A'P + PA + G'B'P + PBG)x < 0 \tag{4.17}$$

Where G can be taken as $G = YP$ provided P (RE solution) is a symmetric matrix, and equation (4.17) can be written as the following after pre and post multiplying with P^{-1}

$$AP^{-1} + P^{-1}A^T + BY + Y^TB^T < 0 \tag{4.18}$$

The above equation can be written as following LMI (Linear Matrix Inequalities) equation

$$AX + XA' + BY + Y'B' < 0, \quad X \in \mathcal{R}^{n\times n}, Y \in \mathcal{R}^{m\times n} \tag{4.19}$$

Where $X = P^{-1}$. This LMI (Linear Matrix Inequality) can be solved with many tools such as with MATLAB, Scilab, and so on, but just a MATLAB procedure to solve LMI is given here. Write $lmiedit$ on the MATLAB command window which will open a figure called LMI editor. In LMI editor, do the following

- Name the LMI system
- Describe the LMIs as MATLAB expressions
- Describe the Matrix variables as S/R/G

  Where S stands for symmetry, R stands for rectangular, and G stands for general.
- Check the view commands option
- Copy the generated code and paste in a script file in MATLAB
- Define the A and B matrices and read the results
- Check if the closed loop system matrix is negative definite.

For more details, please use $\gg$ *help lmiedit* on the command window or read lmiedit guideline available online. **Figure 18** shows the LMI editor window written with LMI equations where X is a positive definite symmetric matrix and Y is a rectangular matrix. **Figure 19** shows the generated code for the defined LMIs.

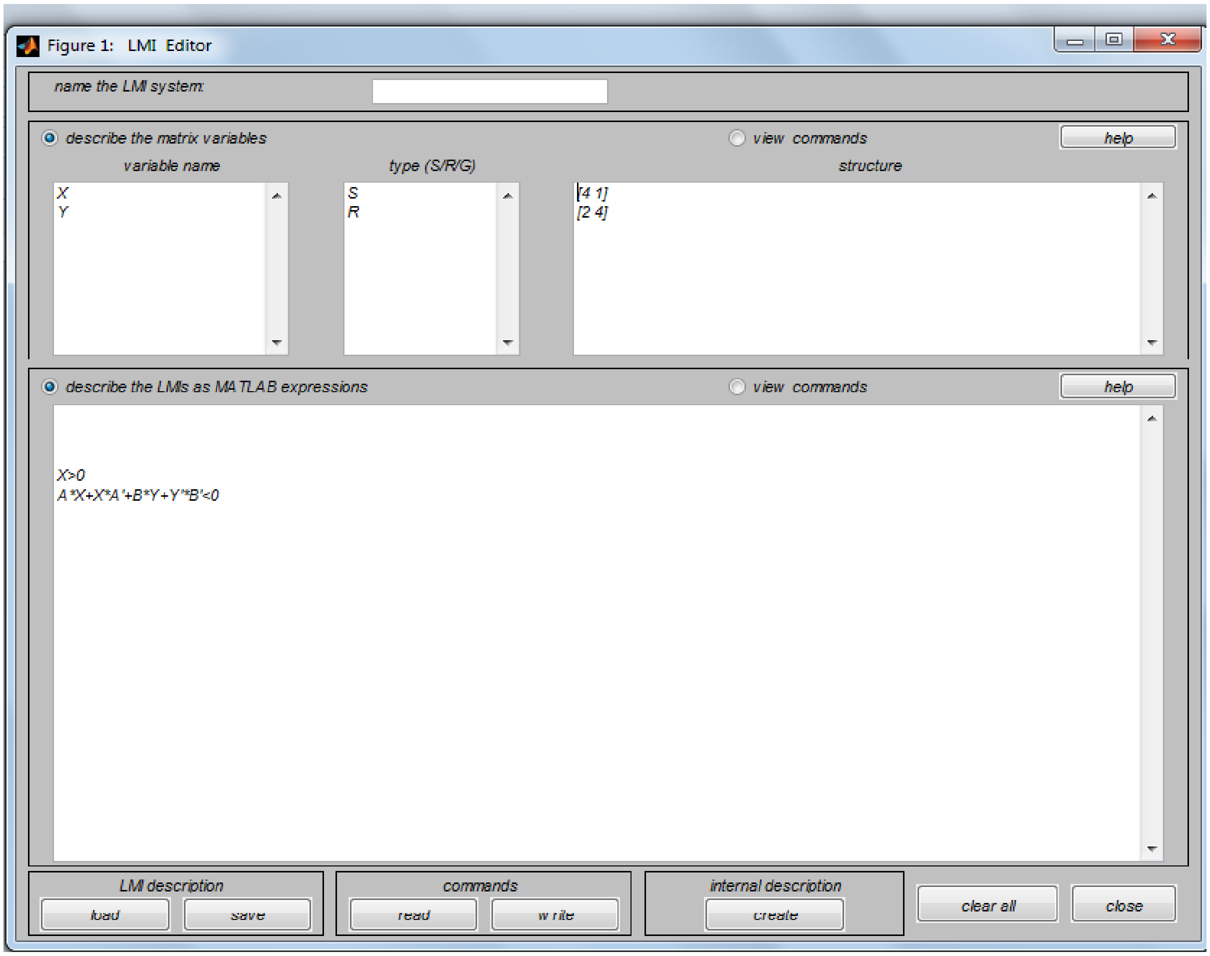

Figure 18 LMI Editor with defined LMI and matrix variables

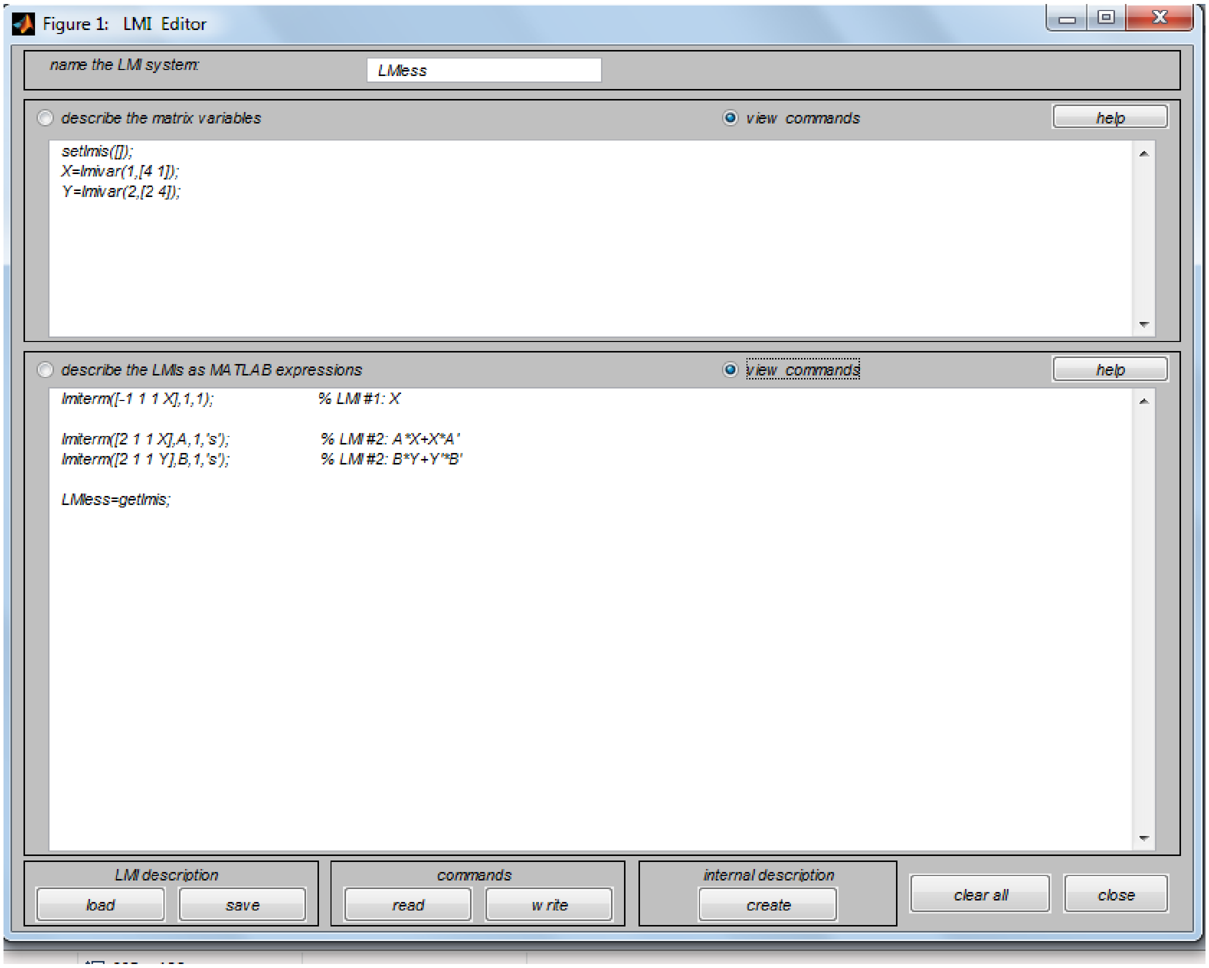

Figure 19 Generated code with *view commands* option

Figure 20 depicts a script file with generated code and defined system matrices. As long as the closed loop system matrix is negative definite, the controller is optimal. The superiority of LMI over an ARE (Algebraic Riccati equation) is because it produces many choices whereas the ARE just produce a unique solution which is not necessarily the best choice user is looking for. In **Figure 20**, $eXval$ produces the eigenvalues of P^{-1} matrix to check if the solution is negative definite which is optimal, and $eval$ checks the eigenvalues of closed loop system matrix $(A + BG)$ to check if the system is negative definite as well, and $gain$ produces the closed loop feedback gains.

Here the results are not shown, but anyone can check the results with the given script file in **Figure 20**.

```
setlmis([]);
X=lmivar(1,[4 1]);
Y=lmivar(2,[2 4]);

A = [0 1 0 0;0 1 1 0;1 1 0 1;1 3 6 7];
B=[0 0;0 1;1 0;1 1];

lmiterm([-1 1 1 X],1,1);                    % LMI #1: X

lmiterm([2 1 1 X],A,1,'s');                 % LMI #2: A*X+X*A'
lmiterm([2 1 1 Y],B,1,'s');                 % LMI #2: B*Y+Y'*B'

LMIess=getlmis;

[tmin, xfeas] = feasp(LMIess,[0,0,10,0,0],-10)
Xsol = dec2mat(LMIess,xfeas,X);
Ysol = dec2mat(LMIess,xfeas,Y);

eXval = eig(Xsol);
eval=eig(A+B*Ysol*inv(Xsol))
echeck = eig(Xsol*A'+A*Xsol+B*Ysol+Ysol'*B')
gain = Ysol*inv(Xsol)
```

Figure 20 A complete LMI script file for a 4x4 plant matrix with a 4x2 input matrix

4.5 The Linear Quadratic Gaussian (LQG) Regulator

The LQG controllers are well established; see, for example,[74, 75, 77-88]. Recall the state-space equation. To begin with, the feedthrough term D is removed from the output equation for simplification:

$$\dot{\boldsymbol{x}}(t) = \boldsymbol{A}\boldsymbol{x}(t) + \boldsymbol{B}\boldsymbol{u}(t) \tag{4.20}$$

$$\boldsymbol{y}(t) = \boldsymbol{C}\boldsymbol{x}(t) \tag{4.21}$$

Assume that the system is composed of process noise and measurement noise; equations (4.20) and (4.21) are rewritten as

$$\dot{\boldsymbol{x}}(t) = \boldsymbol{A}\boldsymbol{x}(t) + \boldsymbol{B}\boldsymbol{u}(t) + \boldsymbol{T}\boldsymbol{w}(t) \tag{4.22}$$

$$\boldsymbol{y}(t) = \boldsymbol{C}\boldsymbol{x}(t) + \boldsymbol{v}(t) \tag{4.23}$$

where $w(t)$ is the process noise and $v(t)$ is the measurement noise. Assume that the noise sources are uncorrelated, zero-mean, Gaussian, white noise random vectors with correlation matrices defined as follows:

$$E\{\boldsymbol{w}(t)\boldsymbol{w}'(t)\} = \boldsymbol{Qn}, \quad E\{\boldsymbol{v}(t)\boldsymbol{v}'(t)\} = \boldsymbol{Rn}, \quad E\{\boldsymbol{w}(t)\boldsymbol{v}'(t)\} = \boldsymbol{Nn} \tag{4.24}$$

Though size of the state weight matrix, Q and the control weight matrix, R are readily available from the LQR cost function due to known states and inputs, one has to determine the size of Q_n, and R_n carefully from the equations (4.22) and (4.23) respectively. If there are other additive terms, one has to consider all of them accordingly. Let A, B, T, and C be $(n \times n), (n \times p), (n \times p), and\ (q \times p)$ respectively. Where n, p, and q are the size of states, inputs, and outputs respectively. From equations (4.22), (4.23), and (4.24) one can find the noise covariance matrices as $Qn(p \times p)$, $Rn(q \times q)$, and $Nn(p \times q)$ which must be positive definite matrices.

The objective of the LQG problem is to find an optimal control that minimizes the performance function $\boldsymbol{J}$:

$$J = \lim_{t \to \infty} E(\boldsymbol{x}^T(t)\boldsymbol{Q}\boldsymbol{x}(t) + \boldsymbol{u}^T(t)\boldsymbol{R}\boldsymbol{u}(t)) \tag{4.25}$$

According to the separation principle, the solution of the LQG problem can be solved by independently solving the optimal regulator problem and the optimal estimation problem [69, 72, 73]. Firstly, we discuss the optimal estimation problem. According to Kalman filter theory [89], we want to minimize the following equation:

$$\lim_{t\to\infty} E([\boldsymbol{x}(t)-\widetilde{\boldsymbol{x}}(t)][\boldsymbol{x}(t)-\widetilde{\boldsymbol{x}}(t)]^{T}) \tag{4.26}$$

where $x(t)$ and $\tilde{x}(t)$ are the true and estimated state vectors, respectively. One can express the estimated state vector $\tilde{x}(t)$ as follows, where a feedback gain K_1 is used to correct the estimate:

$$\dot{\widetilde{\boldsymbol{x}}}(t) = \boldsymbol{A}\widetilde{\boldsymbol{x}}(t) + \boldsymbol{B}\boldsymbol{u}(t) + \boldsymbol{K}_1[\boldsymbol{y}(t) - \boldsymbol{C}\widetilde{\boldsymbol{x}}(t)] \tag{4.27}$$

And $\boldsymbol{K_1} = \boldsymbol{P}\boldsymbol{C^T}\boldsymbol{R^{-1}}$; where $\boldsymbol{P}$ can be obtained from Algebraic Riccati Equation (ARE)

$$\boldsymbol{AP} + \boldsymbol{PA^T} - \boldsymbol{PC^T}\boldsymbol{V^{-1}}\boldsymbol{CP} + \boldsymbol{TWT^T} = 0 \tag{4.28}$$

Secondly, we discuss the optimal regulator problem, similar to the **LQR** problem, by using optimal state estimate $\boldsymbol{x}^*$ to find the optimal control

$$\boldsymbol{u}^*(t) = -\boldsymbol{G}^*\boldsymbol{x}^*(t), \;\; \boldsymbol{G}^* = \boldsymbol{R^{-1}}\boldsymbol{B^T}\boldsymbol{K} \tag{4.29}$$

$\boldsymbol{K}$ is the solution of the algebraic Riccati equation (ARE)

$$A^T K + KA - KBR^{-1}B^T K + Q = 0 \tag{4.30}$$

From the above analysis, it can be found that the **ARE** is solved twice: once for the regulator problem and once for the filter problem. In MATLAB, the command $kalman$ is used to design a Kalman state estimator given a state-space model of the plant and the process and measurement noise covariance data. The syntax, input, and output arguments of $kalman$ are

$$Syntax: \quad [kest, \quad L, \quad P] = kalman(sys, \quad Qn, \quad Rn, \quad Nn)$$

which returns a state-space model $\boldsymbol{kest}$ of the Kalman estimator given the plant model sys and the noise covariance data Qn, Rn, Nn (matrices in equation (4.24). The resulting estimator $\boldsymbol{kest}$ has $[\boldsymbol{u};\ \boldsymbol{y}]$ as inputs and $[\boldsymbol{y}^*;\ \boldsymbol{x}^*]$ as outputs. We can omit the last input argument Nn when $N = 0$. One can check the inputs, outputs, and states of $Kest$ with the following MATLAB command

$$>> \ size(Kest)$$

The minimal realization of the considered coupled system returns 7 (seven) states with one input and one output (SISO). So, the MATLAB command size (Kest) results in as the following:

State-space model with 8 outputs, 2 inputs, and 7 states.

It should be noted that sys must be a state-space model with

$$sys = ss \ \ (msys.a, \quad [B_{control} \ \ msys.b], \quad msys.c, \quad [0])$$

where $\boldsymbol{B_{control}}$ and $\boldsymbol{msys.b}$ are the control force and primary force input matrix, respectively. $\boldsymbol{msys.c}$ is the observed matrix due to the control force. Besides, there are few approaches to begin with LQG controller design. Definitely, LMI based technique to derive a stable system is the best technique to begin with, but one needs to master it first. Anyway, a novice can start with a duality method described by [70] in (p.120-125).

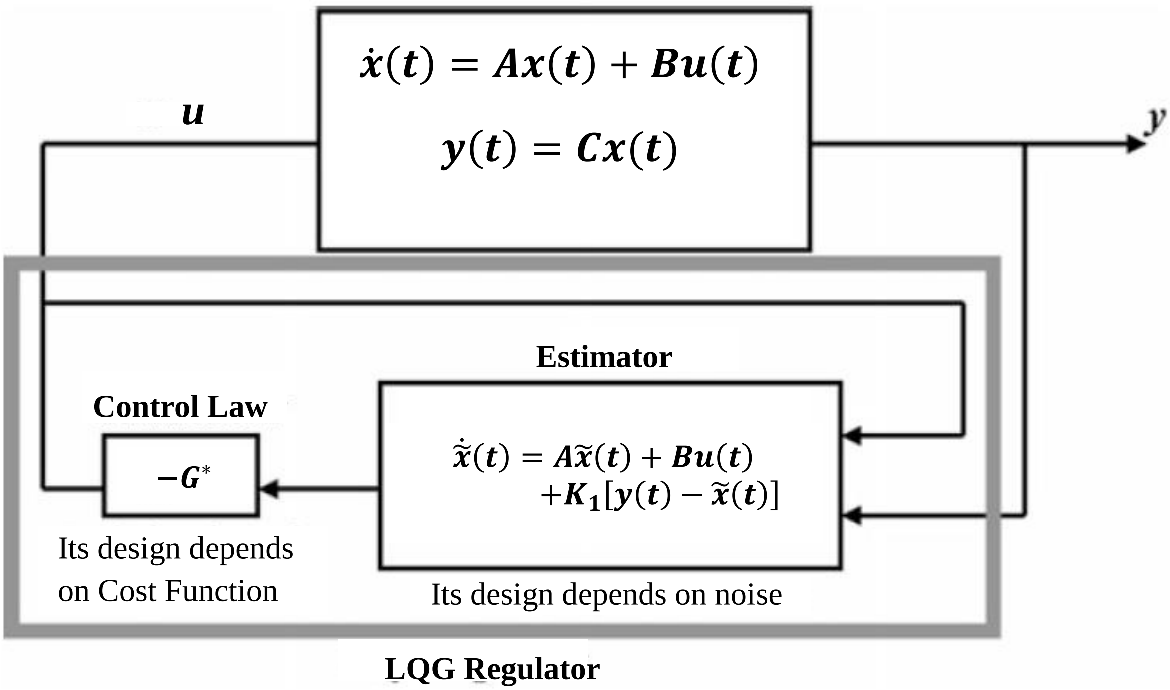

Figure 21 LQG control system design

The LQG problem can be described as Figure **21**. The LQG regulator in Figure **21** can be generated by using the command$\boldsymbol{lqgreg}$

$$rlqg = lqgreg \ (kest, \quad G)$$

which returns the LQG regulator $\boldsymbol{rlqg}$ (a state space model) given the Kalman estimator $\boldsymbol{kest}$ and the optimal state-feedback gain $\boldsymbol{G}$designed with *lqry*. Appendix B shows the MATLAB code used to generate linear quadratic Gaussian (LQG) regulator for SISO case.

Typically, it is impractical to measure all of the states in a system, as required in the linear quadratic regulator (LQR) control scheme. Even if this were possible, the measurement would be contaminated by noise [90]. Actually, there have hardly any system whose all states can be measured in reality except they can be assumed. Though

LQR has infinite gain margins, whereas LQG has finite gain margin, the LQR is scarcely implementable in real applications. Therefore, the LQG control scheme is adopted to design a control system for noise suppression of 3D enclosure with self-sensing piezoelectric actuators.

CHAPTER 5

Results and Discussion

The analytically derived models (equations (3.33) and (3.34)) for the configuration of Figure 22 and Figure 11 are used to obtain the finite dimensional approximate models with the properties and parameters enlisted in Table 3, Table 4 and Table 7. The 3D enclosure shown in Figure 22 is an assumed rectangular wooden box with its top surface being the aluminum plate. Using PZT actuator attached at the center of the plate, this ductile surface can be set into vibrations to generate acoustic disturbance inside the box.

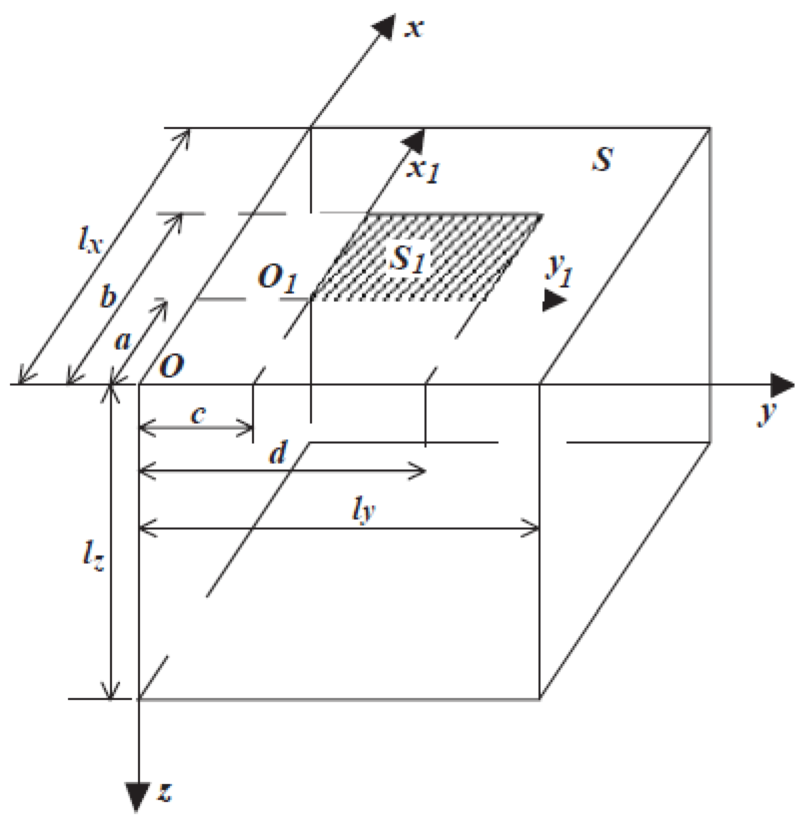

Figure 22 Schematic of 3-D acoustic enclosure[59]

A transfer function model of the system is obtained using equation (3.36) with the parameter values of Table **7** and assumed mode approximation. For this finite dimensional approximation, first five modes in each x, y, and z direction are considered, which yield a total 125 modes. From here a 38th order transfer function (TF) shown in Figure 23 (bode plot) and Figure 24 (magnitude) is derived using a step input bounded by spatial Heaviside function to an assumed microphone located at (127, 152.4, 311.2) mm. Besides, first two and three modes in each x, y, and z direction are considered for the optimal controller design. As it is known fact that a rank deficient system is hardly possible to control, for a minimal realization has been carried out on the system in MATLAB which preserves the original system above all except that it cancels out common pole-zero pairs or removes uncontrollable or unobservable states.

The comparison between original system modeled with the parameters given in Table 7 and the minimal realization of the system is shown in Figure 25. The Linear Quadratic Gaussian (LQG) controller has been applied for the models in three cases such as the followings:

i) Single input single output (SISO)

ii) Multi input single output (MISO)

iii) Multi input multi output (MIMO)

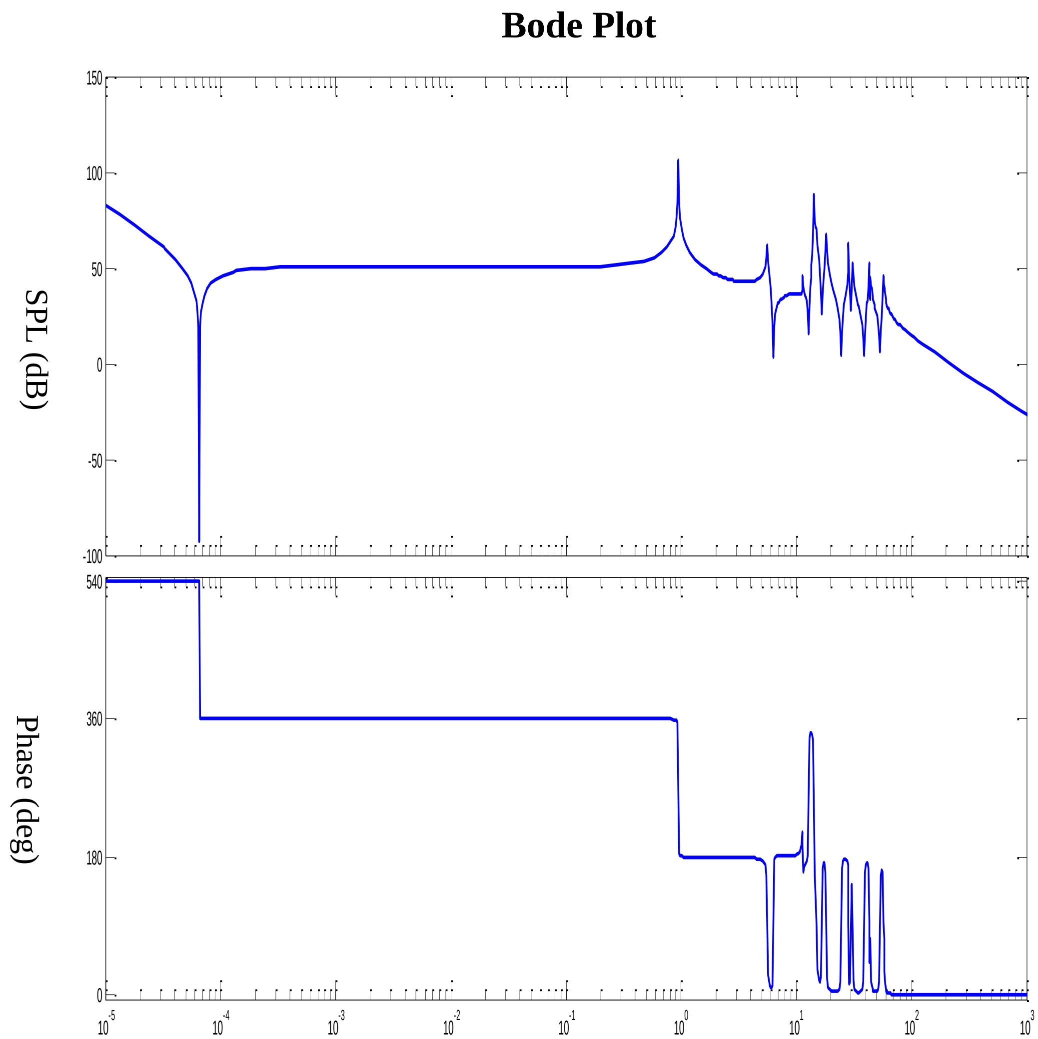

Figure 23 Estimated Transfer Function bode plot from PZT actuator to microphone

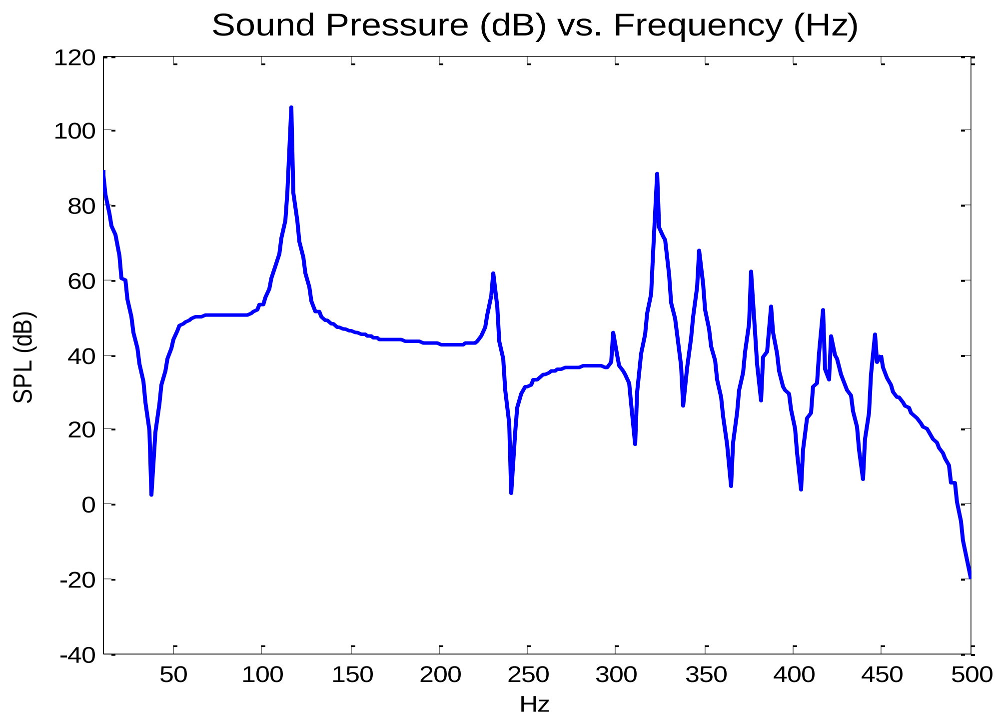

Figure 24 Estimated Transfer Function (magnitude) from microphone SPL to input from actuator

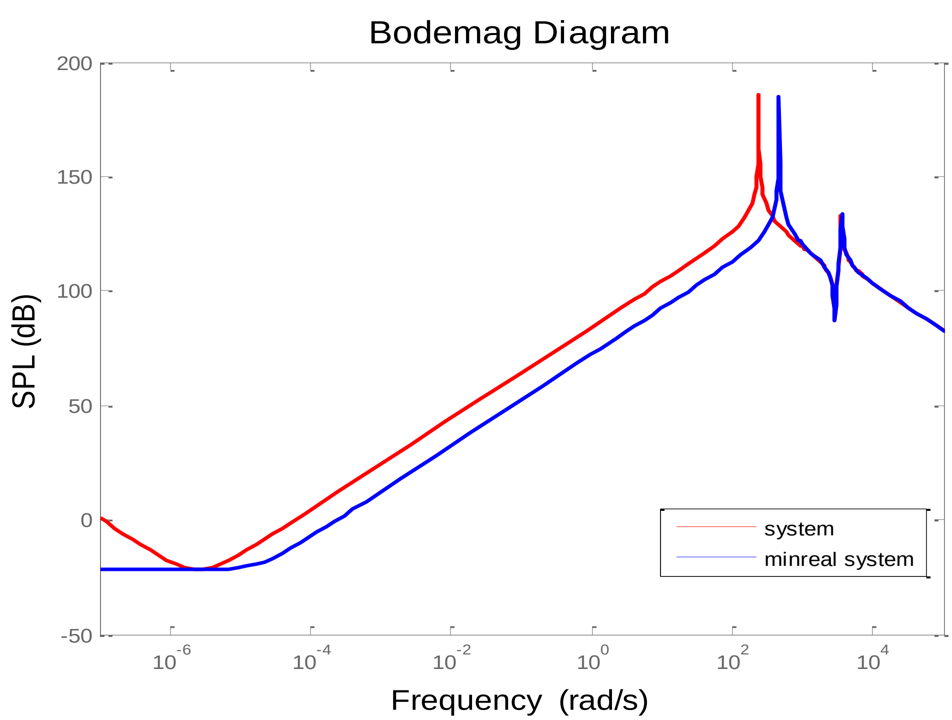

Figure 25 Comparison of magnitude (SPL) between system and minimal realized system

For simulation, first two modes in each x_1; x_2; $and\, x_3$ direction of the cavity are considered, which yield a total of eight (8) modes. Whereas first two modes in each y_1 $and\, y_2$ direction of plate are taken, that returns a total of four (4) modes. Apart from this, other modes are annotated with the figures. Mode numbers of plate are represented with $\boldsymbol{p(m_1, m_2)}$**,** where m_1 $and\, m_2$ are mode numbers in each y_1 $and\, y_2$ direction respectively. Besides, the cavity mode numbers are denoted by $\boldsymbol{c(n_1, n_2, n_3)}$**,** where $n_1, n_2, and\, n_3$ are mode numbers in each $x_1, x_2, and\, x_3$ direction respectively. Moreover, actuator location is shown on the figure except the center location. The results for each case are described below case by case.

5.1 SISO case

Two models with different cavity sizes were developed with the parameter given in the Table 3-4 and Table 7 and controlled for single input single output (SISO). Both models have been attached with a PZT actuator at the center of the models' flexible aluminum plate. Besides PZT actuator patch has been placed at other locations to check the arbitrary feasibility of PZT actuator location to reduce sound pressure level in the cavity. A temporal unit step function has been applied to PZT actuator to create disturbances and vice versa and the controller has been applied to control sound pressure level in the cavity. The sound pressure level (SPL) can be measured at any location in the cavity, but the results presented here are measured at (0.1270, 0.1524, 0.3112) m. The LQG controller has been designed with output weighting, the error penalty matrix and the control penalty matrices which are the followings but not limited to these values, there is a wide range of values the controller works well with and all of them produce optimal results:

$$Qr = 1e1 * eye(rmc) = 10 \times eye(1,1)\ and\ \ Rr = 1e^{-1} * eye(cRx) = 0.1 \times eye(1,1)$$

For Kalman filter, the covariance matrices are selected as,

$$Qe = 100, and\ Re = 10\ or\ Qe = 0.001, and\ Re = 0.1$$

For clarity, we define the **smaller cavity plate** with $\boldsymbol{P_{cs}}(0.3048{,}0.3810)\ m$ and **larger cavity plate** with $\boldsymbol{P_{cb}}(2.00, 0.60)m$. All SISO results for both cavities presented in from Figure 26-43 shows an overwhelming pattern of bounded input problem. Though the PZT-5H bender type patches can work well with the input voltage ranges from -100 Volt to +100 Volt, the input voltage required to control the SPL in the cavities ranges from -5 Volt to +5 Volt, for extra voltage input just make the controlled system track the uncontrolled response forcefully which is wastage of energy. As it can be seen from the Figure 26 and Figure 31, the closed loop response with PZT actuator located at the center of the plate lies below open loop and tracks the open loop response over the entire frequency range of interest indicating uniform broadband reduction without destabilizing higher frequency dynamics. Other locations of PZT actuator taken as the followings

$$x = [(0.0362{,}0.1724), (0.1886{,}0.2486), (0.1886{,}0.2486)]$$
$$y = [(0.1605{,}0.2205), (0.1605{,}0.2205), 0.2558{,}0.3157]$$

The open-loop system response changes due to alteration of the PZT actuator locations. It is clearly evident from Figures 40-48 that the closed loop response sometimes reduces the SPL in the cavity, but the closed loop response hardly tracks the open loop system. So selection of PZT actuator is of tremendous importance, for it changes the overall system dynamics and it is very tedious to track the system if the patch is not located at the right place. Hence, the center location of PZT actuator is superior to those of other locations selected in terms of effectiveness of the LQG regulator. Table 9-10 show the damping achieved for three resonant modes. From the plots, it is clearly seen that there are significant reductions in the gains of those particular resonant frequencies.

Table 9 Damping for few resonant modes in SISO case

Resonant frequency (Hz)	Attenuation (dB)
106.4	7.1
264.8	4

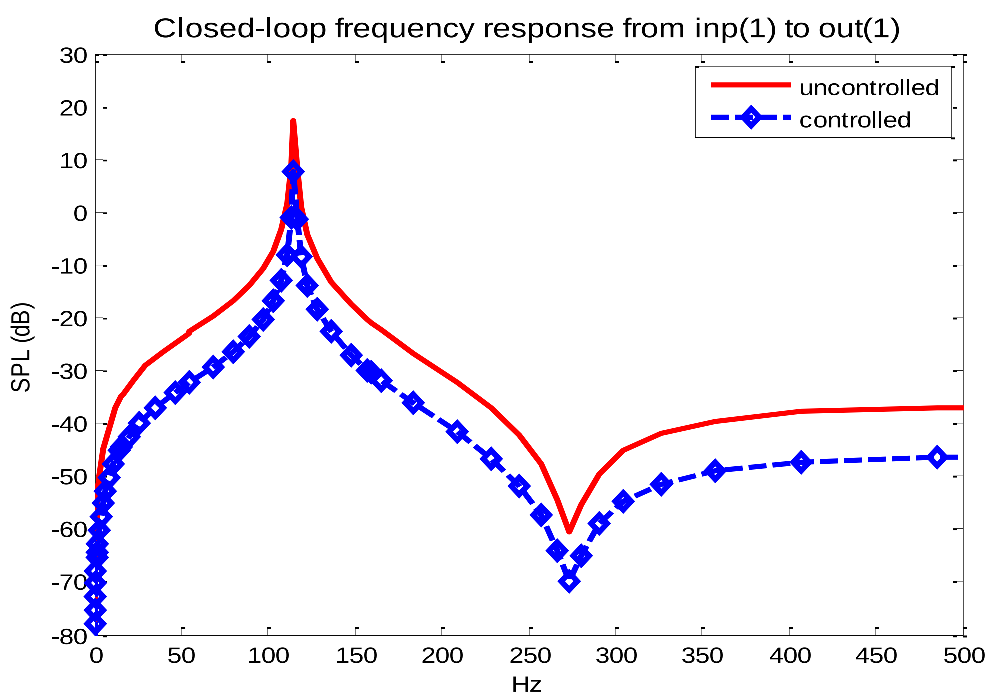

Figure 26 SPL with PZT actuator located at the center of the small cavity $\boldsymbol{P_{cs}}$ with 0.25 Volt (0.0625 N)

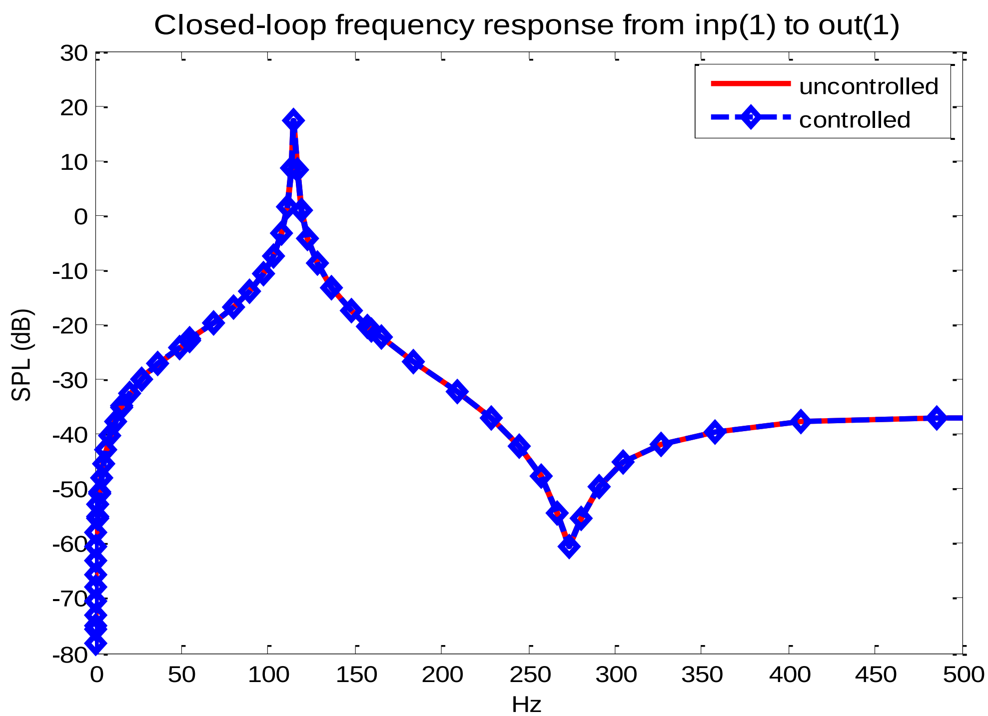

Figure 27 SPL with PZT actuator located at the center of $\boldsymbol{P_{cs}}$ with 0.5 Volt (0.1250 N)

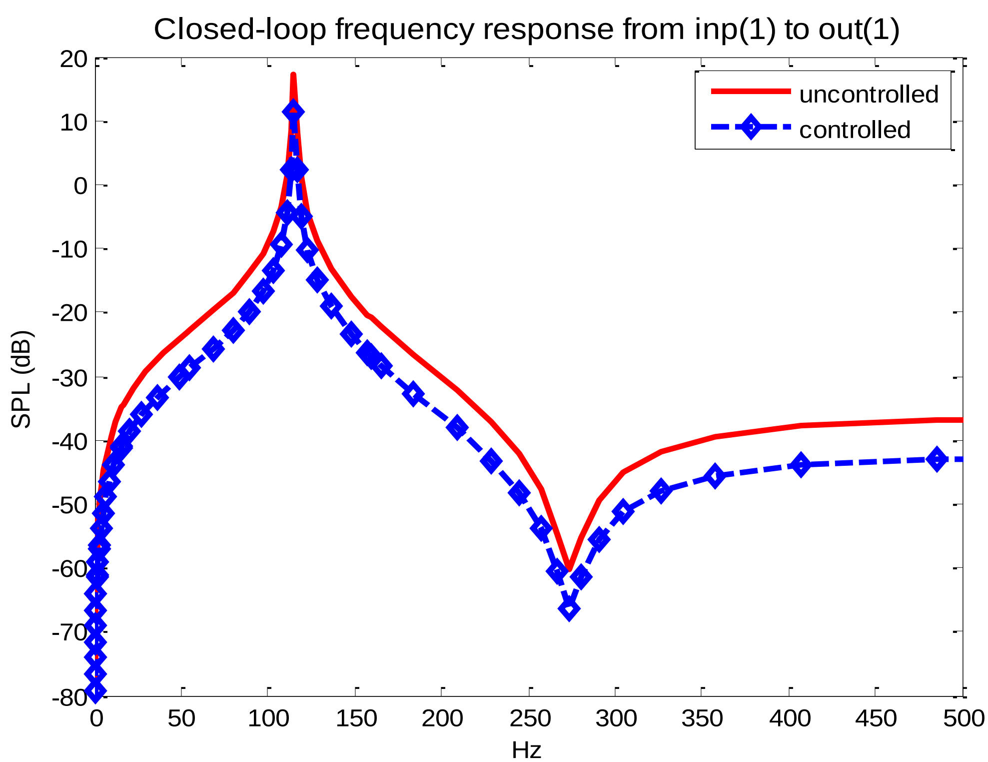

Figure 28 SPL with PZT actuator located at the center of $\boldsymbol{P_{cs}}$ with -1 volt (- 0.2501N)

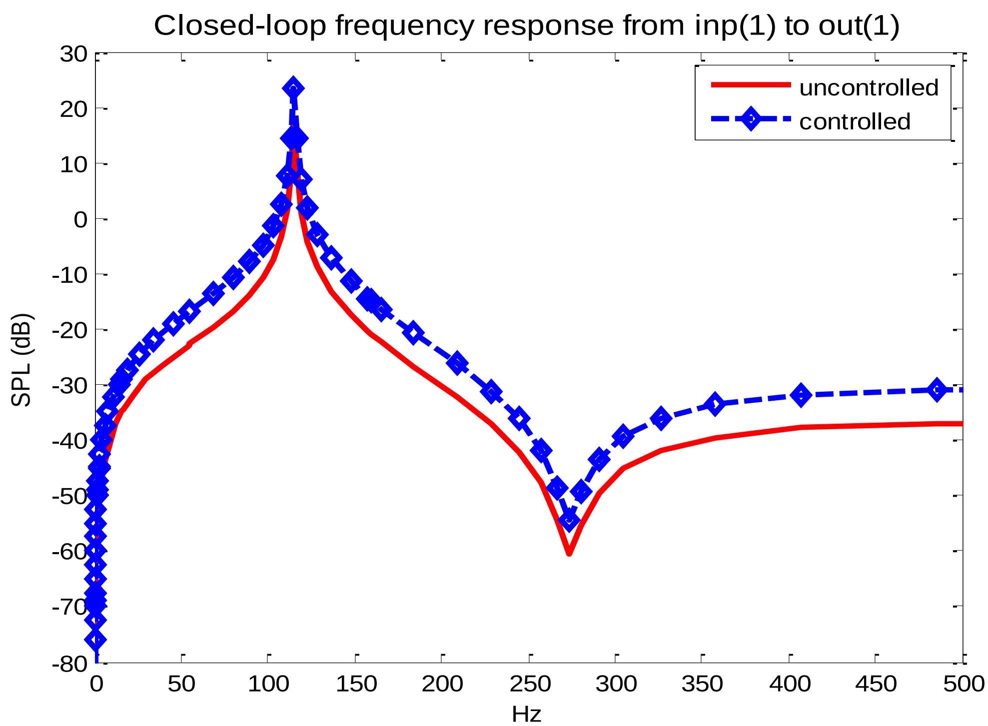

Figure 29 SPL with PZT actuator located at the center of $\boldsymbol{P_{cs}}$ with 2 Volt (0.5002 N)

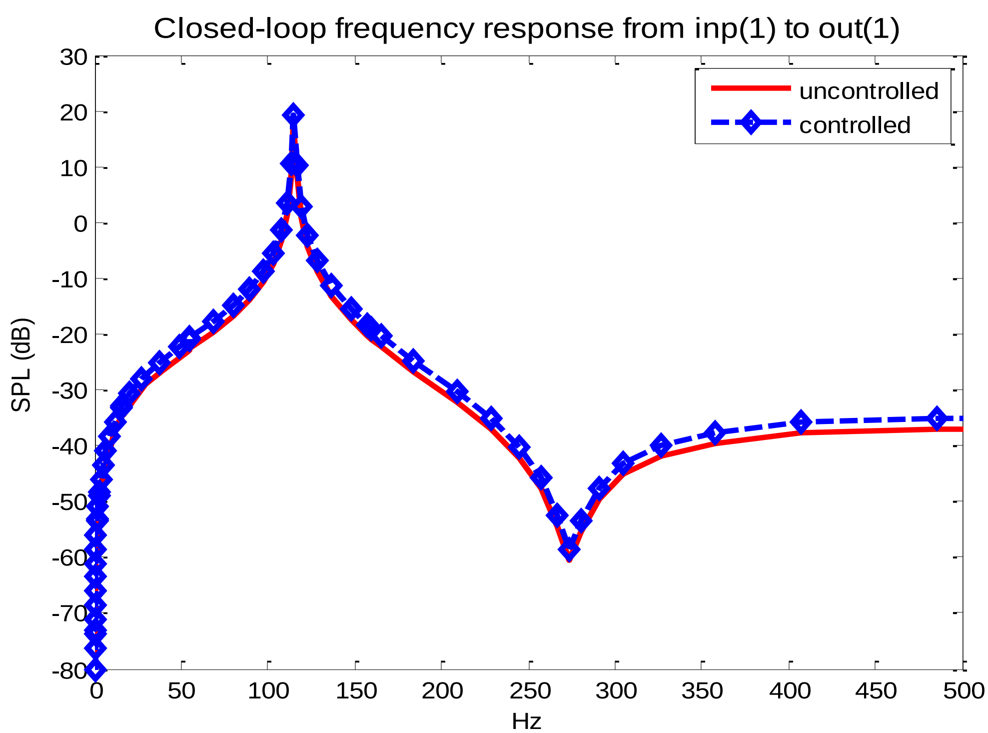

Figure 30 SPL with PZT actuator located at the center of $\boldsymbol{P_{cs}}$ with 5 Volt (1.2504 N)

Table 10 Damping for resonant mode in SISO case for larger cavity

Resonant frequency (Hz)	Attenuation (dB)
51.5	33.5

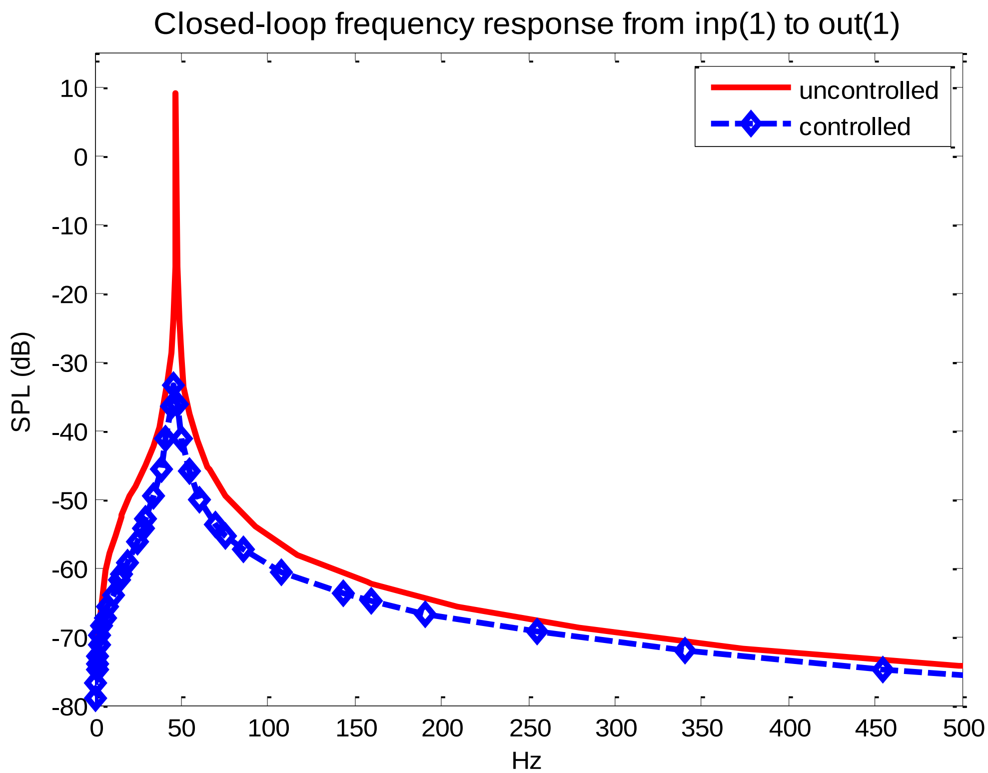

Figure 31 SPL with PZT actuator located at the center of the larger cavity $\boldsymbol{P_{cb}}$ with 0.25 Volt (0.0625 N)

Furthermore, piezoelectric actuator was placed in some other locations. Results from few of them are portrayed in **Figure 34**-43 and schematic placement of single actuator is annotated in these figures. The plate has been divided into four equal parts longitudinally and two equal parts laterally. A, C, and D in the annotated portion of figures represent the PZT patch location in the 1st quarter center, 3rd quarter center, and 3rd quarter center and middle of the second half of the plate respectively.

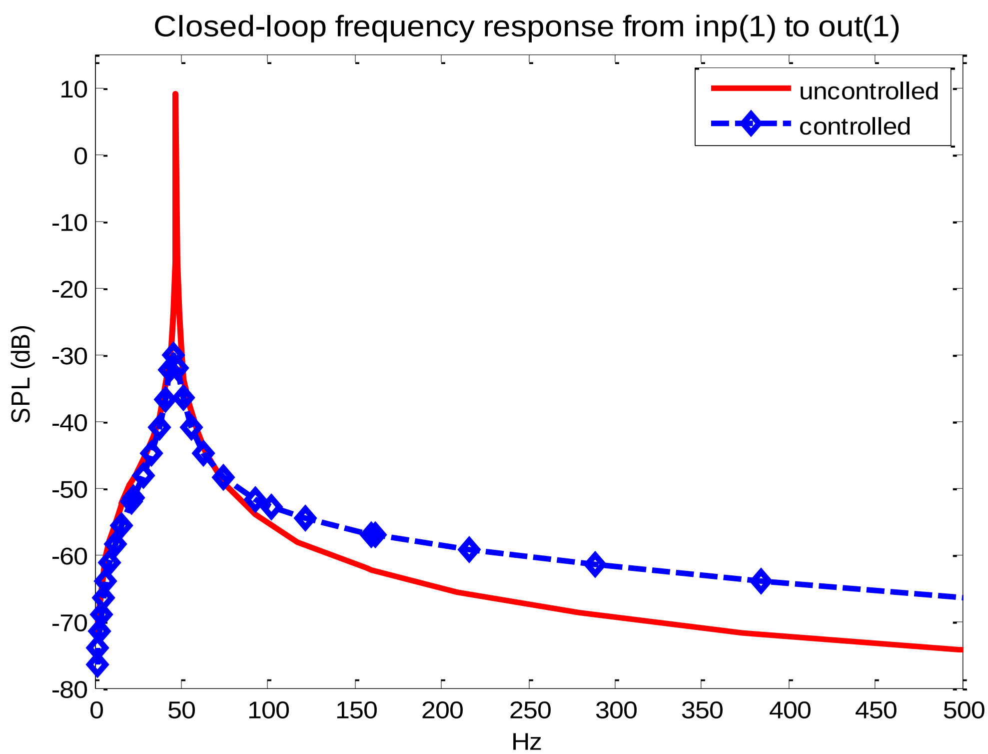

Figure 32 SPL with PZT actuator located at the center of $\boldsymbol{P_{cb}}$ with 0.5 Volt (0.1250 N)

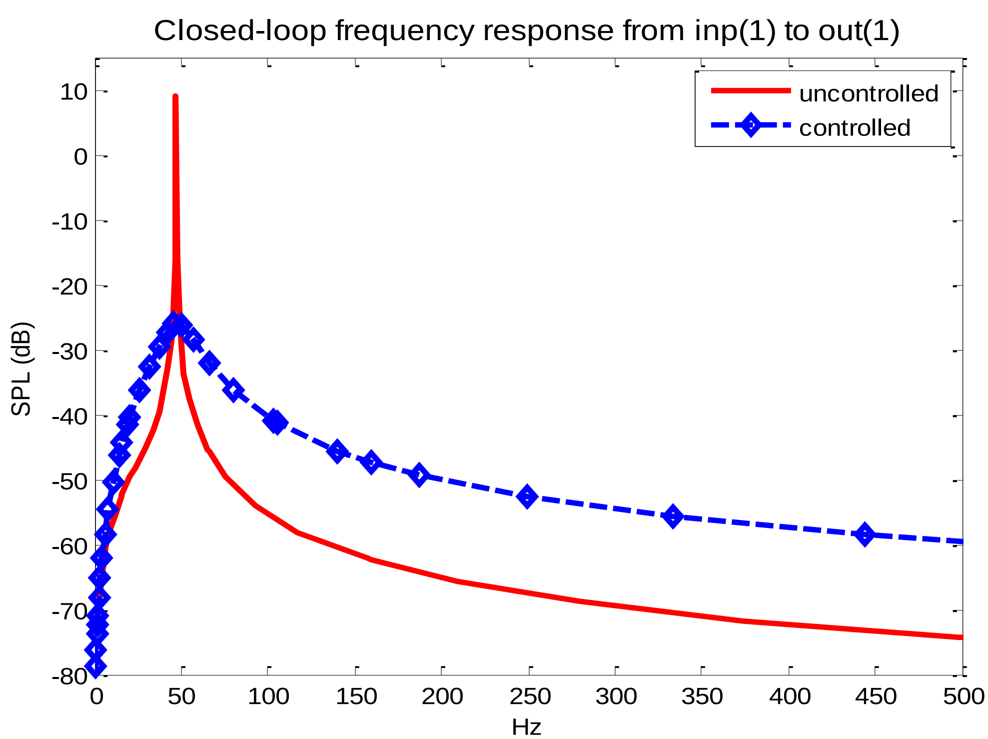

Figure 33 SPL with PZT actuator located at the center of $\boldsymbol{P_{cb}}$ with 1 Volt (0.2501 N)

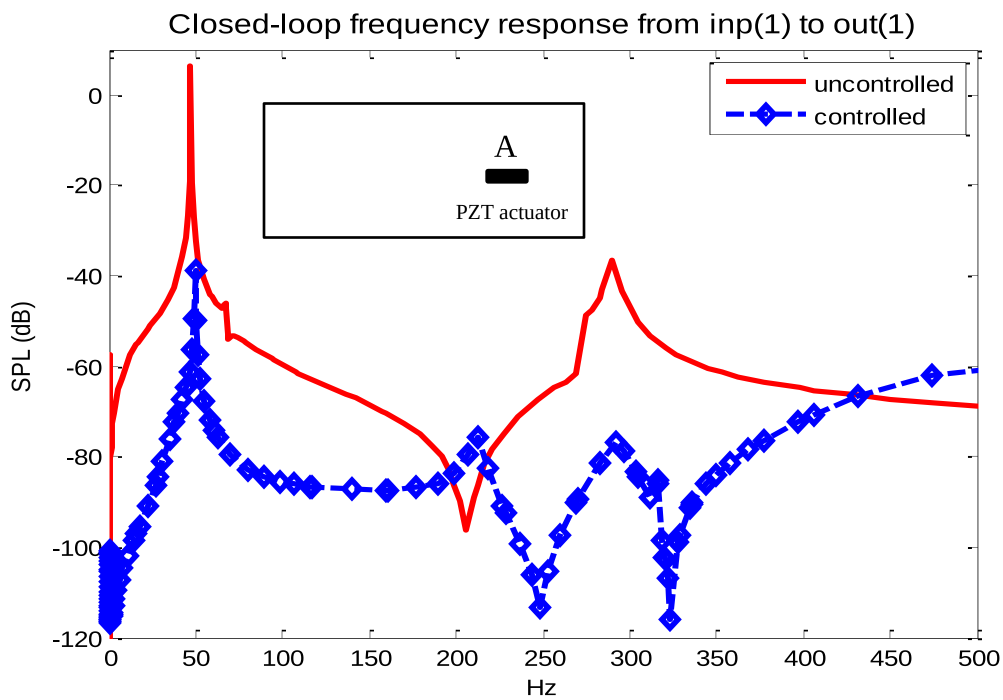

Figure 34 SPL with PZT actuator located at location A of $\boldsymbol{P_{cb}}$ with 1 Volt(0.2501 N)

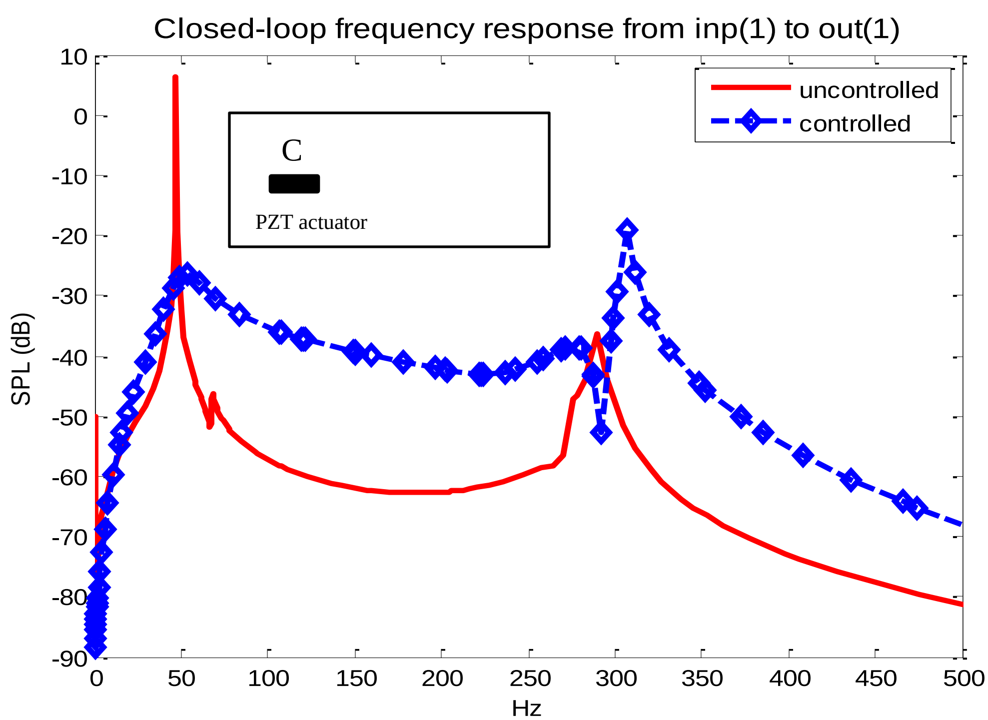

Figure 35 SPL with PZT actuator located at location C of $\boldsymbol{P_{cb}}$ with 1 Volt(0.2501 N)

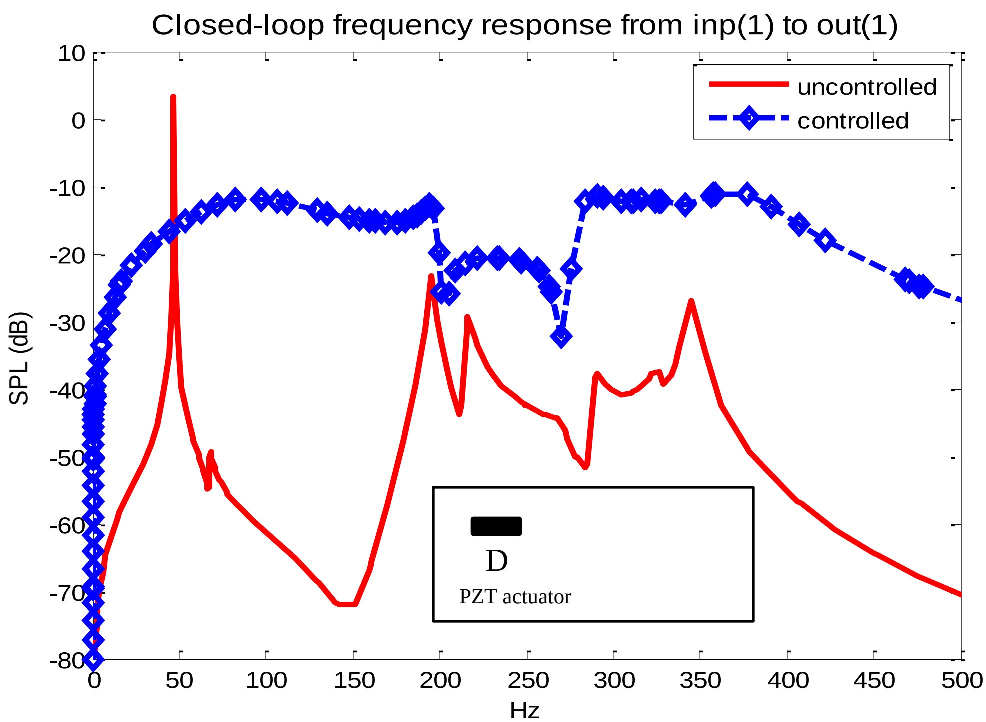

Figure 36 SPL with PZT actuator located at location D of $\boldsymbol{P_{cb}}$ with 1 Volt (0.2501 N)

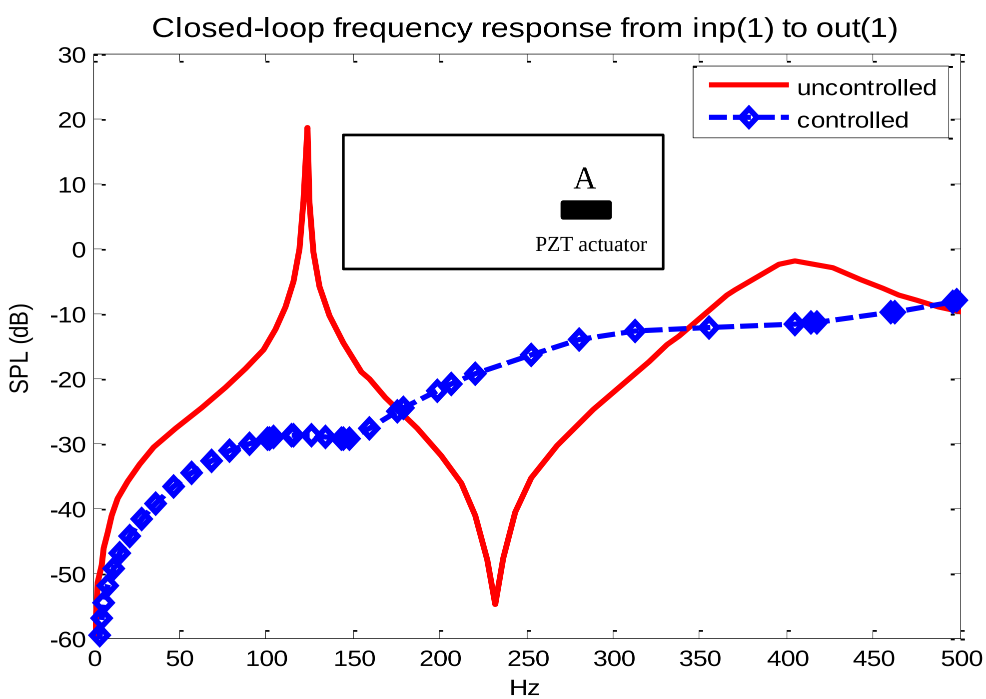

Figure 37 SPL with PZT actuator located at location A of $\boldsymbol{P_{cs}}$ with 0.25 Volt (0.0625 N)

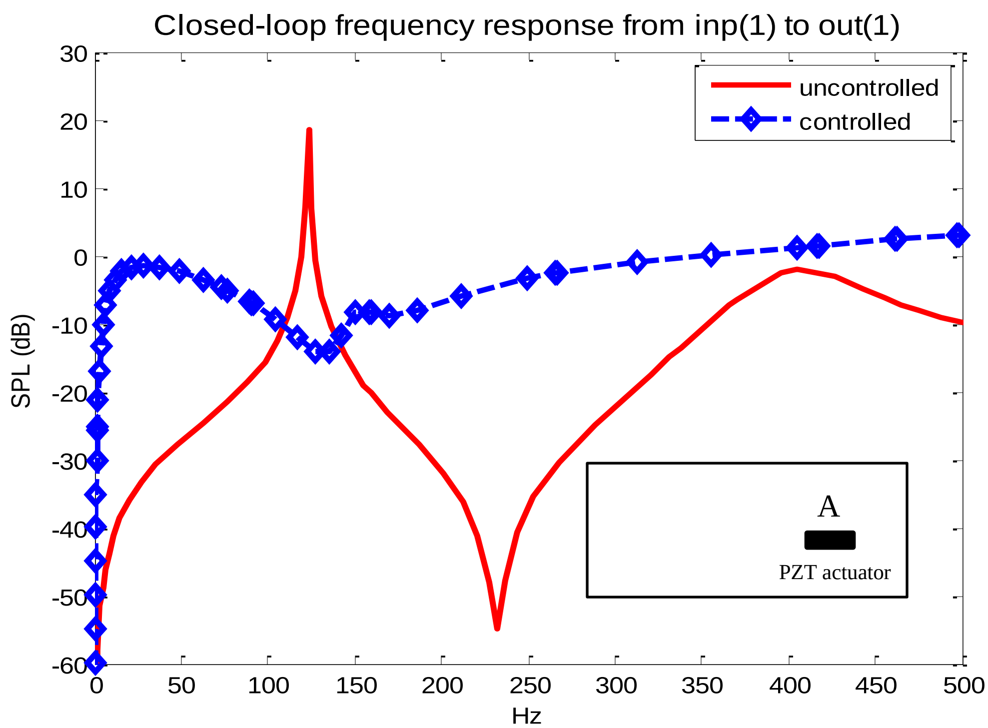

Figure 38 SPL with PZT actuator located at location A of $\boldsymbol{P}_{cs}$ with 1 Volt (0.2501 N)

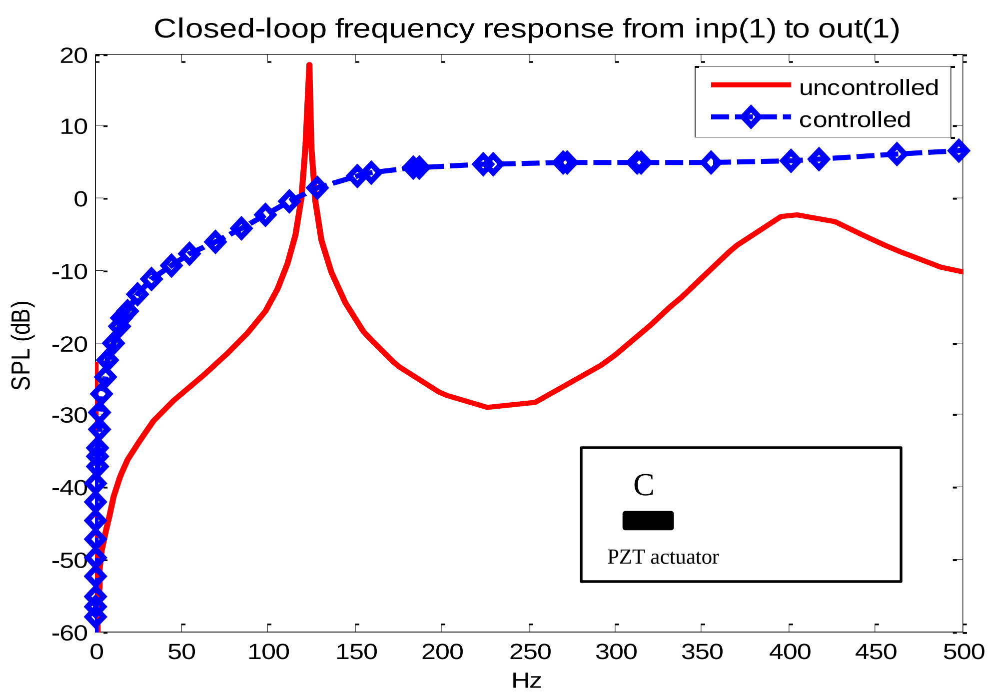

Figure 39 SPL with PZT actuator located at location C of $\boldsymbol{P}_{cs}$ with 1 Volt(0.2501 N)

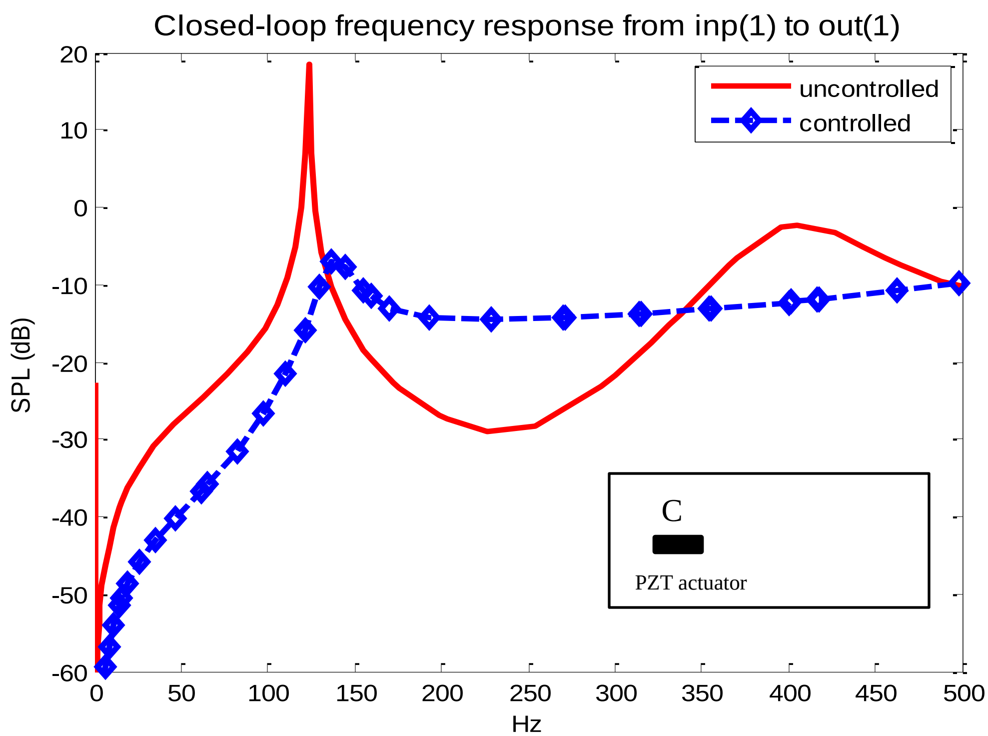

Figure 40 SPL with PZT actuator located at location C of $\boldsymbol{P_{cs}}$ with 0.25 Volt(0.0625 N)

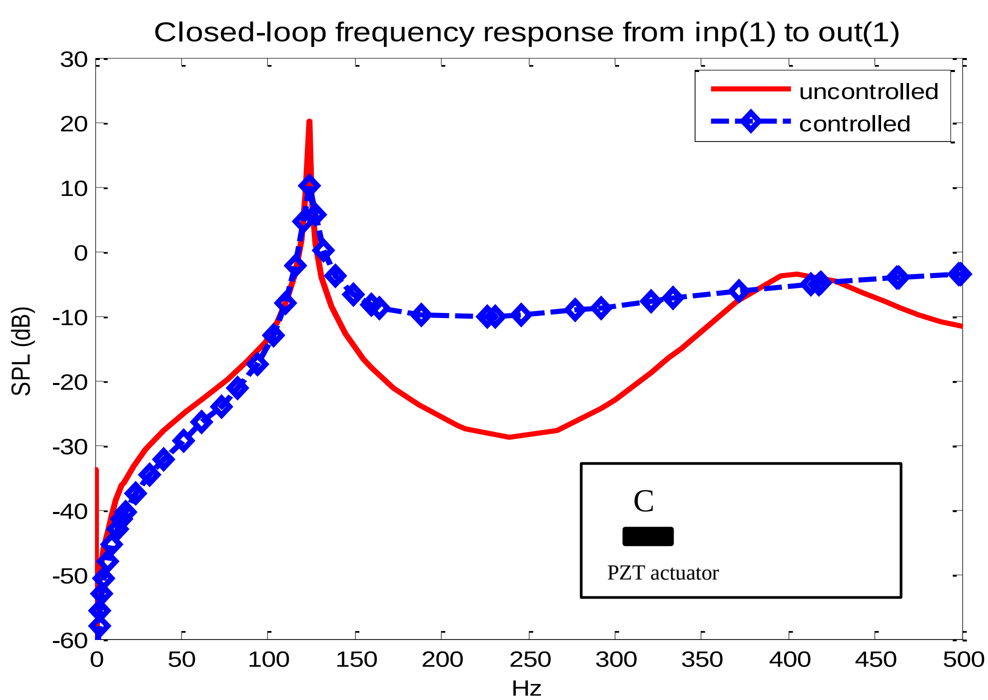

Figure 41 SPL with PZT actuator located at location C of $\boldsymbol{P_{cs}}$ with 0.5 Volt(0.125 N)

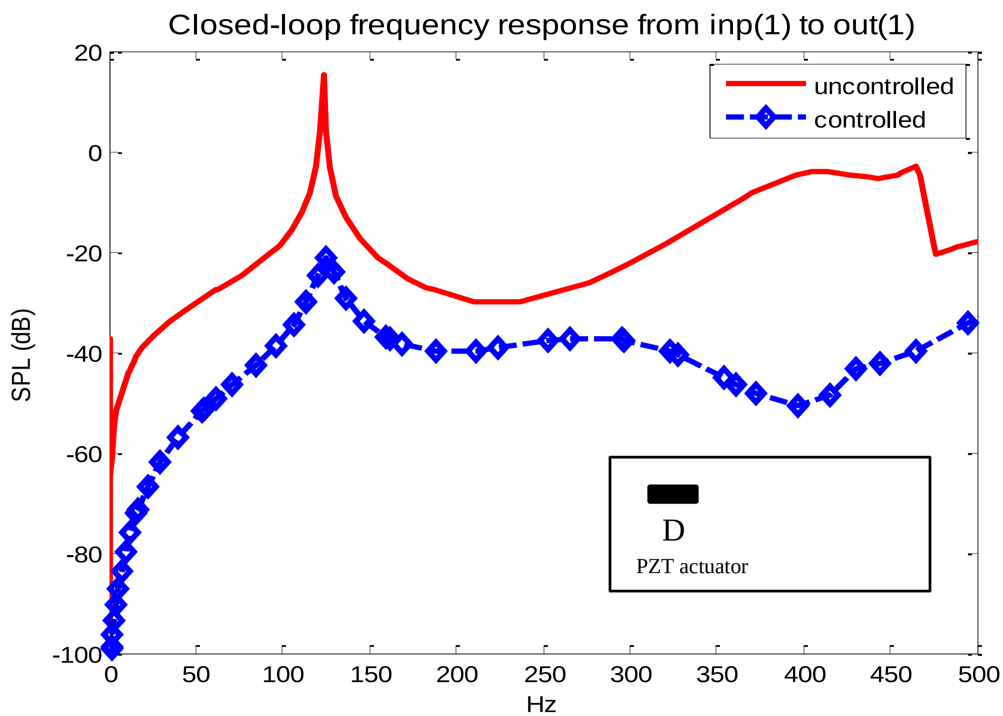

Figure 42 SPL with PZT actuator located at location D of $\boldsymbol{P_{cs}}$ with 1 Volt(0.2501 N)

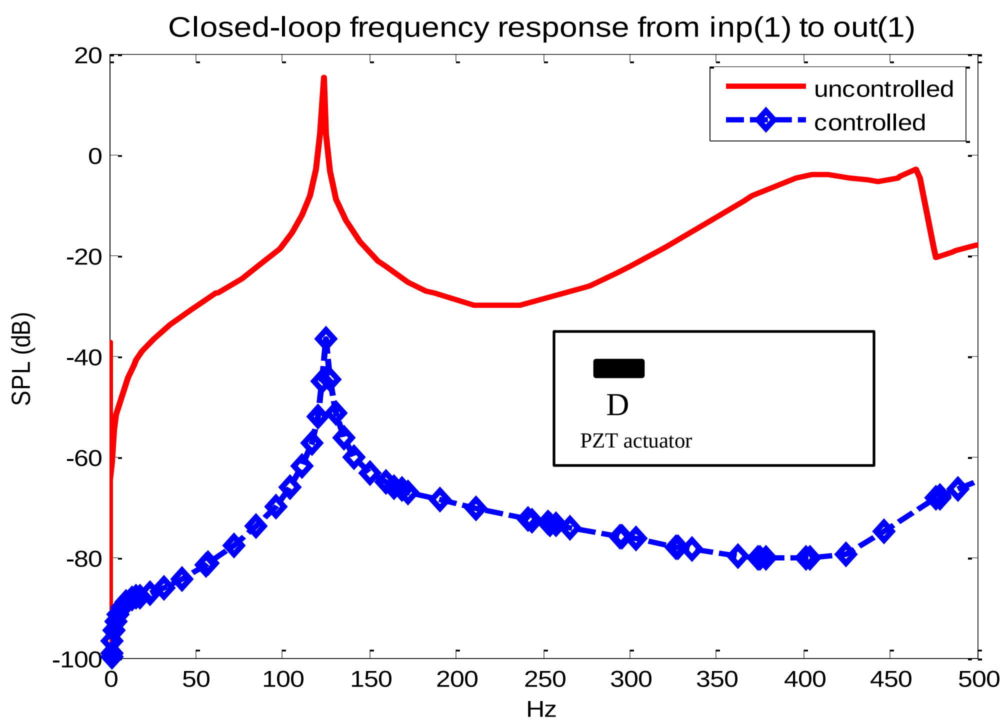

Figure 43 SPL with PZT actuator located at location D of $\boldsymbol{P_{cs}}$ with 0.25 Volt(0.0625 N)

5.2 MISO case

For multi inputs single output (MISO), the model was fitted with three channel PZT actuators on the top of the cavity plate. Different locations have been arbitrary chosen to observe reduction of the sound pressure level (SPL) in the cavity. It is found that different locations of PZT actuators have different impacts in terms of reductions in the sound pressure level in the cavity corresponding to particular eigen-frequencies. For this case, local coordinate for the acoustic sensor (microphone) is chosen as (0.1270, 0.1524, 0.3112) m, and three patches are attached to the plate with the following coordinates

$$\boldsymbol{x} = [(0.627, 0.706), (0.96, 1.04), (1.293, 1.373)]$$
$$\boldsymbol{y} = [(0.27, 0.33), (0.27, 0.33), (0.27, 0.33)]$$

Schematic spatial location of PZT actuator is shown in **Figure 44**, and the length and width of the flexible plate in this figure are represented with $L_x and\ L_y$ respectively. The LQG controller has been designed with output weighting, the error penalty matrix and the control penalty matrices which are the followings but not limited to these values, there is a wide range of values the controller works well with and all of them produce optimal results:

$$Qr = 1e1 * eye(rmc) = e^0 \times eye(1,1), \text{ and}$$

$$Rr = 1e^{-1} * eye(cRx) = 1e^{-4} \times eye(3,3)$$

For Kalman filter, the covariance matrices are selected as

$$Qe = \left(1e^3 \times eye(cRx)\right) = cov\left(1e^3 \times eye(3,3)\right), \text{ and}$$

$$Re = 1e^{1} \times eye(rmc) = 1e^{1} \times eye(1,1)$$

The open and closed-loop frequency response is compared in **Figure 45**-47. From these figures it can be seen that the control effort is only in the frequency band of interest. **Table 11** shows the damping achieved for four resonant modes. From the plots, it is clearly seen that there are significant reductions in the gains of those particular resonant frequencies. Besides, input has been written as inp (1), inp (2), and inp (3). All inputs are applied in voltage. Output is written as out (1) which measure SPL (sound pressure level) at the microphone location corresponding to respective input voltage.

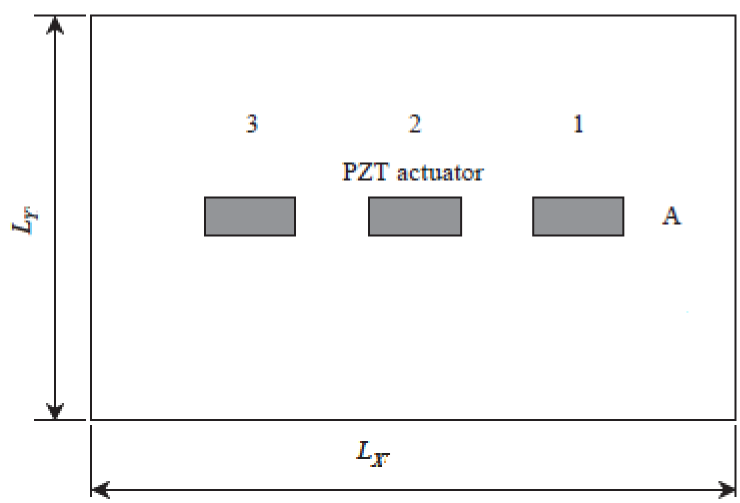

Figure 44 Spatial locations of the PZT actuators on the flexible plate for MISO case

Table 11 Damping for few resonant modes in MISO case

Resonant frequency (Hz)	Attenuation (dB)
51.5	20.2
227.25	4
340.51	5
350.96	13

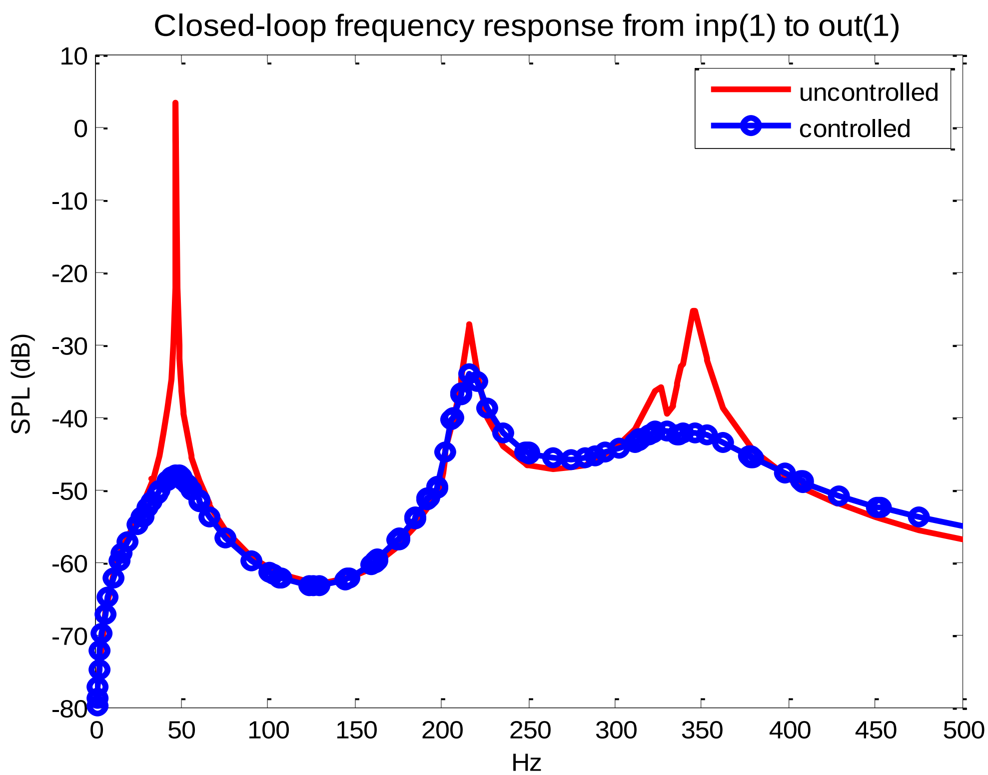

Figure 45 SPL in the cavity from inp (1) to out (1) with applied voltage 1 V (2.2509 N)

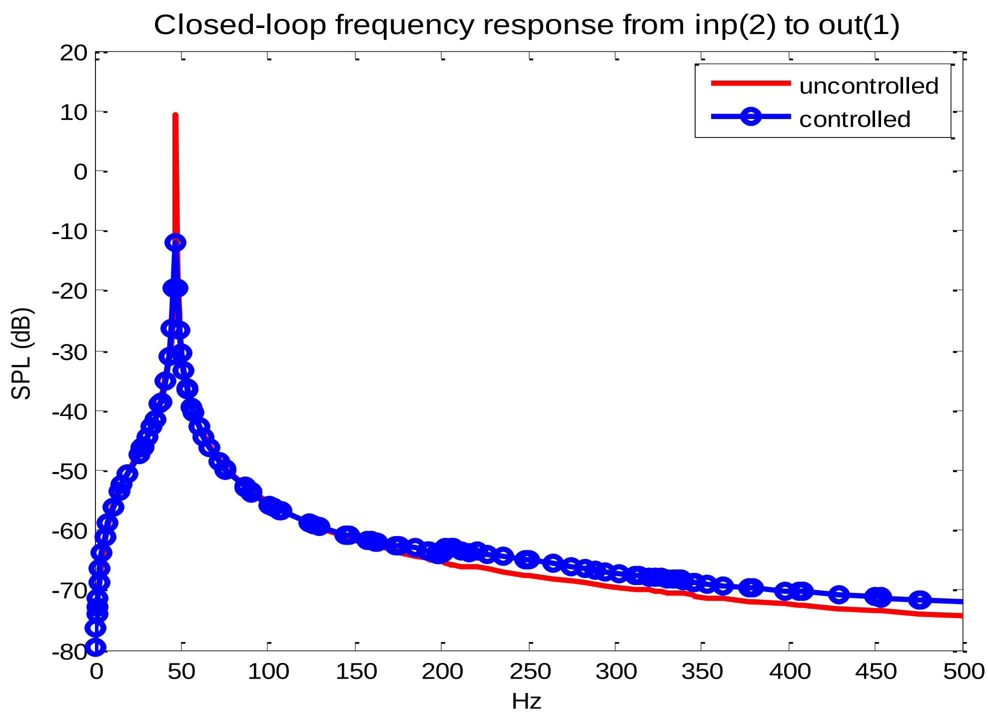

Figure 46 SPL in the cavity from inp (2) to out (1) with applied voltage 1 V (2.2509 N)

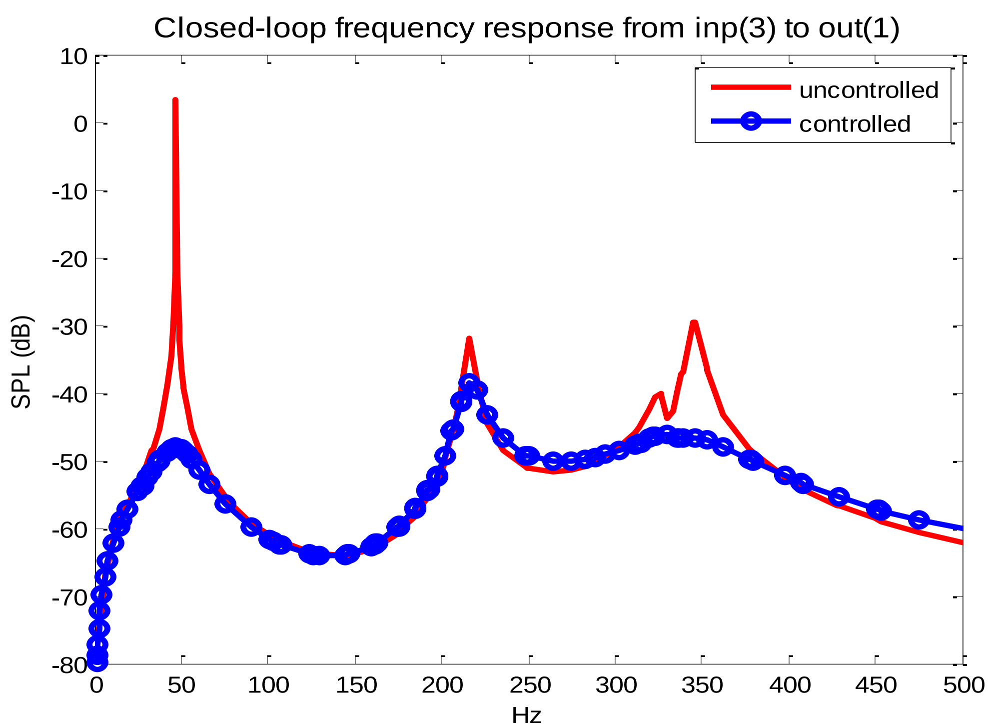

Figure 47 SPL in the cavity from inp (3) to out (1) with applied voltage 1 V (2.2509 N)

5.3 MIMO case

For multi inputs multi outputs (MIMO), the model modeled with the parameters enlisted in Table 3-4 has been attached with three channel PZT actuators on the top of the cavity plate. Schematic spatial location of PZT actuator and PVDF sensor is shown in **Figure 48**. Each channel consists of three PZT patches and all patches are connected in parallel to each other in a channel so that potential difference applied to a channel is equal to each patch actuator. All channels are equidistant from each other, so do the patches in a channel. The channels are located at the end of first quarter, second quarter, and third quarter of the length and across the width of the plate. First, two modes have been taken along each direction of the cavity and plate which ends up with a system after minimal realization which removes four states such as following

$$\gg size(msys)$$

$$State - space\ model\ with\ 3\ outputs, 3\ inputs, and\ 20\ states.$$

Then, the linear quadratic Gaussian (LQG) regulator is applied to the system, and the open and closed-loop frequency responses are read and plotted after converting the cavity response to sound pressure level (SPL) using the following equation:

$$magdb\ (SPL)\ =\ 20 * log10(mag)$$

Bode magnitude of the system response in absolute units, returned as a 3-D array with dimensions (number of outputs) × (number of inputs) × (number of frequency points). For MIMO systems, mag(i, j, k) gives the magnitude of the response from the jth input to the ith output. The cavity responses have been measured with two assumed microphones in two locations such as the followings:

$$(\boldsymbol{x}, \boldsymbol{y}, \boldsymbol{z}) = [(1.00, 0.30, 0.30), (1.00, 0.30, 0.60)]$$

Moreover, an assumed PVDF sensor is placed on the plate to measure the plate displacements and the location is the following $(x, y) = [(0.10, 0.20)] and\ (x, y) = [(0.90, 0.30)]$ respectively. Besides the plate materials have been changed from aluminum to steel and the frequency responses are measured at the same locations. Some of the results presented in Figure 49-64 show the attenuation of some resonant modes are spectacular. But comparing the results from both the aluminum plate cavity and steel plate cavity, it is clear that aluminum plate is more adaptable to the PZT patch compared to that of steel plate, for the aluminum has a material strength which is almost in the same range of the given PZT actuator material. Another fact is that the output results varies from location to location, so choosing the best location is very challenging as the results portrayed in Figure 55-64 show it clearly. The response measured at $(x, y) = [(0.10, 0.20)]$ shown at Figure 55 and Figure 56 for aluminum plate cavity and steel plate cavity respectively. Another measurement taken at $(x, y) = [(0.90, 0.30)]$ is presented at Figure 57 only for aluminum plate cavity.

Likewise, four modes are taken along each of the x, and y direction of the plate, and three modes are taken along each x, y, and z direction of the cavity which ends up with a system after minimal realization which removes two unobservable states such as following

$$>> size(msys)$$

$$State - space\ model\ with\ 3\ outputs, 3\ inputs, and\ 84\ states.$$

In this case, the LQG controller has been designed with output weighting, the error penalty matrix and the control penalty matrices which are the followings

$$Qr = 1e^{-4} * eye(rmc) = e^{0} \times eye(3{,}3)\text{, and}$$

$$Rr = 1e^{0} * eye(cRx) = 1e^{-4} \times eye(3{,}3)$$

For Kalman filter, the covariance matrices are selected as

$$Qe = \left(1e^{-2} \times eye(cRx)\right) = cov\left(1e^{-2} \times eye(3{,}3)\right)\text{, and}$$

$$Re = 1e^{1} \times eye(rmc) = 1e^{1} \times eye(3{,}3)$$

Though there are other values that work well and produce optimal results, but it becomes tedious to choose proper weighting matrices as the system size increases. The responses presented in Figures 58-64 clearly show the controller considerably reduces response in terms of attenuation of some resonant modes along with tracking the system which is expected from a regulator performance point of view. Table 12 shows the damping achieved for few resonant modes. From the plots, it is clearly seen that there are significant reductions in the gains of those particular resonant frequencies.

Besides, the results depicted in Figure 63 and Figure 64, clearly show the aluminum plate is a better host structure to the PZT actuator considered here than to that of steel plate. Besides, input has been written as inp (1), inp (2), and inp (3). All inputs are applied in voltage. Output is written as out (1), out (2), and out (3). Out (1), and out (2) measure SPL (sound pressure level) at the microphone locations corresponding to respective input, and out (3) measures displacemnt (μm) on the plate at the specified location corresponding to respective input voltage.

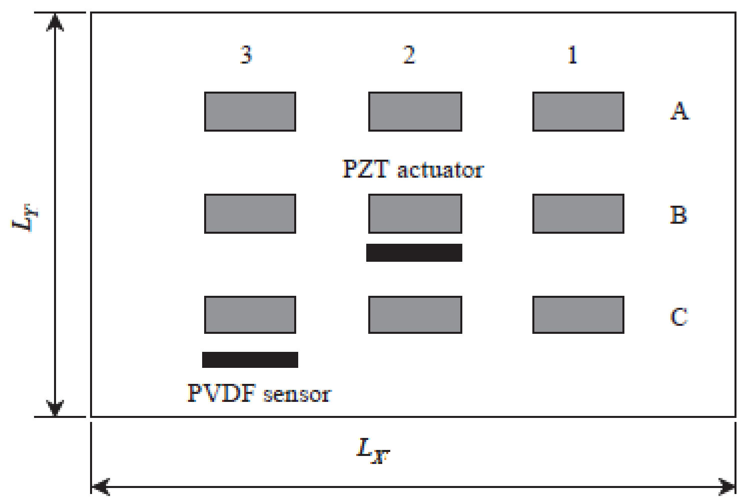

Figure 48 Spatial locations of the PZT actuators on the flexible plate for MIMO case

Table 12 Minimum damping for few resonant modes in MIMO case

Resonant frequency (Hz)	Attenuation (dB)
51.4995	4.1
85.5176	6
153.5537	3.2
193.2414	7
312.4	8.1
345.8	4.4

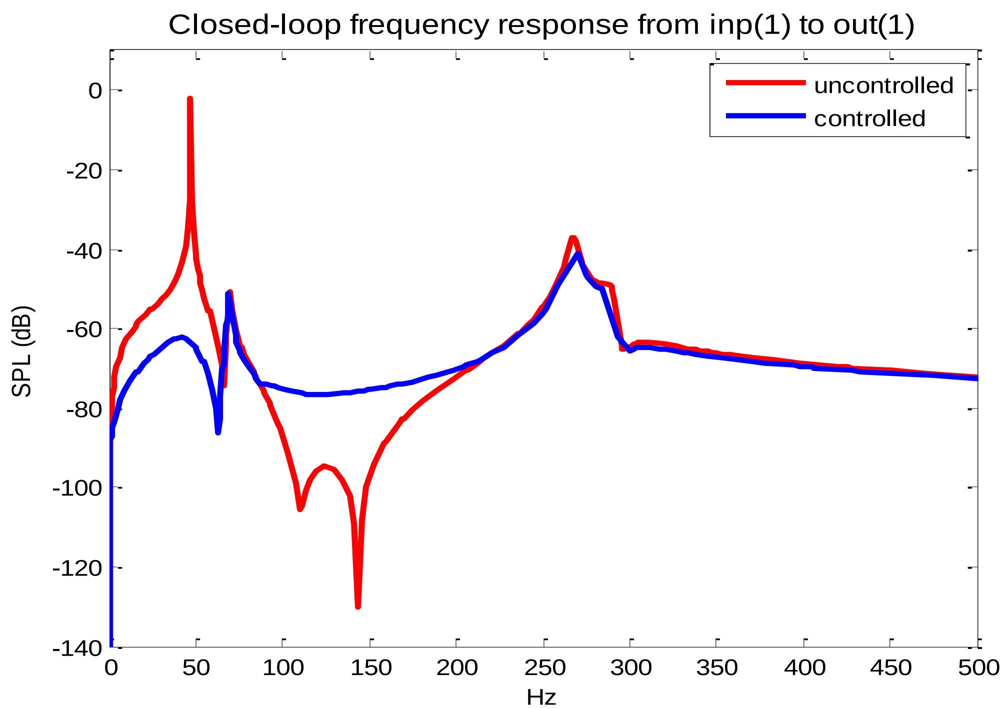

Figure 49 SPL in the cavity from inp (1) to out (1) with applied voltage 1 V (2.2509 N)

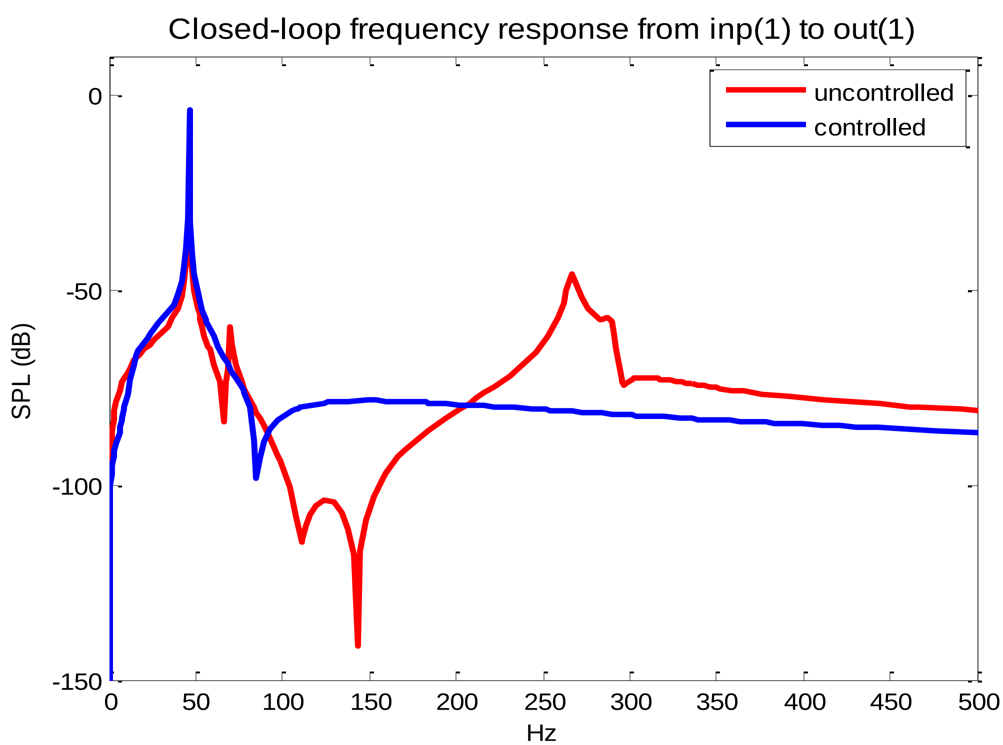

Figure 50 SPL in the cavity with applied voltage 1 V with steel plate (2.2509 N)

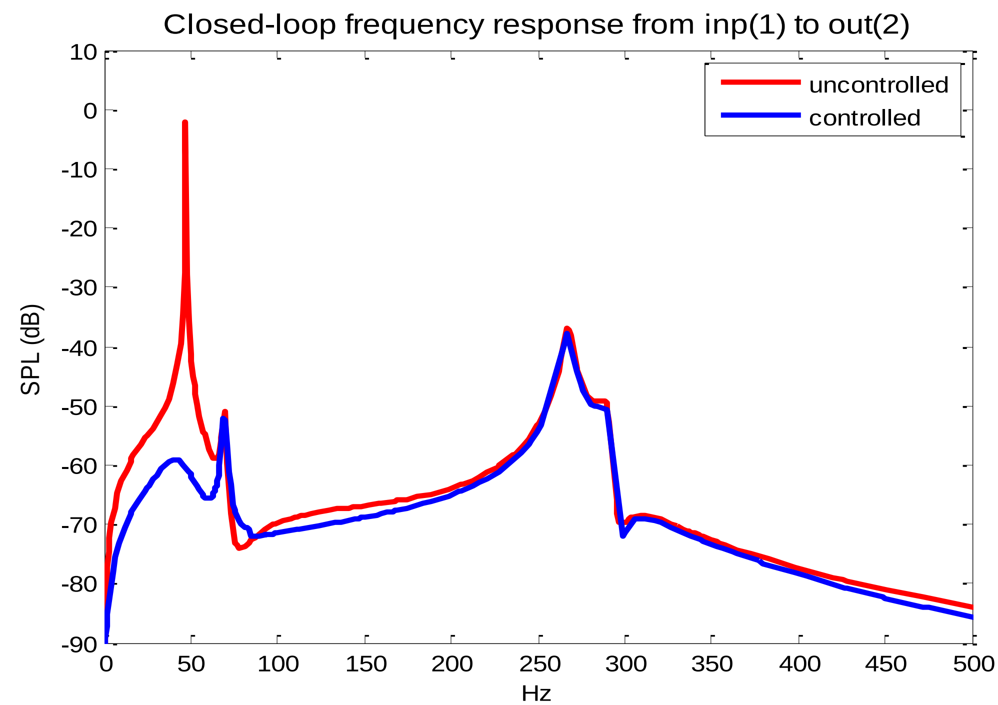

Figure 51 SPL in the cavity from inp (1) to out (2) with applied voltage 1 V (2.2509 N)

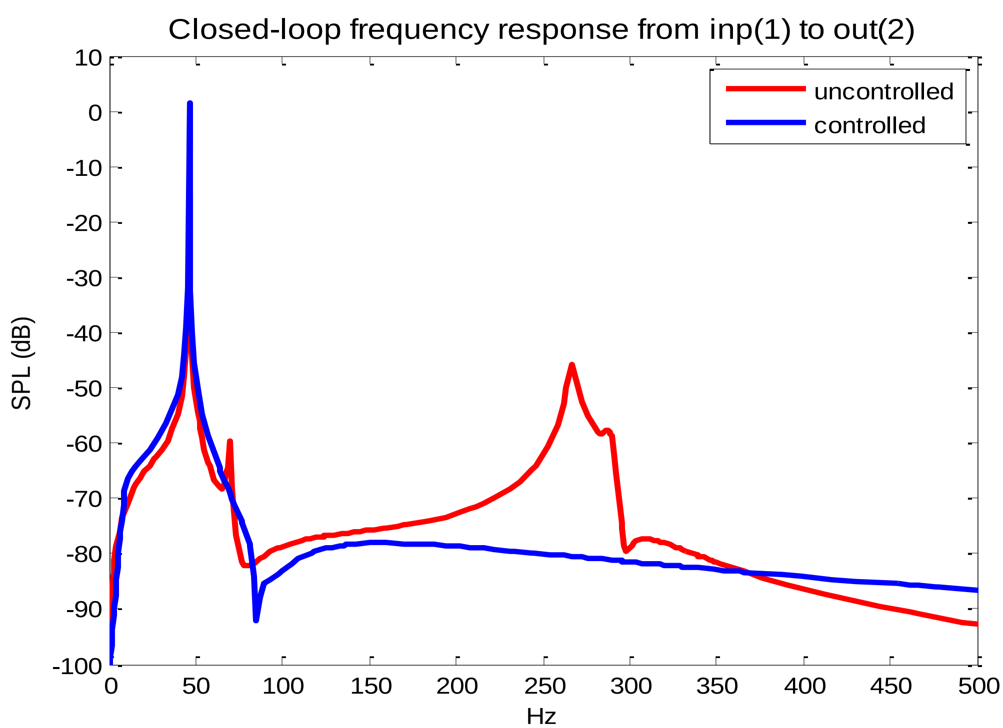

Figure 52SPL in the cavity with applied voltage 1 V with steel plate (2.2509 N)

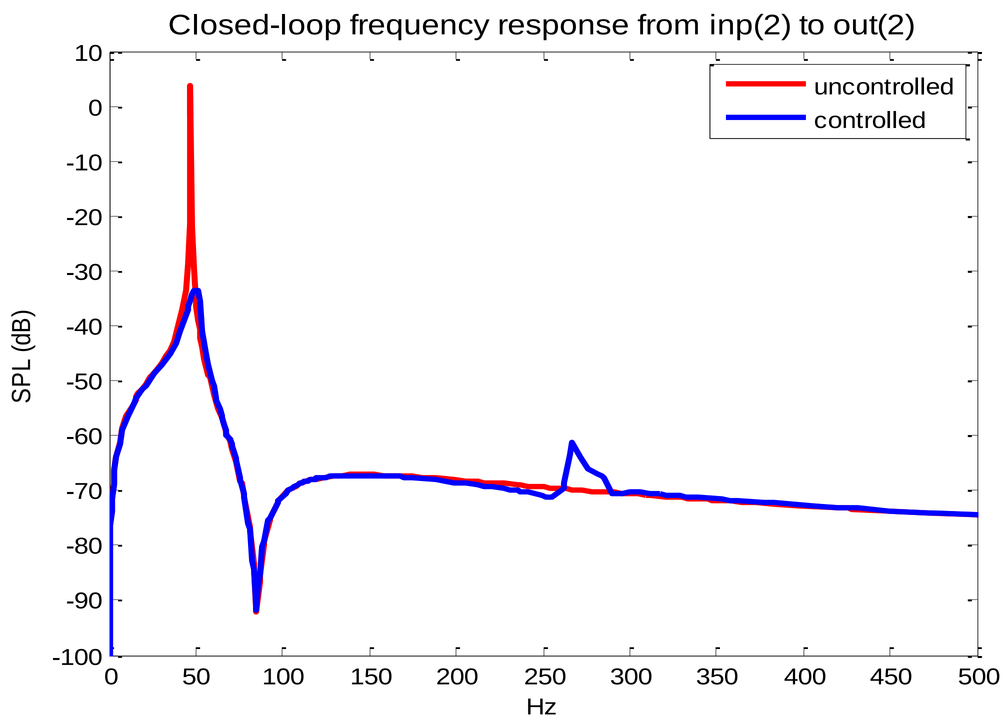

Figure 53 SPL in the cavity from inp (2) to out (2) with applied voltage 1 V (2.2509 N)

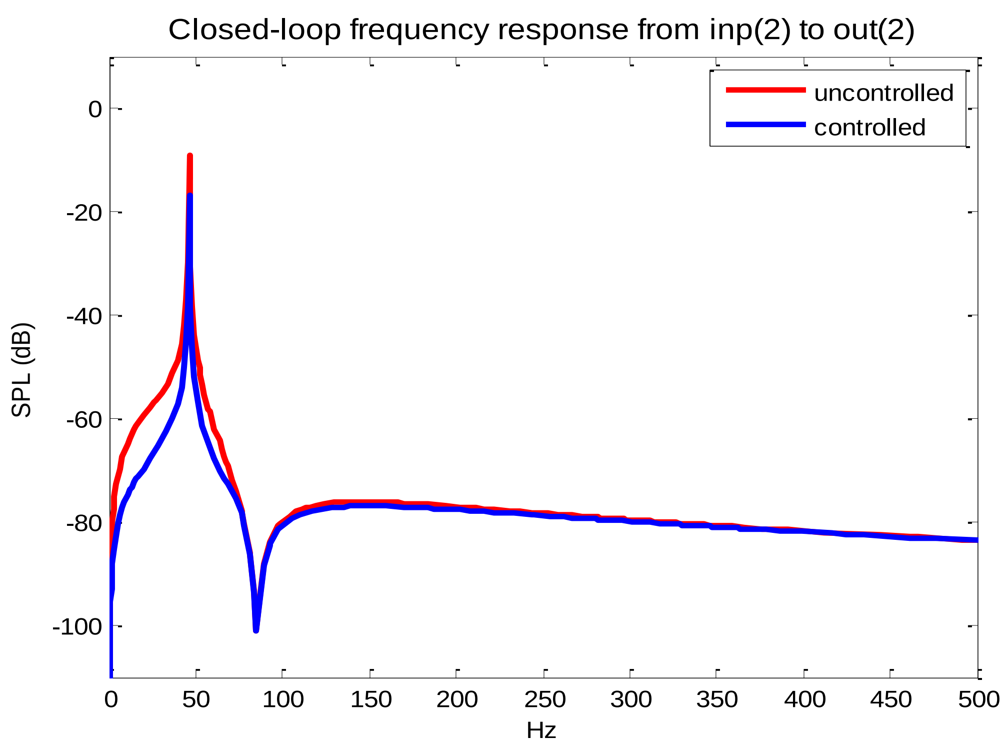

Figure 54 SPL in the cavity with applied voltage 1 V with steel plate (2.2509 N)

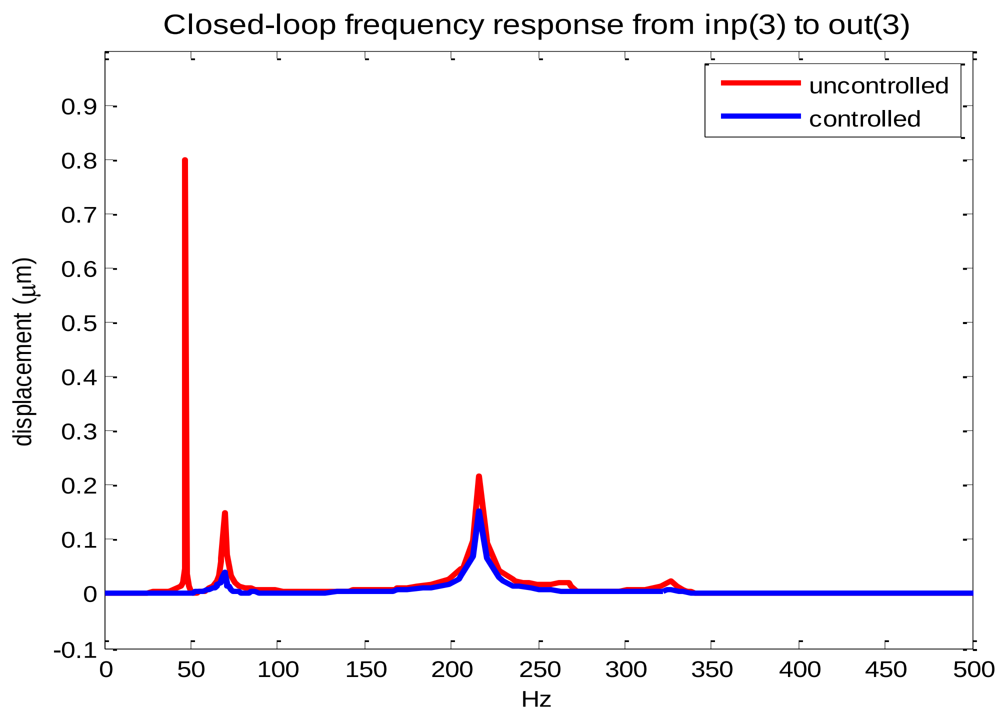

Figure 55 Frequency response from inp (3) to out (3) with applied voltage 1 V (2.2509 N)

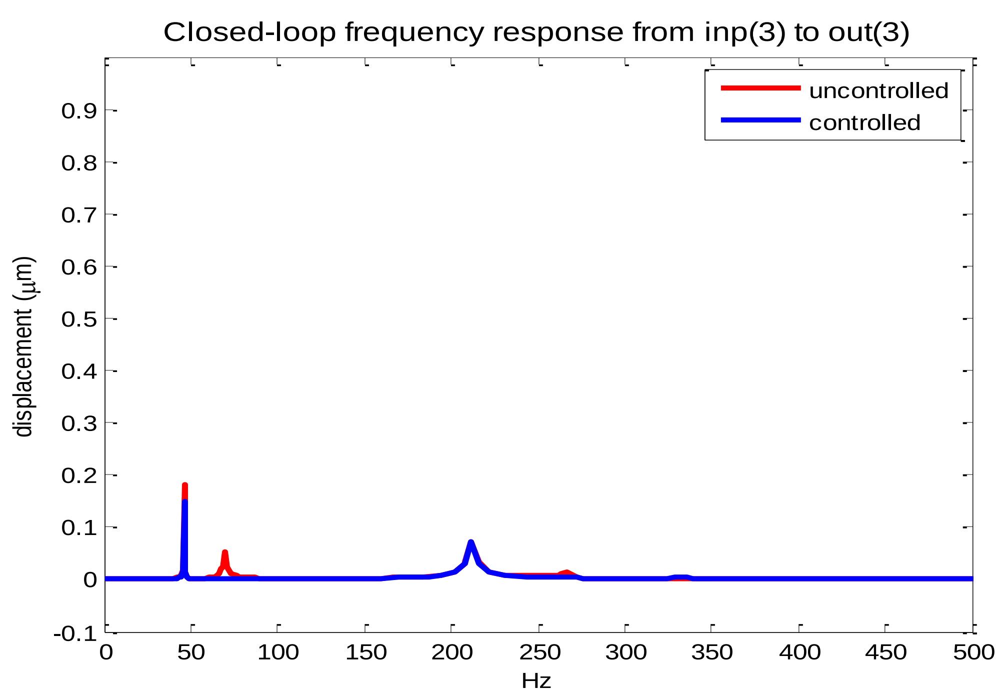

Figure 56 Open and Closed-loop frequency response with applied voltage 1 V with steel plate (2.2509 N)

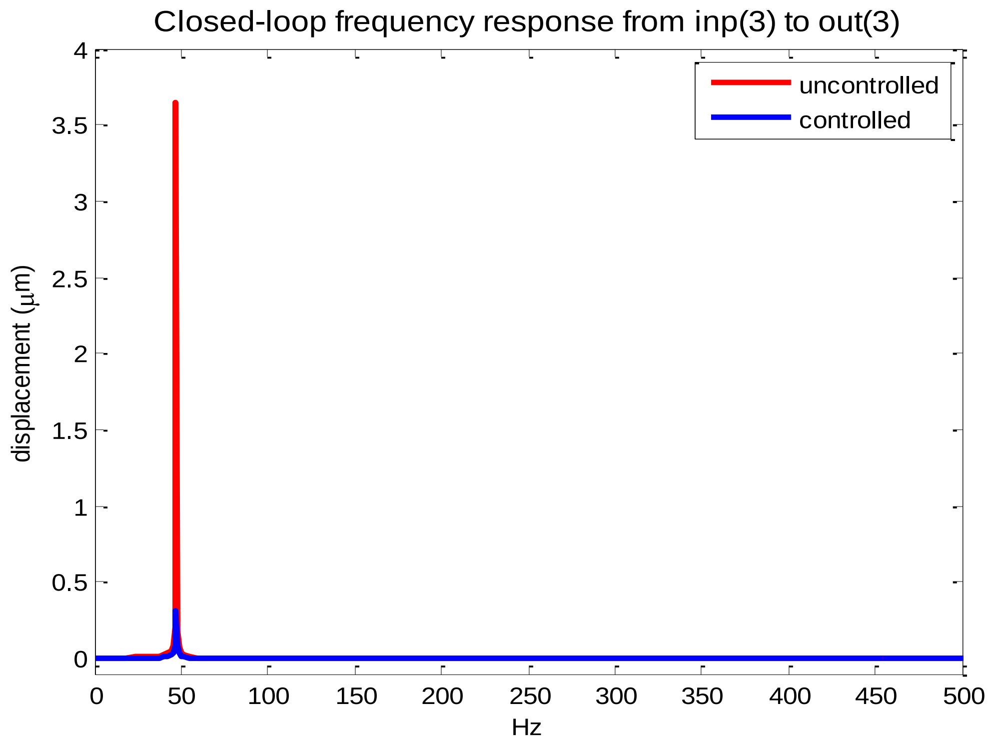

Figure 57 Frequency response with applied voltage 1 V at PVDF sensor location (0.90, 0.30) m (2.2509 N)

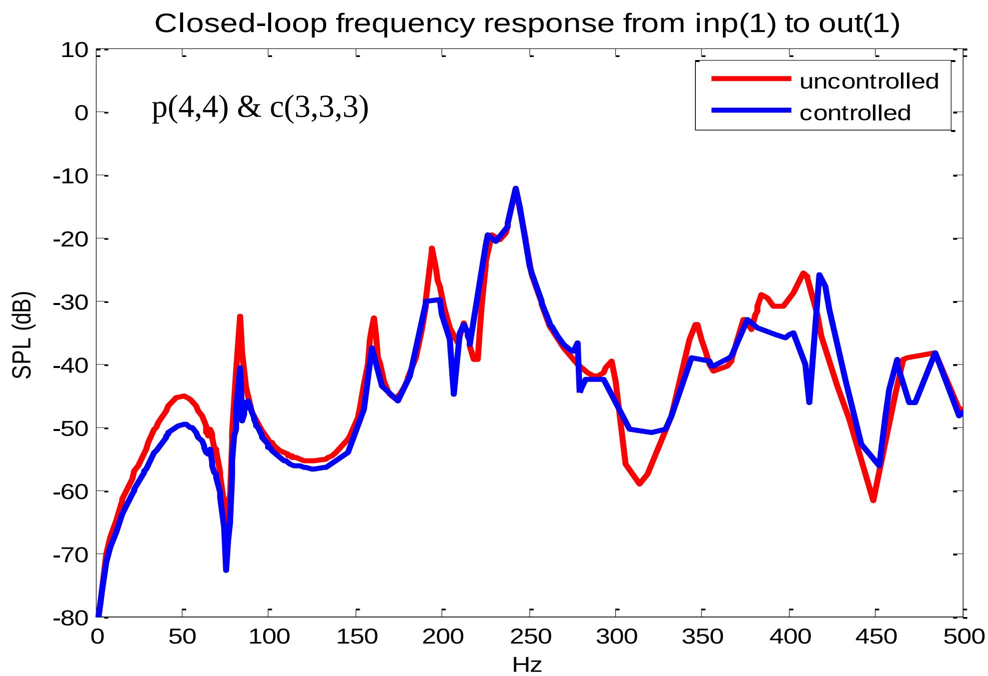

Figure 58 SPL in the cavity from inp (1) to out (1) with applied voltage 1 V (2.2509 N)

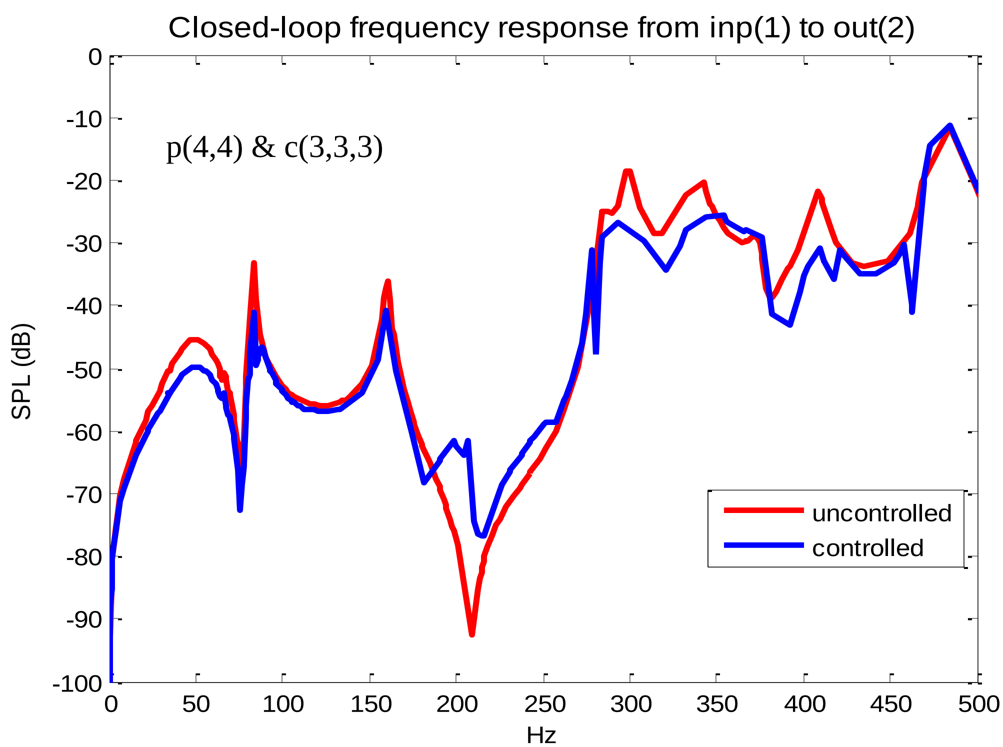

Figure 59 SPL in the cavity from inp (1) to out (2) with applied voltage 1 V (2.2509 N)

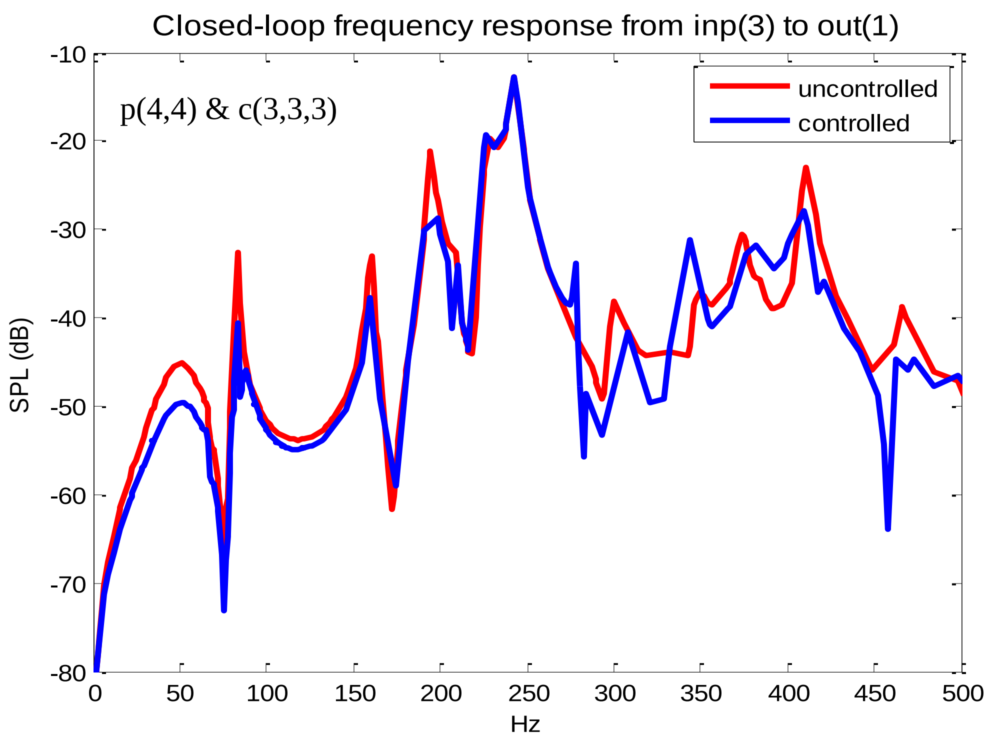

Figure 60 SPL in the cavity from inp (3) to out (1) with applied voltage 1 V (2.2509 N)

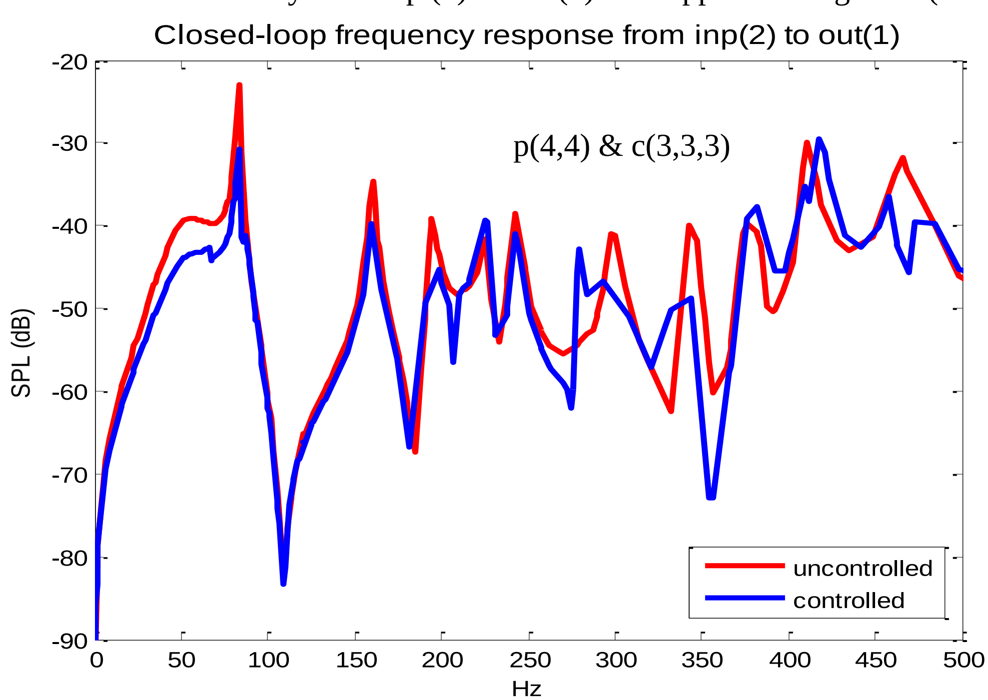

Figure 61 SPL in the cavity from inp (2) to out (1) with applied voltage 1 V (2.2509 N)

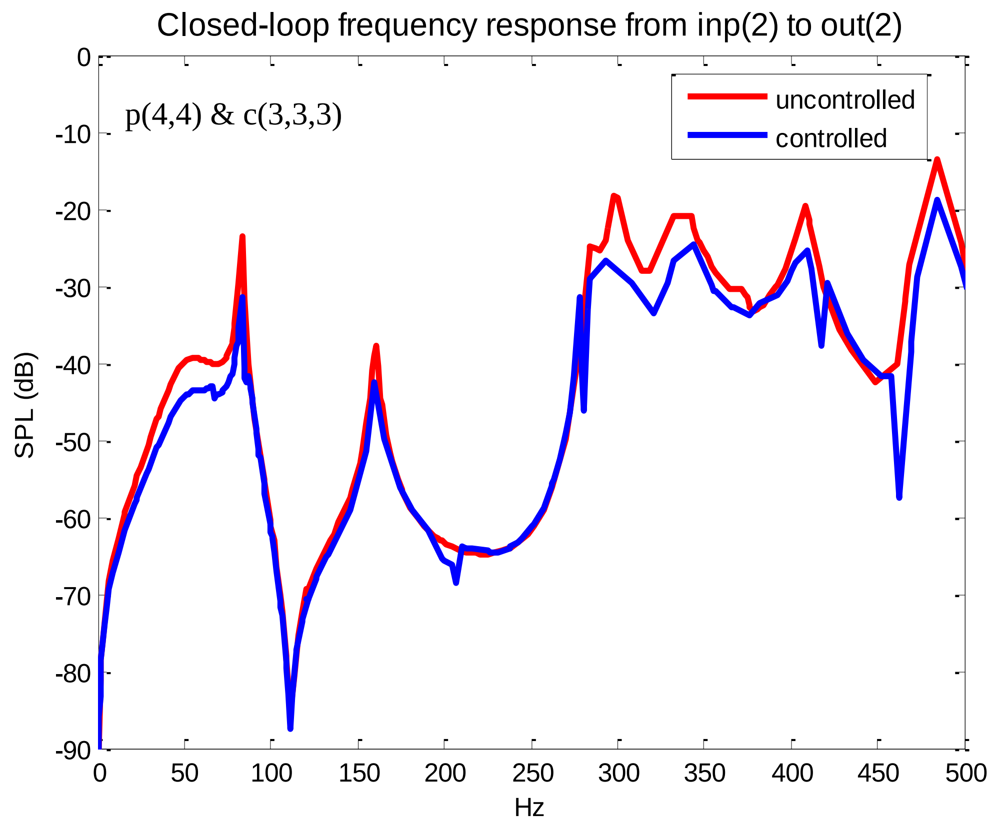

Figure 62 SPL in the cavity from inp (2) to out (2) with applied voltage 1 V (2.2509 N)

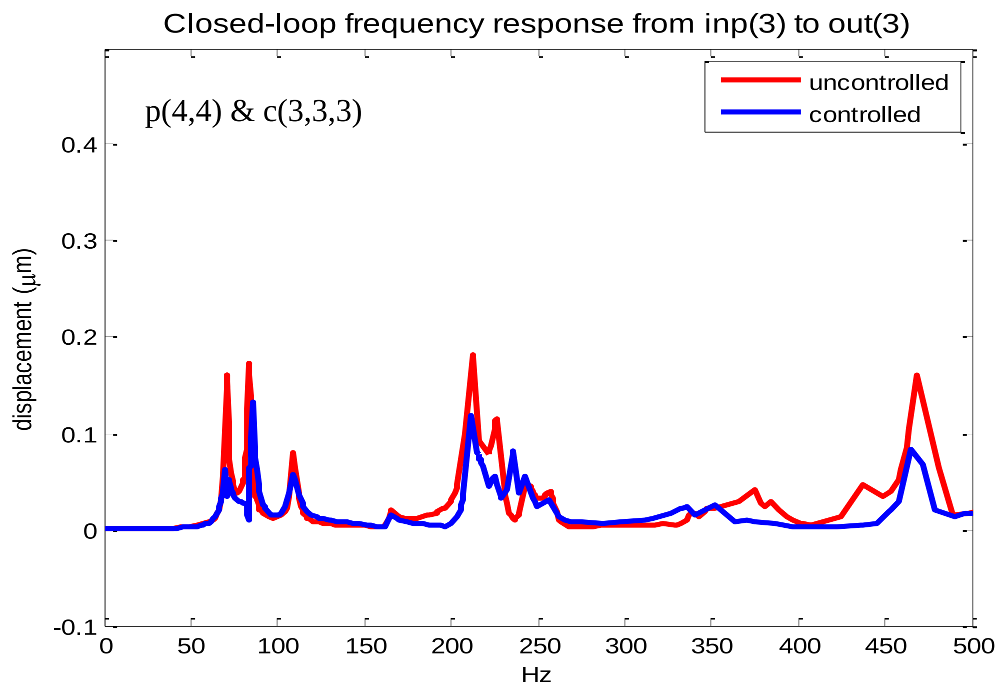

Figure 63 Frequency response from inp (3) to out (3) with applied voltage 1 V (2.2509 N)

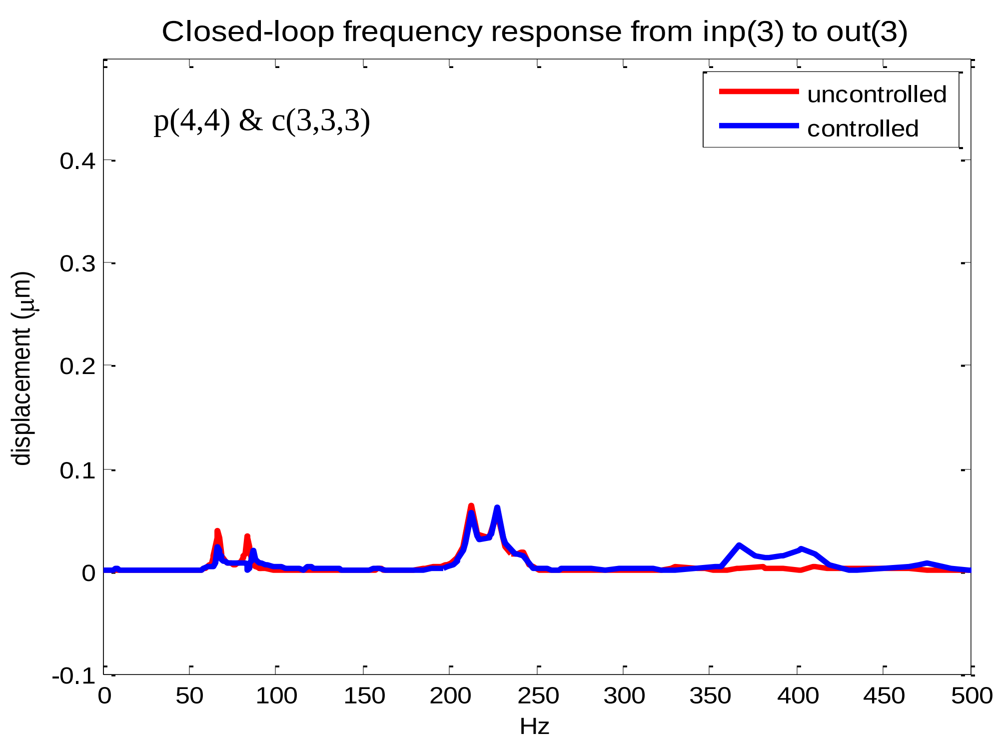

Figure 64 Frequency response with applied voltage 1 V with steel plate

CHAPTER 6

Conclusions

6.1 Summary

A thorough literature review has been conducted on active structural acoustic control (ASAC) of a rectangular enclosure. There has been much work on ASAC ranging from simple beam to smart building. But there is hardly any work in the literature that addresses active structural acoustic control in a 3D enclosure with systematic Linear Quadratic Gaussian (LQG) controller design. The remainder of the thesis work can be summed up as followings.

First, an active noise control of a 1-D rectangular Duct has been validated using passive and semi-active shunt circuits which work as proportional and PID controller respectively. Comparing validation result, it is obvious that the semi-active shunt loudspeaker works well and easy to develop.

Second, an active acoustic-structure coupled system has been modeled and developed and eigen-frequency of the developed model has been validated against the available analytical and experimental eigen-frequency of a 3D enclosure pertaining to active structural acoustic control (ASAC).

Third, this thesis work answers if it is possible to develop and implement SISO, MISO, and MIMO controllers based on Linear Quadratic Gaussian (LQG) regulator that ensure some robustness but still have the necessary performance for meaningful reductions of sound pressure level (SPL)in the 3D enclosure.

Finally, the controller implemented results have been discussed case by case for SISO, MISO, and MIMO controllers respectively. Besides, two types of plates such as aluminum and steel plate have been used as a host structure of PZT actuators. The results show that an aluminum plate is much better to that of steel plate due to its adaptability with the PZT actuators due to closeness of the material strength (Young Modulus). Moreover, it is clear from the simulation results that the LQG based controller can reduce considerable system noise while keeping track to the system response. But LQG based controller becomes pretty tedious when the mode numbers increase, for it is very challenging to select proper weighting matrices for the system with orders more than few hundreds.

6.2 Recommendations for future work

- Optimization of PZT patches locations on the host plate using genetic algorithms.
- Improved estimation of states considering the missing dynamics of the systems.
- In the present work LQG control strategies were considered, for the most part to show that the numerical model is a useful design tool. Based on the results presented in the thesis, it can be stated that LQG control strategies have potential for reducing the sound radiation. However, it may be

worthwhile to consider other control strategies better suited for the current control problem.

Appendix A

$$\boldsymbol{v_{PZT}^{T}} = [V_{PZT}^{1} \;\dots\; V_{PZT}^{N_{PZT}}]$$

$$\boldsymbol{A_{11}} = diag(A_{11}^{m})_{2N_p\times 2N_p},\;\; \boldsymbol{A_{22}} = diag(A_{22}^{n})_{2(N_a+1)\times 2(N_a+1)}$$

$$\boldsymbol{E_{11}} = I_{2N_p\times 2N_p},\;\; \boldsymbol{E}_{22} = I_{2(N_a+1)\times 2(N_a+1)}$$

$$\boldsymbol{A_{11}^{m}} = \begin{bmatrix} 0 & 1 \\ -\omega_{p,m}^{2} & -2\xi_{p,m}\omega_{p,m} \end{bmatrix} m = 1,\dots,N_p$$

$$\boldsymbol{A_{22}^{n}} = \begin{bmatrix} 0 & 1 \\ -\omega_{a,n}^{2} & -2\xi_{a,n}\omega_{a,n} \end{bmatrix} \qquad\qquad n = 0,1,\dots,N_a$$

$$\boldsymbol{A_{12}} = \begin{bmatrix} 0 & 0 & \cdots & 0 & 0 \\ c_{0,1} & 0 & & c_{N_a,1} & 0 \\ \vdots & & \ddots & \vdots & \\ 0 & 0 & \cdots & 0 & 0 \\ c_{0,N_p} & 0 & & c_{N_p,N_a} & 0 \end{bmatrix}_{2N_p\times 2(N_a+1)}$$

$$\boldsymbol{E_{21}} = \begin{bmatrix} 0 & 0 & \cdots & 0 & 0 \\ 0 & c_{0,1} & & 0 & c_{0,N_p} \\ \vdots & & \ddots & \vdots & \\ 0 & 0 & \cdots & 0 & 0 \\ 0 & c_{N_a,0} & & 0 & c_{N_a,N_p} \end{bmatrix}_{2(N_a+1)\times 2N_p}$$

$$\boldsymbol{D_{PZT}} = \begin{bmatrix} 0 & 0 & \cdots & 0 & 0 \\ B_{PZT,1,1} & B_{PZT,1,2} & & B_{PZT,1,(N_{PZT}-1)} & B_{PZT,1,N_{PZT}} \\ & \vdots & \ddots & & \vdots \\ 0 & 0 & \cdots & 0 & 0 \\ B_{PZT,N_p,1} & B_{PZT,N_p,2} & & B_{PZT,N_p,(N_{PZT}-1)} & B_{PZT,N_p,N_{PZT}} \end{bmatrix}_{2N_p\times N_{PZT}}$$

$$\boldsymbol{B_{11}} = \begin{bmatrix} 0 \\ \gamma_{11} \\ \dots \\ 0 \\ \gamma_p \end{bmatrix}_{\boldsymbol{2N_p}\times\boldsymbol{1}}$$

$$\boldsymbol{d}_{PW}^{T} = \frac{1}{m_p}[0 \quad g_{p,1} \cdots 0 \quad g_{p,N_p}]\_(1\times 2N_p)$$

Appendix B

```
% Read the plant, input, disturbance, and output matrices from %workspace

Ax = A0;% Plant matrix
Bx = Dpztp; % Input matrix
Cx0 =[Cx];% Output matrix
[rCx,cCx]=size(Cx0);
[rBx,cBx]=size(Bx);
Dx = zeros(rCx,cBx);
sys_0 = ss(Ax,Bx,Cx0,Dx);% Actual system
%%%% generate state feedback controller %%%%
[msys] = minreal(sys_0,1); % minimal realized system
[rmc, cmc]=size(msys.c);
[rRx,cRx]=size(msys.b);

Qr = 1e2*eye(rmc);% Error penalty matrix imposed on output
Rr = 1e-4*eye(cRx);%Control penalty matrix
G = lqry(msys.a,msys.b,msys.c,msys.d,Qr,Rr); %State-feedback gain %matrix with output weighting

Qe = (1e-1*eye(cRx));% process noise data
Re = (1e-2*eye(rmc));%measurement noise data

Bcontrol = (msys.b)*-1*[1];   % Control Input (Voltage)
Bpp = Bd(1:length(msys.b),1); %Disturbance Input

Ksys = ss(msys.a,[Bcontrol Bpp],msys.c,[msys.d msys.d]);
[Kest] = kalman(Ksys,Qe,Re); % Kalman state estimator
sys_k = -lqgreg(Kest,G); %LQG regulator
feedin = [1];
feedout = [1];
sys_c  =  feedback(msys, sys_k,feedin,feedout); %Closed-loop %system with lqgreg feedback
```

References

1. Lueg, P., *Process of silencing sound oscillations, US Patent, 2 043 416*. 1934, Application.
2. Lueg, P., *PBOCESS OF SILENCING SOUND*. 1936, Google Patents.
3. Olson, H.F., *Electronic control of noise, vibration, and reverberation.* The Journal of the Acoustical Society of America, 1956. **28**: p. 966.
4. Olson, H.F. and E.G. May, *Electronic sound absorber*. The Journal of the Acoustical Society of America, 1953. **25**: p. 1130.
5. Snyder, S., L. Brooks, and D. Moreau, *Active control of noise and vibration*. Vol. 1. 2013: CRC Press.
6. Hong, J., et al., *Modeling, identification, and feedback control of noise in an acoustic duct.* Control Systems Technology, IEEE Transactions on, 1996. **4**(3): p. 283-291.
7. Li, D., *Active control of aircraft cabin noise and vibration using a physical model*. 2003.
8. Fuller, C., C. Hansen, and S. Snyder, *Active control of sound radiation from a vibrating rectangular panel by sound sources and vibration inputs: an experimental comparison.* Journal of Sound and Vibration, 1991. **145**(2): p. 195-215.
9. Snyder, S. and C. Hansen, *Mechanisms of active noise control by vibration sources.* Journal of Sound and Vibration, 1991. **147**(3): p. 519-525.
10. Snyder, S. and C. Hansen, *The design of systems to control actively periodic sound transmission into enclosed spaces, part II: mechanisms and trends.* Journal of sound and vibration, 1994. **170**(4): p. 451-472.
11. Grewal, A., et al., *Active control of aircraft cabin noise using smart structures.* AIAA/ASME/AHS Adaptive Structure Form, 1996.
12. Gerner, C., D. Sachau, and H. Breitbach. *Active noise control in an aircraft cabin*. in *Proc of IMAC-XXII, conference on structural dynamics*. 2004.
13. Dorling, C., et al., *A demonstration of active noise reduction in an aircraft cabin.* Journal of Sound and Vibration, 1989. **128**(2): p. 358-360.
14. Elliot, S., et al., *In-flight experiments on the active control of propeller-induced cabin noise.* Journal of Sound and Vibration, 1990. **140**(2): p. 219-238.
15. Kuo, S.M. and D.R. Morgan, *Active noise control: a tutorial review.* Proceedings of the IEEE, 1999. **87**(6): p. 943-973.
16. Macmartin, D.G., *Collocated structural control for reduction of aircraft cabin noise.* Journal of sound and vibration, 1996. **190**(1): p. 105-119.
17. Radcliffe, C. and S. Southward, *Global active noise control of a one-dimensional acoustic duct using a feedback controller.* Journal of Vibration and Acoustics, 1993. **115**: p. 488-494.
18. Beier, T.H., et al., *High speed research program structural acoustics multi-year summary report.* NASA TM, 2005. **213536**.

19. Bullmore, A., et al., *The active minimization of harmonic enclosed sound fields, part II: A computer simulation.* Journal of Sound and Vibration, 1987. **117**(1): p. 15-33.
20. Elliott, S., et al., *The active minimization of harmonic enclosed sound fields, Part III: Experimental verification.* Journal of Sound and Vibration, 1987. **117**(1): p. 35-58.
21. Elliott, S.J. and P.A. Nelson, *Active noise control.* Signal Processing Magazine, IEEE, 1993. **10**(4): p. 12-35.
22. Gonzalez, A., et al., *Sound quality of low-frequency and car engine noises after active noise control.* Journal of Sound and Vibration, 2003. **265**(3): p. 663-679.
23. Montazeri, A., J. Poshtan, and M.H. Kahaei, *Modal analysis for global control of broadband noise in a rectangular enclosure.* noise notes, 2007. **6**(4): p. 41-56.
24. Nelson, P., et al., *The minimum power output of free field point sources and the active control of sound.* Journal of Sound and Vibration, 1987. **116**(3): p. 397-414.
25. Wright, R.I., *A hierarchical noise control system using adaptable tuned vibration absorbers*. 2003, Citeseer.
26. Fuller, C.R. and G.P. Gibbs. *Active control of interior noise in a business jet using piezoceramic actuators*. in *Noise Con 1994: Proceedings of the 1994 National Conference on Noise Control Engineering*. 1994.
27. Balachandran, B., A. Sampath, and J. Park, *Active control of interior noise in a three-dimensional enclosure.* Smart materials and structures, 1996. **5**(1): p. 89.
28. Baumann, W.T., F.S. Ho, and H.H. Robertshaw, *Active structural acoustic control of broadband disturbances.* The Journal of the Acoustical Society of America, 1992. **92**(4): p. 1998-2005.
29. Bullmore, A., P. Nelson, and S. Elliott, *Theoretical studies of the active control of propeller-induced cabin noise.* Journal of sound and vibration, 1990. **140**(2): p. 191-217.
30. Fuller, C. and J. Jones, *Experiments on reduction of propeller induced interior noise by active control of cylinder vibration.* Journal of Sound and Vibration, 1987. **112**(2): p. 389-395.
31. Fuller, C.R., et al., *Active control of interior noise in model aircraft fuselages using piezoceramic actuators.* AIAA journal, 1992. **30**(11): p. 2613-2617.
32. Kajikawa, Y., W.-S. Gan, and S.M. Kuo, *Recent advances on active noise control: open issues and innovative applications.* APSIPA Transactions on Signal and Information Processing, 2012. **1**: p. e3.
33. Koshigoe, S., J. Gillis, and E. Falangas, *A new approach for active control of sound transmission through an elastic plate backed by a rectangular cavity.* The Journal of the Acoustical Society of America, 1993. **94**(2): p. 900-907.
34. Koshigoe, S., A. Teagle, and A. Gordon, *A time domain study of active control of sound transmission due to acoustic pulse excitation.* The Journal of the Acoustical Society of America, 1995. **97**(1): p. 313-323.
35. Lyon, R.H., *Noise reduction of rectangular enclosures with one flexible wall.* The Journal of the Acoustical Society of America, 1963. **35**: p. 1791.
36. Dowell, E. and H. Voss, *The effect of a cavity on panel vibration.* AIAA journal, 1963. **1**(2): p. 476-477.

37. Pretlove, A., *Free vibrations of a rectangular panel backed by a closed rectangular cavity by a closed rectangular cavity.* Journal of Sound and Vibration, 1965. **2**(3): p. 197-209.
38. Pretlove, A., *Forced vibrations of a rectangular panel backed by a closed rectangular cavity.* Journal of Sound and Vibration, 1966. **3**(3): p. 252-261.
39. Dowell, E., G. Gorman, and D. Smith, *Acoustoelasticity: general theory, acoustic natural modes and forced response to sinusoidal excitation, including comparisons with experiment.* Journal of Sound and Vibration, 1977. **52**(4): p. 519-542.
40. Narayanan, S. and R. Shanbhag, *Sound transmission through elastically supported sandwich panels into a rectangular enclosure.* Journal of Sound and Vibration, 1981. **77**(2): p. 251-270.
41. Al-Bassyiouni, M. and B. Balachandran, *Sound transmission through a flexible panel into an enclosure: structural–acoustics model.* Journal of Sound and Vibration, 2005. **284**(1): p. 467-486.
42. Mohamady, S., et al., *Modeling and Eigenfrequency Analysis of Sound-Structure Interaction in a Rectangular Enclosure with Finite Element Method.* Advances in Acoustics and Vibration, 2010. **2009**.
43. Du, J.T., et al., *Vibro-acoustic analysis of a rectangular cavity bounded by a flexible panel with elastically restrained edges.* The Journal of the Acoustical Society of America, 2012. **131**(4): p. 2799-2810.
44. Kulah, S., U. Aridogan, and I. Basdogan, *Investigation of an Active Structural Acoustic Control System on a Complex 3D Structure*, in *Topics in Modal Analysis, Volume 7*. 2014, Springer. p. 715-721.
45. Guicking, D., K. Karcher, and M. Rollwage. *Active control of the acoustic reflection coefficient at low frequencies*. in *INTER-NOISE and NOISE-CON Congress and Conference Proceedings*. 1983. Institute of Noise Control Engineering.
46. Glaese, R.M., *Impedance matching for structural-acoustic control*. 1997, Massachusetts Institute of Technology.
47. Bassyiouni, M.A. and B. Balachandran, *Sound transmission through a flexible panel into an enclosure:structural–acoustics model.* Journal of Sound and Vibration, 2005(284): p. 467–486.
48. Fang, B., et al., *Modelling, system identification, and control of acoustic–structure dynamics in 3-D enclosures.* Control Engineering Practice, 2004. **12**(8): p. 989-1004.
49. Li, D., L. Cheng, and C. Gosselin, *Optimal design of PZT actuators in active structural acoustic control of a cylindrical shell with a floor partition.* Journal of sound and vibration, 2004. **269**(3): p. 569-588.
50. Rao, M.D., *Recent applications of viscoelastic damping for noise control in automobiles and commercial airplanes.* Journal of Sound and Vibration, 2003. **262**(3): p. 457-474.
51. Qiu, J. and H. Ji, *The application of piezoelectric materials in smart structures in China.* International Journal of Aeronautical and Space Science, 2010. **11**(4): p. 266-284.

52. Fleming, A.J., et al., *Control of resonant acoustic sound fields by electrical shunting of a loudspeaker*. Control Systems Technology, IEEE Transactions on, 2007. **15**(4): p. 689-703.
53. Pietrzko, S. and Q. Mao. *Noise Reduction in a duct using passive/semi-active shunt loudspeakers*. in *The Sixteenth International Congress on Sound and Vibration*. 2009.
54. Bies, D. and C. Hansen, *Engineering noise control: theory and practice*. 2009: Taylor & Francis.
55. Nelson, P.A., S.J. Elliott, and J.E.F. Williams, *Active control of sound.* Physics Today, 1993. **46**: p. 75.
56. Doria, A., *Control of acoustic vibrations of an enclosure by means of multiple resonators.* Journal of sound and vibration, 1995. **181**(4): p. 673-685.
57. McKelvey, T., H. Akçay, and L. Ljung, *Subspace-based multivariable system identification from frequency response data.* Automatic Control, IEEE Transactions on, 1996. **41**(7): p. 960-979.
58. Hanifzadegan, M. and A. Ohadi. *Global Active Control of Transmitted Sound Into Acoustic Cavity With Speakers and Piezoelectric Patch Actuators*. in *ASME 2009 International Mechanical Engineering Congress and Exposition*. 2009. American Society of Mechanical Engineers.
59. Liu, F., B. Fang, and A. Kelkar, *Energy Extraction-Based Robust Linear Quadratic Gaussian Control of Acoustic-Structure Interaction in Three-Dimensional Enclosure.* Journal of Vibration and Acoustics, 2014. **136**(4): p. 041008.
60. Bryson, A.E., *Applied optimal control: optimization, estimation and control*. 1975: CRC Press.
61. Chesi, G., *LMI techniques for optimization over polynomials in control: a survey.* Automatic Control, IEEE Transactions on, 2010. **55**(11): p. 2500-2510.
62. Ibrir, S., *Convex optimization approach to observer-based stabilization of uncertain linear systems.* Journal of dynamic systems, measurement, and control, 2006. **128**(4): p. 989-994.
63. Meirovich, L., *Fundamentals of Vibrations*. 2001: McGraw-Hill Higher Education.
64. Kim, S.M., Brenna, M.J., *Active control of harmonic sound transmission into an acoustic enclosure using both structural and acoustic actuators.* Journal of the Acoustical Society of America, 2000. **107**(5): p. 2523-2534.
65. Qiua, Z., Zhang, X., Wu, H., Zhang, H., *Optimal placement and active vibration control for piezoelectric smart flexible cantilever plate.* Journal of Sound and Vibration, 2007. **301**: p. 521-543.
66. Pota, H.R. and A.G. Kelkar, *Modeling and control of acoustic ducts.* Journal of vibration and acoustics, 2001. **123**(1): p. 2-10.
67. Blevins, A.J., *Formulas for Natural Frequency and Mode Shapes*. 1979, Melbourne, FL: Krieger.
68. Elliott, S.J., *Signal processing for active control*. 1999: Academic, London.
69. Fuller, C.C., S. Elliott, and P.A. Nelson, *Active control of vibration*. 1996: Academic Press.

70. Lin, F., *Robust control design: an optimal control approach*. Vol. 18. 2007: John Wiley & Sons.
71. Elliott, S.J., *A review of active noise and vibration control in road vehicles.* 2008.
72. Lurie, B. and P. Enright, *Classical feedback control: with MATLAB*. 2000: CRC Press.
73. Hansen, C. and S. Snyder, *Active control of noise and vibration, 1997.* E&FN Spon, London.
74. Anderson, B.D. and J.B. Moore, *Optimal control: linear quadratic methods*. 2007: Courier Dover Publications.
75. Skogestad, S. and I. Postlethwaite, *Multivariable feedback control: analysis and design*. Vol. 2. 2007: Wiley New York.
76. Zhou, K., J.C. Doyle, and K. Glover, *Robust and optimal control*. Vol. 40. 1996: Prentice Hall New Jersey.
77. Habib, H., et al. *Internal reference model based optimal LQG controller for atomic force microscope*. in *Control Automation Robotics & Vision (ICARCV), 2012 12th International Conference on*. 2012. IEEE.
78. Hendrix, C.D., M.J. Veth, and R.W. Carr. *LQG control design for a hovering micro air vehicle using an optical tracking system*. in *Aerospace conference, 2009 IEEE*. 2009. IEEE.
79. Dačić, D.B. and D. Nešić, *Quadratic stabilization of linear networked control systems via simultaneous protocol and controller design.* Automatica, 2007. **43**(7): p. 1145-1155.
80. Selvam, K., et al., *Feedback–feedforward individual pitch control for wind turbine load reduction.* International Journal of Robust and Nonlinear Control, 2009. **19**(1): p. 72-91.
81. Semeraro, O., et al., *Feedback control of three-dimensional optimal disturbances using reduced-order models.* Journal of Fluid Mechanics, 2011. **677**: p. 63-102.
82. Fisco, N. and H. Adeli, *Smart structures: part I—active and semi-active control.* Scientia Iranica, 2011. **18**(3): p. 275-284.
83. Gawronski, W., *Linear quadratic controller design for the deep space network antennas.* Journal of guidance, control, and dynamics, 1994. **17**(4): p. 655-660.
84. Gawronski, W., *Control and pointing challenges of large antennas and telescopes.* Control Systems Technology, IEEE Transactions on, 2007. **15**(2): p. 276-289.
85. Gawronski, W.K., C. Racho, and J.A. Mellstrom, *Application of the LQG and feedforward controllers to the deep space network antennas.* Control Systems Technology, IEEE Transactions on, 1995. **3**(4): p. 417-421.
86. Pulthasthan, S. and H.R. Pota, *The optimal placement of actuator and sensor for active noise control of sound–structure interaction systems.* Smart Materials and Structures, 2008. **17**(3): p. 037001.
87. Vasques, C. and J. Dias Rodrigues, *Active vibration control of smart piezoelectric beams: Comparison of classical and optimal feedback control strategies.* Computers & structures, 2006. **84**(22): p. 1402-1414.
88. Wills, A.G., et al., *Model predictive control applied to constraint handling in active noise and vibration control.* Control Systems Technology, IEEE Transactions on, 2008. **16**(1): p. 3-12.

89. Grewal, M.S. and A.P. Andrews, *Kalman filtering: theory and practice using MATLAB*. 2011: John Wiley & Sons.
90. Choi S. B. and Young M. H, *Vibration Control of Flexible Structure*, in *Piezoelectric Actuators*. 2010, CRC Press. p. 23-64.

Vitae

Name	: MD TARIQUE BIN HAMID
Nationality	: Bangladeshi
Date of Birth	: 03/01/1987
Email	: tbinhamid@gmail.com
Address	: Mashila, Chaugacha, Jessore, Bangladesh
Academic Background	: MS in Aerospace Engineering
	KFUPM, Dhahran 2015
	BEng. in Aerospace Engineering
	International Islamic University Malaysia 2011